The background of the slide is a complex, colorful pattern. It features a large, bright yellow and orange area at the bottom, which transitions into a blue area at the top. The pattern has a textured, almost crystalline appearance, with various shades of blue, green, and yellow. The overall effect is reminiscent of a microscopic view of a particle filter or a water treatment process.

Numerical and experimental design of ultrasonic particle filters for water treatment

H.J. Cappon

Numerical and experimental design of ultrasonic particle filters for water treatment

Hendrik Jannis Cappon

Thesis committee

Promotor

Prof. Dr G. van Straten
Professor of Systems and Control
Wageningen University

Co-promotor

Dr K.J. Keesman
Associate professor, Biomass Refinery and Process Dynamics
Wageningen University

Other members

Prof. Dr C.J. Buisman, Wageningen University
Prof. Dr A.F.W. van der Steen, Erasmus University, Rotterdam
Dr J. Hawkes, University of Manchester, UK
Dr M. Mayer, EasyMeasure, Amersfoort

This research was conducted under the auspices of the Netherlands Research School for the Socio-Economic and Natural Sciences of the Environment (Sense)

Numerical and experimental design of ultrasonic particle filters for water treatment

Hendrik Jannis Cappon

Thesis

submitted in the fulfilment of the requirements for the degree of doctor
at Wageningen University
by the authority of the Rector Magnificus
Prof. Dr M.J. Kropff,
in the presence of the
Thesis Committee appointed by the Academic Board
to be defended in public
on Wednesday 5 March 2014
at 11 a.m. in the Aula.

H.J. Cappon

Numerical and experimental design of ultrasonic particle filters for water treatment,
202 pages.

PhD thesis, Wageningen University, Wageningen, NL (2014)

With references, with summaries in Dutch and English

ISBN 978-94-6173-859-2

CONTENTS

1	Introduction and outline	13
1.1	Background	14
1.2	Problem formulation	15
1.3	Objective	15
1.4	Thesis outline	16
2	Acoustic separation principle	19
2.1	Theoretical background	20
2.2	State of the art	26
2.2.1	Physical separators	26
2.2.2	1D models and designs	27
2.2.3	2D models and designs	29
2.2.4	3D models and designs	31
2.2.5	Applications and new concepts	31
2.3	Demonstrator	33
2.3.1	Materials and methods	33
2.3.2	Results	34
3	Model of the piezoelectric transducer	39
3.1	Introduction	40
3.2	Background	40
3.2.1	Piezo modelling basics	42
3.2.2	Boundary conditions	45
3.3	Materials and Methods	46

3.3.1	Experiments	46
3.3.2	Finite element model	47
3.3.3	Optimisation routine	47
3.3.4	Initial estimate	49
3.4	Results	50
3.4.1	Experiments	50
3.4.2	Simulations	51
3.4.3	Sensitivity study	54
3.5	Discussion	55
3.6	Conclusion	58
4	Model of an ultrasonic separator	61
4.1	Introduction	62
4.2	Materials and Methods	63
4.2.1	Device description	63
4.2.2	Experimental approach	64
4.2.3	Numerical model	65
4.2.4	Calibration and validation strategy	67
4.3	Results	68
4.3.1	Experiments	68
4.3.2	Calibration	68
4.3.3	Validation	70
4.4	Discussion	70
4.5	Conclusions	71
5	Basic design for an industrial separator	81
5.1	Introduction	82
5.2	Materials and methods	83
5.2.1	Transducer positioning and flow direction	84
5.2.2	Flow lane design	84

5.2.3	Optimisation criteria	85
5.3	Results	87
5.4	Conclusions and discussion	88
6	Industrial scale separator design	93
6.1	Introduction	94
6.2	Materials and methods	94
6.2.1	Methodology	94
6.2.2	Basic configuration	95
6.2.3	FE model	95
6.2.4	Design criteria and variables	97
6.2.5	Simulation strategy	99
6.3	Results	100
6.3.1	Acoustics	100
6.3.2	Flow characteristics	101
6.4	Compromised design	103
6.4.1	Particle tracing	105
6.5	Discussion	106
6.6	Conclusions	110
7	Industrial scale separator evaluation	113
7.1	Introduction	114
7.2	Materials and Methods	114
7.2.1	Experimental setup configuration	114
7.2.2	Concentration calibration	116
7.2.3	Batch mode operation	117
7.2.4	Sampling and efficiency	117
7.3	Results	118
7.4	Discussion	119
7.5	Conclusions	124

8	Flow control in acoustic separators	125
8.1	Introduction	126
8.2	Acoustic separation principle	126
8.3	Materials and Methods	127
8.3.1	Experiments	127
8.3.2	Piece-wise linear state space model	128
8.4	Results	131
8.4.1	Optimal pump rate ratio	131
8.4.2	Steady state analysis	132
8.4.3	Dynamic data analysis	134
8.4.4	Model validation	135
8.4.5	Optimal switching control	136
8.5	Discussion	138
8.6	Conclusions	140
9	Discussion and conclusions	141
9.1	Discussion	142
9.1.1	Design methodology	142
9.1.2	Finite element modelling	142
9.1.3	Parameter identification	144
9.1.4	Optimisation	145
9.1.5	Experiments	146
9.2	Conclusions	148
10	Synthesis and future perspective	151
10.1	Industrial size separators	152
10.2	Modes of operation	152
10.3	Fields of application	154
10.4	Model enhancements	155

A Sensitivity study on the final design	157
B Energy consumption of the final design	159
C Turbidity and efficiency measurements	163
D Steady state parameter estimation	167
Summary	187
Samenvatting	191
Acknowledgements	195
Curriculum Vitae	197

1. INTRODUCTION AND OUTLINE

1.1 Background

Almost all industrial and agricultural processes in the world use water for a wide variety of purposes. Water resources in the world, however, are limited. About 2.9% of the water in the world is fresh water, of which about 2.2% resides in glaciers and polar caps [46]. Mean while industrial development and growth of the world's population increases the demand for drinking water, food and products, thus increasing the pressure on these limited water resources. Therefore, intake of fresh water and disposal of communal and industrial wastewater is a subject of general concern. This being recognised by many governments, companies and farmers, urges them to search for technologies to limit their water usage and maximise reuse. Besides that, more stringent environmental regulations also force industry to minimise spills, both of water as well as the constituents thereof. Hence, there is a growing need for water recycling, recovery and multi-sourcing strategies. In almost all cases of water usage or reuse some sort of water treatment is needed to obtain the water quality needed.

Water technology incorporates the water treatment techniques used for water purification and content recovery. Water treatment often consists of several steps, each of them removing different kinds of constituents or pollutants. These steps, called "unit operations" can be divided into chemical, biological or physical processes and hybrids thereof. A chemical treatment process may involve a chemical reaction resulting in insoluble solids precipitation, which is then followed by physical settling or filtering. Biological processes use micro-organisms like bacteria or algae to remove dissolved organic matter, nitrogen and phosphorus from (waste)water. Physical processes use the laws of physics and constituent properties to purify water, like gravitational settling, centrifugation, granular media filtering and evaporation. The type of treatment chosen depends mainly on the substances which need to be removed. These substances in water can be divided into three main categories:

- soluble matter, like salts and organic acids;
- insoluble matter, like oil and fat, but also particulate matter, like sand, clay and insoluble salts and organics;
- micro-organisms, like bacteria, algae and viruses.

The increasing need for water and material reuse drives the innovation of new technology. One of the new technologies being investigated for water purification and recycling or constituent recovery is ultrasonic particle separation, which

is the subject of the current study. In this technique, mainly known from cell harvesting in biotechnology [9, 20, 31], high frequency ultrasound (MHz range) is used to concentrate suspended particles in water. This technique is especially interesting for harvesting or removal of particles with an almost neutral buoyancy with respect to the surrounding liquid [30].

Other comparable techniques available mainly consist of various types of filters, like depth filters (sand/anthracite), surface filters (cloth) and microfiltration units [63]. The disadvantage of these types of filters is that they always use a medium: the material that causes some particles to pass the filter, while others are retained. This filter usually becomes clogged at some point in time, causing the performance to deteriorate. At that point the filter needs cleaning, usually in the form of a backwash operation: clean water flushes the filter for a short time with a flow opposite to the direction of flow used during the filtering operation. Moreover, filters get polluted by bacterial growth, which is generally a problem in filtration membranes. Thorough cleaning of these conventional filters usually requires additional chemicals to reduce biological growth and scaling. Recovery of valuable (biological) particulate matter with conventional filtering techniques is usually not effective, since the particulate tends to clog the filter and becomes difficult to reclaim. An alternative techniques to recover particulate matter is centrifugation¹, which imposes large shear stress to the particles and usually is not energy efficient.

1.2 Problem formulation

For both water purification and particle recovery, it would be very beneficial if a filter exists, which does not use a filter medium, but which filters on a basis other than a porous structure. Acoustic filtration using ultrasound might be a viable alternative, because it does not show any of the above mentioned disadvantages, simply because there is no filter medium.

1.3 Objective

The objective is to develop an ultrasonic separation device for particle recovery and water purification, which is fit for industrial applications, rather than biotechnology or related medical fields. This change of focus from biotechnology to

¹Hydrocyclones can also be used for particle removal/recovery, but are less effective for near-neutral buoyant particles.

process industry incorporates device scaling, which in turn involves issues related to optimal size, efficient control strategies, separation efficiency and energy demand. Therefore, the research questions imposed are:

- What is the optimal size and configuration for an acoustic separator capable of handling large flows of several cubic meters per hour?
- What separation efficiency can be obtained with this device and how will efficiency be determined?
- What is the minimum power required, given a predefined efficiency and flow rate, to acoustically filter small, near neutral particles ($> 10 \mu\text{m}$, 1100 kg/m^3) from water?
- What control strategy should be used for optimal operation of an industrial scale acoustic separator?

In order to investigate these issues in a consistent and reproducible manner, a combined numerical-experimental approach is proposed. Numerical simulations are continuously cross-checked with experimental findings in a design loop, thus validating the design approach taken. An important advantage of numerical simulations is the speed at which design changes can be evaluated and adapted without the need to construct any of the intermediate products. The main disadvantage of simulations is that there is always a certain extent of uncertainty with respect to the real situation. Nevertheless, simulations also allow robust design, which eliminates the effect of small discrepancies encountered in reality. In this study, system optimisation using a step-wise numerical-experimental approach is applied to improve the performance of ultrasonic separators, contributing to the feasibility of these devices for industrial use. Optimisation of macro-scale ultrasonic separators by this approach has not been reported in literature.

1.4 Thesis outline

The background of acoustic separation and its applications are presented in Chapter 2. The theory is backed up with an experimental and numerical demonstration of the principle in ambient air. The combination of experimental work and numerical simulations was adopted in the analysis and redesign of the separation chamber. The initial design studies focused on modelling and validation of the piezoelectric transducer, the actuator of the system, as outlined in Chapter 3. Secondly modelling and validation of an existing separator chamber (cuvette)

was performed and described in Chapter 4. The basic design principles of a new ultrasonic separator is the subject of Chapter 5, which was then extended to an optimised new design in Chapter 6. The numerically optimised design was built and evaluated as presented in Chapter 7. The entire study concludes with a model-based open loop control strategy and associated efficiency for separator performance control in Chapter 8. Finally, the discussions and conclusions, followed by a synthesis and future perspectives are covered in the last two chapters.

2. ACOUSTIC SEPARATION PRINCIPLE

2.1 Theoretical background

Acoustic separation is based on the principle that acoustic pressure exerts forces on particles with different density / sound propagation properties in a fluid or gas. The technology has been under investigation only during the last two decades, even though the theory for this technique was established already in the first half of the past century. In 1934 King [47] derived an equation to calculate the forces acting on a particle in a one-dimensional, acoustic field. Gor'kov used a different approach to establish similar results, though in an arbitrary acoustic field [27]. An extensive derivation of the acoustic radiation force F^{rad} [N] acting on a particle is given by Bruus [10], based on the work of King and Gor'kov.

In summary, the analysis by Bruus starts with the conservation of fluid mass inside a given volume, resulting in the continuity equation,

$$\frac{\partial \rho}{\partial t} = -\nabla \cdot (\rho \mathbf{v}) \quad (2.1)$$

with ρ the fluid density in [kg/m³], \mathbf{v} the fluid velocity in [m/s] and $\nabla = [\frac{\partial}{\partial x} \frac{\partial}{\partial y} \frac{\partial}{\partial z}]^T$. Equation 2.1 states that the change of density of a small volume of fluid in time is similar to the net mass flow into this same volume. Then the Navier-Stokes equation for fluid flow is derived from the conservation of momentum, giving,

$$\rho \left[\frac{\partial \mathbf{v}}{\partial t} + (\mathbf{v} \cdot \nabla) \mathbf{v} \right] = -\nabla p + \eta \nabla^2 \mathbf{v} + \beta \eta \nabla (\nabla \cdot \mathbf{v}) + \rho \mathbf{g} \quad (2.2)$$

with p the fluid pressure [N/m²], η the dynamic viscosity [Ns/m²], β the viscosity ratio of the compressible fluid [-] and \mathbf{g} the gravity vector. Equation 2.2 states that the sum of the change of momentum in time and the convection is equal to the sum of the negative pressure gradient, viscous terms and external forces (gravity), which is the equation of motion for fluid flow.

Taking these two equations and introducing small, first order perturbations to ρ ($\rho = \rho_0 + \rho_1$) and p ($p = p_0 + c_f^2 \rho_1$, with c_f the speed of sound in the fluid [m/s]) and assuming $\mathbf{v} = \mathbf{v}_0 + \mathbf{v}_1$ with $\mathbf{v}_0 = \mathbf{0}$, while also neglecting external forces, the following expressions are found

$$\frac{\partial \rho_1}{\partial t} = -\rho_0 \nabla \cdot \mathbf{v}_1 \quad (2.3)$$

$$\rho_0 \frac{\partial \mathbf{v}_1}{\partial t} = -c_f^2 \nabla \rho_1 + \eta \nabla^2 \mathbf{v}_1 + \beta \eta \nabla (\nabla \cdot \mathbf{v}_1) \quad (2.4)$$

Taking the time derivative of equation 2.3 and inserting equation 2.4 with $\nabla \cdot \nabla = \nabla^2$, $\nabla \cdot \nabla^2 \mathbf{v}_1 = \nabla^2(\nabla \cdot \mathbf{v}_1)$, because ∇^2 is a scalar operator, and assuming time harmonic signals with angular frequency ω in [rad/s] (with $\omega = 2\pi f$ and $\partial e^{-i\omega t} / \partial t = -i\omega e^{-i\omega t}$) gives

$$\frac{\partial^2 \rho_1}{\partial t^2} = -\nabla \cdot \left(\rho_0 \frac{\partial \mathbf{v}_1}{\partial t} \right) \quad (2.5)$$

$$= -\nabla \cdot \left(-c_f^2 \nabla \rho_1 + \eta \nabla^2 \mathbf{v}_1 + \beta \eta \nabla(\nabla \cdot \mathbf{v}_1) \right) \quad (2.6)$$

$$= c_f^2 \nabla^2 \rho_1 - (1 + \beta) \eta \nabla^2(\nabla \cdot \mathbf{v}_1) \quad (2.7)$$

$$= c_f^2 \left[1 + \frac{(1 + \beta) \eta}{\rho_0 c_f^2} \frac{\partial}{\partial t} \right] \nabla^2 \rho_1 \quad (2.8)$$

$$= c_f^2 \left[1 - i\omega \frac{(1 + \beta) \eta}{\rho_0 c_f^2} \right] \nabla^2 \rho_1 \quad (2.9)$$

The second term at the right-hand side of equation 2.7, which define the damping factor, are quite small (10^{-6}) for waves in water with frequencies above 1 MHz. Neglecting these terms and using $p_1 = c_f^2 \rho_1$ results in the undamped wave equation:

$$\nabla^2 p_1 = \frac{1}{c_f^2} \frac{\partial^2 p_1}{\partial t^2} \quad (2.10)$$

In case of time harmonic signals with $\mathbf{v}_1 = \mathbf{v}(\mathbf{r}) e^{-i\omega t}$, generally true for sound waves, $\rho_0 \frac{\partial \mathbf{v}_1}{\partial t} = -c_f^2 \nabla \rho_1$ results in

$$\mathbf{v}_1 = -i \frac{1}{\rho_0 \omega} \nabla p_1 = \nabla \phi_1, \quad (2.11)$$

$$\phi_1 = \frac{-i}{\rho_0 \omega} p_1 \quad (2.12)$$

in which ϕ_1 in [m²/s] is the acoustic velocity potential, which also fulfils the wave equation, and which is used by Gor'kov to derive the acoustic radiation force.

Bruus extended the analysis to the acoustic radiation force and showed that there exists a secondary acoustic force. This secondary acoustic force is not just harmonic about an equilibrium state, as is the primary acoustic force, but is able to propel the particle in both a travelling and a standing wave field. The assumptions that were applied, are as follows:

- The fluid surrounding the particle is an ideal, compressible fluid;
- The particle is non-deformable, though compressible;
- The size of the particle is much smaller than the wavelength of the ultrasound;
- There is no interaction between particles in the suspension;
- There is no disturbance of the acoustic wave field by the particles themselves;
- The particle scatters the incident sound wave radially.

Bruus (and Gor'kov) defined the acoustic radiation force \mathbf{F}^{rad} as a gradient of the radiation force potential U^{rad} [Nm] as:

$$\mathbf{F}^{rad}(r) := -\nabla U^{rad}(r) \quad (2.13)$$

with r the (x, y, z) position of the particle in the acoustic field.

Gor'kov showed that the acoustic radiation force potential in a one-dimensional acoustic field with space variable x is given by:

$$U^{rad}(x) = -\frac{4\pi a^3}{3} \left[\frac{1}{2} (\kappa_f - \kappa_p) \langle p(x)_{in}^2 \rangle - \frac{3}{4} \rho_f \frac{2(\rho_p - \rho_f)}{2\rho_f + \rho_p} \langle v(x)_{in}^2 \rangle \right] \quad (2.14)$$

with a the particle diameter in [m], κ_p and κ_f the compressibility of the particle and the fluid in [m^2/N], ρ_p and ρ_f the densities of particle and fluid [kg/m^3] and $\langle p_{in}^2 \rangle$ and $\langle v_{in}^2 \rangle$ the time-averaged squared incident pressure [N^2/m^4] and squared velocity [m^2/s^2] of the acoustic wave, respectively.

The fluid pressure and fluid velocity field are given by:

$$p_{in} = p_a \cos(kx) \sin(\omega t) \quad (2.15)$$

and

$$v_{in} = -\frac{p_a}{\rho_f c_f} \sin(kx) \cos(\omega t) \quad (2.16)$$

with p_a the magnitude of the pressure of the acoustic wave [N/m^2], x the axial position in the planar wave field [m] and k the wavenumber in [$1/\text{m}$] and with c_f the speed of sound in the fluid.

Since for the time averages hold: $\langle \cos^2(\omega t) \rangle = \frac{1}{2}$ and $\langle \sin^2(\omega t) \rangle = \frac{1}{2}$ and the compressibility is defined as $\kappa_f = 1/(\rho_f c_f^2)$, the radiation potential of a one-dimensional plane wave follows from equation 2.14 and is given by:

$$U^{rad}(x) = -\pi a^3 k p_a^2 \left[\left(\frac{\kappa_f - \kappa_p}{3\kappa_f} \right) \cos^2(kx) - \frac{1}{2} \rho_f \frac{2(\rho_p - \rho_f)}{2\rho_f + \rho_p} \sin^2(kx) \right] \quad (2.17)$$

Consequently, the one-dimensional radiation force in a plane standing wave becomes

$$\begin{aligned} F^{rad} &:= \frac{\partial U^{rad}}{\partial x} \\ &= \frac{4}{3} \pi k a^3 \Phi(\kappa, \rho) E_{ac} \sin(2kx) \end{aligned} \quad (2.18)$$

with the acoustic energy density E_{ac} in [J/m³] defined by:

$$E_{ac} := \frac{p_a^2}{4\rho_f c_f^2} \quad (2.19)$$

and the acoustic contrast factor $\Phi(\kappa, \rho)$ defined by:

$$\Phi(\kappa, \rho) := \frac{5\rho_s - 2\rho_f}{2\rho_s + \rho_f} - \frac{\kappa_s}{\kappa_f} \quad (2.20)$$

The acoustic energy density E_{ac} can only be estimated from measurements of (either) the acoustic pressure or the particle trajectories and known particle properties. The formulas shown here (2.1 - 2.20) are the basis for the numerical simulations performed throughout this study.

The wavelength of an acoustic wave at 2 MHz is 0.75 mm. Incompressible particles up to approximately 50 μm can therefore be subjected to the radiation force equation without significant errors. The current study aims at separation of particles of about 10 μm with ultrasonic standing waves (USW). In this thesis, the source of the acoustic wave is a piezoelectric transducer, which is modelled in Chapter 3. The transducer is attached to a glass matching layer, which vibrates with the transducer and couples the transducer to the fluid, forming an acoustic separator modelled in Chapter 4.

In the analysis of transducer and resonator, admittance (the inverse of impedance) plays a key role as this system property can be measured by an impedance analyser. In both analyses, the system can be considered as a multi-degree-of-freedom

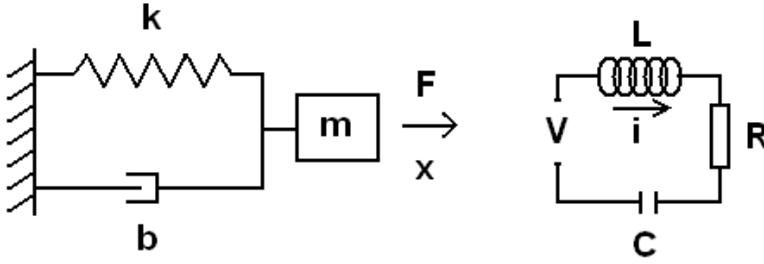


Figure 2.1: Single degree of freedom (SDOF) systems: a mechanical mass-spring-damper system (left) and an electrical inductor-resistor-capacitor system (right).

(MDOF) system. For a 1D single-degree-of-freedom (SDOF) mass-spring-damper or inductor-resistor-capacitor model (Figure 2.1), under the assumption that the system behaviour is linear, the following mathematical analysis can be given.

The differential equation of motion in displacement x of a mass-spring-damper system is written as:

$$m\ddot{x} + b\dot{x} + kx = Fe^{i\omega t} \quad (2.21)$$

with m the system mass in [kg], b the damping factor in [Ns/m], k the stiffness in [N/m] and $Fe^{i\omega t}$ a time harmonic excitation force in [N].

With a time harmonic signal $x = Ae^{i\omega t}$, with A the amplitude of vibration in [m], this becomes

$$(-A\omega^2 m + iA\omega b + Ak)e^{i\omega t} = (-\omega^2 m + i\omega b + k)x = Fe^{i\omega t} \quad (2.22)$$

And the solution in x is:

$$x = \frac{Fe^{i\omega t}}{-\omega^2 m + i\omega b + k} \quad (2.23)$$

$$= \frac{Fe^{i\omega t}}{i\omega(b + i(\omega m - \frac{k}{\omega}))} \quad (2.24)$$

with the first derivative in t :

$$\dot{x} = \frac{Fe^{i\omega t}}{b + i(\omega m - \frac{k}{\omega})} \quad (2.25)$$

The mechanical impedance Z_m of this system is written as

$$Z_m = R_m + iX_m \quad (2.26)$$

with resistance $R_m = b$ and reactance $X_m = (\omega m - k/\omega)$ for a mass-spring-damper system. The undamped eigenfrequency is found when the imaginary part of the impedance is zero: $\omega_0 = \sqrt{k/m}$

For the electrical analogy, an inductor-resistor-capacitor (LRC) system, excited with voltage V , the solution in current I becomes:

$$I = \frac{V e^{i\omega t}}{R + i(\omega L - \frac{1}{\omega C})} \quad (2.27)$$

with R the resistance in [Ω], L the inductance in [henry = Ω s] and C the capacitance in [farad = s/ Ω]. In this case the electrical resistance is $R_e = R$ and the reactance is $X_e = (\omega L - 1/\omega C)$.

In practical MDOF electro-mechanical systems, like piezoelectric transducers and electrically driven acoustic separators, the impedance (or admittance) depends on both the electrical and mechanical (acoustical) properties of the system, as shown in Chapter 3, resulting in a series of eigenfrequencies, which were measured with an impedance analyser.

A state of resonance (vibration at an eigenfrequency) in the separation chamber improves the separation efficiency, because forces resulting from standing waves are much higher than forces from travelling plane waves [30]. Under standing wave conditions, the particles within the fluid are forced to the nodal or antinodal pressure areas of the chamber, depending on the physical properties of both the medium and the particles [30]. A positive contrast factor Φ indicates that the particles will move towards the pressure nodes of the acoustic wave field, whereas a negative contrast factor forces the particles towards the pressure antinodes. These areas can be discrete spots as well as nodal lines or planes [57].

Since Gor'kov assumes an ideal fluid in his derivation, there is no attenuation of the acoustic wave while travelling through the fluid. In reality attenuation leads to several types of acoustic streaming, summarised by Wiklund et al [68]. Generally speaking, a gradient in the time-averaged acoustic momentum flux in the fluid, gives rise to acoustic streaming or, in other words, the attenuation in the fluid causes the acoustic energy to be transformed into kinetic energy of the fluid particles, thus causing acoustic streaming. Practically speaking, the effect of acoustic streaming is that vortices may occur inside the resonance chamber, depending on the acoustic energy flux, the acoustic pressure and the frequency

applied. In case of acoustic separators with a length much larger than the wavelength, typical for the industrial separators in this thesis, Eckart streaming is the dominant factor. This type of streaming causes a reverse fluid flow in areas with a lower acoustic flux. In case of standing waves with as little attenuation as possible, the effects on acoustic streaming will be small, which can be verified by means of experiments.

The acoustic radiation force is not the only influencing factor in acoustic particle filtering. The particles are also subject to drag forces, according to the Stokes equation for viscous fluids:

$$F^{drag} = -6\pi\eta av_p \quad (2.28)$$

with η the dynamic viscosity of the fluid and v_p the velocity of the particle relative to the fluid. Both forces F^{rad} and F^{drag} determine the particle acceleration and velocity in the acoustic wave field, and thus the particle trajectory. The role of gravity and buoyancy in acoustic separation of small, near-buoyant particles is negligible¹. Once the particles start to form flocs due to interacting particle forces, gravity becomes important, causing the agglomerated particle flocs to settle.

In the next sections the state of the art is presented, followed by a demonstration of the separation principle in ambient air.

2.2 State of the art

2.2.1 Physical separators

A physical separator consists of a stack of separate layers, one of which is the fluid layer in which the separation of particles takes place (see figure 2.2). Each layer has its own function and characteristics:

1. The first layer is the transducer, usually a piezoelectric ring or plate, which supplies the energy or vibration to the separator. A single element piezoelectric transducer consists of piezoelectric material with a very thin electrode on both sides. This electrode usually covers the entire area of the piezoelectric material. In fact, the transducer consists of three layers in itself, but the characteristics of the electrodes are not always taken into account, since they are very thin (approximately 10 μm);

¹With a particle diameter of 10 μm and density of 1100 kg/m^3 the steady state particle velocity will be about 5 $\mu\text{m/s}$. The particles will therefore not settle due to gravity.

2. The second layer is the so called matching or coupling layer, which separates the transducer from the liquid, thus preventing direct contact between the two. The matching layer transfers the acoustic waves generated by the transducer to the fluid. The thickness of the matching layer is extremely important for the efficiency of the separator, as will be shown later;
3. The third layer is the resonance chamber with (flowing) fluid in which separation of fluid and particles takes place. The acoustic waves result in acoustic radiation forces on the particles, thus causing them to concentrate at the pressure (anti-)nodes in the chamber. The particles can be forced to a separate (second) outlet of the chamber (see for instance Hawkes et al. [34] and Townsend et al. [65]) or can be held inside the chamber until saturation takes place, which is then followed by a (back) flush to remove the concentrate;
4. The fourth layer is the reflector, which reflects the acoustic waves back into the resonant chamber, thus causing standing waves (resonance) in the chamber. Usually this layer is the last and it radiates into the surrounding air (sometimes air is referred to as the backing layer). In the case of larger separation devices, the reflector can be replaced by another matching layer and a second transducer.

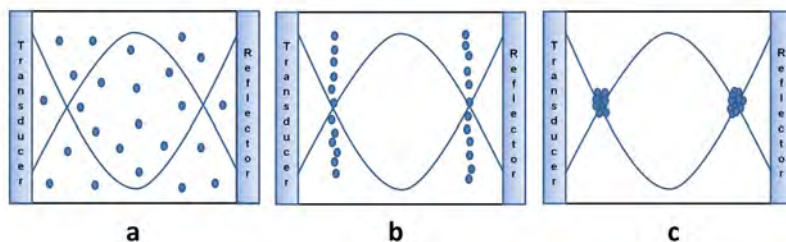


Figure 2.2: Sketch of ultrasonic particle trapping using standing waves. The transducer (left) and the reflector (right) build the standing wave field (with two nodes) in the intermediate fluid layer. Particles are first scattered (a), immediately line up (b) and agglomerate (c) in the nodes.

2.2.2 1D models and designs

The fundamentals of acoustic separators in the one-dimensional case were summarised by Gröschl [30, 23] based on a large amount of earlier studies by others,

Table 2.1: *Studies on ultrasonic standing wave separation units and particle manipulators, highlighting the mainstream of the modelled and evaluated systems.*

Study	Year	Scale	Model / Experiment	Result	Evaluation [Yes / No]
Aboobaker et al. [3]	2005	mm	1D/exp.	particle trajectory	Y
Andrade et al. [5]	2010	cm	2D/exp.	particle trajectory	Y
Bekker et al. [7]	1997	cm	exp.	36 kHz separator	N
Benes et al. [8]	2001	cm	1D/exp.	multiple wavelength separator	Y
Dain et al. [19]	1995	mm	2D	particle trajectory	N
Gorenflo et al. [26]	2002	cm	exp.	separation efficiency	N
Haake and Dual [32]	2004	mm	3D	particle manipulator	Y
Hawkes and Coakley [35]	2001	mm	2D/exp.	particle concentrator	Y
Hawkes et al. [33]	2002	cm	1D/exp.	half-wavelength separator	Y
Hill et al. [36, 37]	2002 2008	sub-mm	1D/exp.	particle manipulator	Y
Kapishnikov et al. [43]	2006	sub-mm	2D	particle sorting	Y
Neild et al. [57, 56]	2006 2007	sub-mm	2D	particle manipulator	Y
Nowotny and Benes [58, 59]	1987 1991	-	1D	theory	N
Townsend et al. [65]	2004	sub-mm	2D/exp.	particle trajectories	Y
Townsend et al. [64]	2008	sub-mm	1D/exp.	quarter-wavelength separator	Y

including Gor'kov. In part I of this review it is explained how to calculate forces on particles in a known acoustic field and what secondary forces exist in the acoustic separator, which should be taken into account. The review also shows how to account for attenuation (damping) and how electro-mechanical parameters of a piezoelectric transducer can be taken into account. An important issue in this study is that performance numbers are defined, based on the energy used to separate particles in comparison to energy losses, in order to compare the efficiency of acoustic resonators. In part II of his study, he shows how to design a physical ultrasonic separator with the best dimensions of different layers, the piezoelectric transducer and the frequency control unit of the amplifier. In this part it is not entirely clear whether the device made was truly tested and whether improvements were possible. Despite the fact that this review is only applicable to a 1D case, it has been used extensively for the design of ultrasonic separation devices. Various studies in which 1D, 2D and 3D models were applied are summarised in Table 2.1.

One-dimensional matrix models - describing mechanical and electrical displacement in relation to stress and electric potential - in multi-layered systems (see Figure 2.2), were developed by Nowotny and Benes [58, 59]. These models included a model of the piezoelectric transducer and all layers in an acoustic

resonator. Such matrix models were also applied by Benes et al. [8] for multiple wavelength separators and by Hawkes et al. [33] for modeling of half-wavelength resonators. Both of these were also experimentally evaluated. Moreover, a series of studies of Hill and co-authors [36, 37, 64] were dedicated to 1D modelling of the layered structure of the resonator, studying the effects of frequency, layer thickness and modelling detail. On the basis of this modelling study it was shown that the optimal frequency of operation of a separator was not automatically at the design frequency, due to interactions of the modes of each layer. The frequency at which maximum separation efficiency occurs, corresponded to the frequency of maximum acoustic energy in the fluid layer, but did not correspond to the main eigenfrequency (peak admittance) of the multi-layer resonator system. Benes [8] and Hawkes [33] found similar results. Later studies have extended this work to include fluid flow and resistant (drag) forces to thus predict particle paths inside the fluid layer [65].

Particle trajectories were calculated analytically and evaluated experimentally by Aboobaker et al. [3] for a one-dimensional trajectory in a standing wave field and by Andrade et al. [5] for progressive waves. Aboobaker also extended the analytical model to a particle concentration simulation, which was not evaluated. Townsend et al. [65] modelled the particle path of yeast cells ($3\ \mu\text{m}$) exposed to ultrasonic standing waves inside the fluid flow of a half-wavelength separator. Good agreement was found between simulated particle concentration and experimental values at various frequencies.

2.2.3 2D models and designs

One of the most detailed studies on the design of a 2D separator and its performance was documented by Hawkes and Coakley [35]. A half wavelength concentrator was made of stainless steel with 0.25 mm wide channels. The forces on the particles and thus the direction of concentration was perpendicular to the fluid flow. It was shown that this system, although designed for 3 MHz, performs better at 3.1 MHz. The reason for this phenomenon, as demonstrated by Hill [36], is that a system with two (or more) coincident resonances creates separate peaks near the assumed resonance and anti-resonance at the frequency where resonance would be expected. Therefore, the optimal frequency of operation is not at the assumed resonance but somewhat higher or lower. Precise dimensions and specifications of Hawkes and Coakley's device and measurement system are specified in the publication. In the experiments a more than 1000-fold clearance was achieved using $5\ \mu\text{m}$ yeast cells and a flow rate of 6 ml/min. Moreover, it was shown that theoretical clearance is close to the experimental clearance when sim-

ply using first order effects (primary particle forces) and low excitation voltages. It was suggested that more detail in both the experimental setup and the theoretical approach, like particle momentum and particles size dependent viscous correction, would make the model more suitable to be applied at higher voltages (and corresponding higher acoustic particle forces). An important note in the study is that cavitation (air bubble implosion) by low US frequencies should be avoided in order to obtain a laminar undisturbed flow.

Dain et al. [19] performed a 2D analytical study on particle movement using a parameter perturbation method. As model input an oscillating wall (acoustic source) was applied and a convex reflector, which forced the particles towards specific spots in the acoustic field. The analysis was purely mathematical and not validated with any experiment.

Kapishnikov et al. [43] used a numerical model to predict the particle trajectory of particles (2.5, 5 and 10 μm) and blood cells in microchannel flows (half and quarter wavelength) and demonstrated the possibility to sort various particle sizes by means of USW with an efficiency near 100% for a concentration of 1% and a flow rate of 162 nl/s. The approach was similar to the experimental analysis with 3 and 8 μm particles in Laurell et al. [50].

Lipkens et al. [54] calculated the particle trajectories through a straight channel, which is interrupted by an acoustic chamber in which the particles were exposed to standing waves and waves with stepped frequency sweeps. In the theoretical model it was found that particles could be swept from the central main stream into the quiescent area of the chamber. This method was evaluated in a subsequent study [55] and proved to be able to separate 6 μm polystyrene beads from a 150 ml/min water flow at a speed of around 5 mm/s. Clearances or efficiencies of the process were not specified.

2D model simulations using a Finite Element (FE) approach, were performed by Neild et al. [57, 56], using a partly cut piezoelectric transducer to generate surface waves beneath a fluid layer. The surface waves typically created nodal lines at which particles were concentrated. It was shown that FE modelling is necessary to find all the resonance modes of a separator/concentrator system, since the analytical 1D approach does not identify all possible resonance frequencies. The location of the concentrated particles could be predicted numerically and these locations were verified experimentally.

2.2.4 3D models and designs

Haake and Dual [32] have used a 3D approach to both model and design a particle manipulator. The aim was to concentrate particles at specified locations using a vibrating plate, excited by a piezoelectric element. Haake and Dual used a glass plate connected to a piezoelectric transducer, which was excited in shear mode. Their analytical 3D approach of this separator was used to predict the positions of particle concentration. Their results were verified with experiments and show the strength of this relatively simple approach.

Lilliehorn et al. [53] developed a micro-electromechanical system (MEMS). This device was specifically meant for 3D microparticle manipulation, similar to the approach in [32] and [57]. The device operated at frequencies from 2.4 up to 12.5 MHz and at a maximum flow rate of 1 mm/s. Good agreement was said to be found between the numerical and experimental approach, although the evaluation was only made on a visual basis. The studies demonstrate that it is possible to trap particles at specific, predefined locations in the 3D field of the particle concentrator. An angular spectrum approach (ASA) was applied to calculate the near field pressure of an acoustical particle trap. The approach was not further explained and little evidence was presented on the validity of this ASA method in this application.

2.2.5 Applications and new concepts

Bosma et al. [9] took an existing, commercially available separator, the BioSep (Applikon B.V., Schiedam, the Netherlands), and tested this device for harvesting (micro)algae and found the method not to be feasible for this application. This conclusion is related to the device tested, but seemed to be extrapolated to the entire method of ultrasonic separation as such. If the device were dedicated to the harvesting of microalgae, it might well be feasible, yet no device as such existed at that moment.

Bekker et al. [7] used a 36 kHz transducer to separate talcum powder (with unspecified properties) from water in a 120 mm long, 20 mm wide tube by directing the flow perpendicular to the transducer surface. The maximum efficiency was 65% at a flow rate of 2.5 ml/s. It was suggested to further optimise the separator used, especially towards smaller particle sizes to treat cooling tower blowdown water.

Gorenflo et al. [26] tested the efficiency of a BioSep 200L acoustic cell retention system using CHO (Chinese Hamster Ovary) cells (15 μ m) at various flow rates

(50-400 l/day) and power levels (60-90 W). Efficiencies varying from 57% at 400 l/day up to 96% at 50 l/day were found using 60 W of input power. When varying the input power from 60 W up to 90 W the efficiency increased from 78% to 82%. Therefore, acoustic separator performance seems more dependent on flow rate than on input power.

Gröschl et al. [31] evaluated the separation efficiency of a prototype cell harvesting separator at various flow rates (24-60 l/day) and input powers (14-58 W) using hybridoma cells. The efficiency varied between 60% (60 l/day @ 24 W) and near 100% (24 l/day @ 52 W), comparable to the results found in [26]. According to the figures presented in this study, the separation efficiency seemed to increase linearly with power (below 95% efficiency) and was more profound as the flow rate increased (0.3%/W @ 36 l/day up to 1.1%/W @ 60 l/day). Above 95% efficiency the relation was no longer linear. The separation efficiency decreased non-linearly with flow rate i.e. the higher the flow rate, the higher the decline in efficiency (estimated at 5% up to 15% decline per 12 l/day).

A most interesting study was performed by Ahrens and Patterson [4], investigating the use of ultrasound for improving the sedimentation process of a paper mill for whitewater clarification. The conventional technique used a Dissolved Air Flotation (DAF) unit. The evaluated ultrasound technique showed that investment costs were reduced by 50%, operational costs by 33% and estimated energy costs by 46%. These estimates were based on a pilot unit which processed 40 l/min and were extrapolated to a 7500 l/min full scale unit.

Whitworth et al. [67] used modulated ultrasound to transport 9 μm polystyrene particles along a central axis of a cylindrical container. Two piezoelectric transducers were fixed at both ends of the container and excited with slightly different frequencies. The particles formed clumps and these could be transported along the axis at a maximum velocity of 24 mm/s with a frequency difference of 100 Hz (main frequency 3 MHz). Other methods, like ramping the frequency, pulsed/burst sound (2.5 s) followed by sedimentation (2.5 s) and sedimentation, after switching the sound off completely, all resulted in less clearance of the suspension than applying the frequency difference.

Glynne-Jones et al. [24] investigated the concept of parallel particle separation with multiple channels in a brass plate, excited with a single piezoelectric device. The idea was that the piezoelectric device would create resonances in the channel walls, which had a perfectly rectangular cross section. If the channel walls vibrated with a given eigenfrequency (natural mode), thus creating standing waves in the channel, it should be possible to create parallel particle filters with a single transducer. Unfortunately, the vibration of the plate with the channels was dom-

inated by Lamb (surface) waves, so that resonances in each of the channels were not as expected. Further study was recommended to solve this problem.

The most recent studies on ultrasonic standing wave applications focus on particle manipulation and positioning, thus improving sensing and characterisation capabilities. Most of these studies integrate numerical design and experimental validation or evaluation for system development. Courtney et al. [18] proposed a method of positioning particles in a standing wave field by means of phase controlled sinusoidal signals. They found that it is possible to translate $5\ \mu\text{m}$ particles across several wavelengths within the separator. Earlier work by Glynne-Jones [25] used mode-switching to position particles in specific locations or bands inside a resonance chamber by switching between subsequent eigenfrequencies, thus moving the nodal positions in small steps. This method was used to line up 10 and $20\ \mu\text{m}$ particles in any location inside a quarter wavelength separator within a flow. Dron et al. [21] aimed to improve Particle Image Velocimetry (PIV) measurements by acoustic focusing of particles. They investigated the influence of particle concentration, particle diameter ($2\text{-}7\ \mu\text{m}$) and acoustic pressure amplitude (excitation voltage $3\text{-}10\ \text{V}$) on the focusing time of particles in a standing wave field, without and with fluid flow. Also the effect of acoustic streaming was taken into account. Grinenko et al. [29] constructed an entire ring of piezoelectric transducers, each of which could be controlled separately. The system was able to move the particle in almost any desired position within this ring.

The current study will focus on macro-scale, industrial applications of ultrasonic standing waves. The development of macro-scale devices was not continued after the work of Bekker [7] and the introduction of BioSep more than a decade ago [26, 66].

2.3 Demonstrator

2.3.1 Materials and methods

In this study, the separation principle was demonstrated using large polystyrene particles in ambient air (typically $20^\circ\ \text{C}$., pressure $1030\ \text{mbar}$ and relative humidity $35\ \%$). The separation unit consisted of four low budget $50\ \text{W}$ piezo tweeters (Conrad TE-300, range $5\text{-}40\ \text{kHz}$), a signal generator (Velleman PCGU 1000) and a car audio amplifier (Raveland XCA 1200) with a $12\ \text{V}$, $3\ \text{A}$ DC power supply. The horns of the tweeters were removed and each remaining speaker unit was mounted on a perspex (PMMA) stand allowing it to radiate in a horizontal

plane. Each speaker was connected to each of four amplifier outputs: two opposite speakers to the "front" output and the two others to the "rear" output. The four mounts with tweeters were set up perpendicularly to create a resonance field in between them (Figure 2.3). Hence, the setup basically consists of a signal generator, an audio amplifier and four audio tweeters.

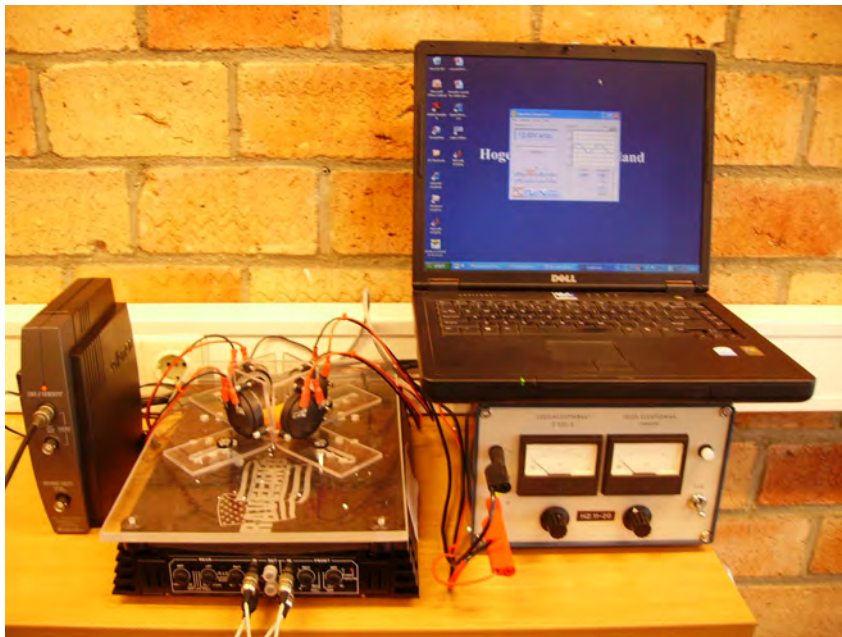


Figure 2.3: Experimental setup of an acoustic separator in air. Four piezo tweeters were mounted perpendicularly on a transparent base plate and driven by an amplified sinusoidal signal creating a resonance field.

Polystyrene particles of various sizes (0.5-3 mm) were randomly placed in the resonance area on a slightly elevated piece of cardboard in order to have them centred in the horizontal plane of the resonance field. On the cardboard a metric mm scale was drawn aimed at observing the process more accurately. The rectangular area between the speakers, being about 5×7 cm, was captured using a home video Sony HC30 PAL digital camera.

2.3.2 Results

On the basis of wave theory one would expect a range of eigenfrequencies occurring in the given experimental setup. However, only one resonance frequency was found by trial and error, being 12.6 kHz. There were slight indications of

another eigenfrequency at 22 kHz, but results were not consistent. Most likely, the piezoelectric speakers were not able to generate enough acoustic power at other eigenfrequencies in both the lower and higher frequency range of its specifications. At the resonance frequency of 12.6 kHz the particles were consistently separated in three bands (Figure 2.4), which are assumed to be the nodal bands of the resonance area. The separation took place in less than three video frames of 0.04 s (50 Hz interlaced = 25 fps) each, thus hardly visible to a regular camera. The three bands shown indicated that the resonance field was asymmetrical: the center was a nodal line, instead of an anti-node. Hence two opposite speakers were driven out of phase by a full 180 degrees. Switching off the two nearest speakers resulted in a similar particle division, which indicates that the effect of the nearest speakers was not as large as the effect of the other two. Note also that in the right panel of Figure 2.4 the nodal bands are not straight but slightly curved about the centre of the resonance field. Even the central streak was not perfectly straight.

The experimental results were subsequently used to calculate the acoustic pressure in the wave field as well as the radiation force acting on the particles. The motion of the particle is governed by two forces: the acoustic force and the drag force. The latter is composed of friction with the surface and the surrounding air. For the subsequent analysis it was assumed that the drag force was linearly related to the particle velocity. Moreover, the experiments showed that there was no overshoot in the particle displacement, so that the displacement was (over)critically damped. Thus, the unknown drag force should be as large as to allow a non-oscillatory movement of the particle to its final location. The acceleration $a(t)$, the velocity $v(t)$ and the position $x(t)$ of the particle were thus described by

$$a(t) = \frac{F^{rad}(x) + F^{drag}(v)}{m_p} \quad (2.29)$$

$$\frac{dv}{dt} = a(t)$$

$$\frac{dx}{dt} = v(t)$$

with appropriate initial conditions and where F^{drag} is the velocity dependent drag force, F^{rad} the location dependent acoustic radiation force and m_p the mass of the particle.

The trajectory was calculated iteratively, as the force field changes with the position of the particle, with a time step of 10^{-5} seconds. The calculated particle

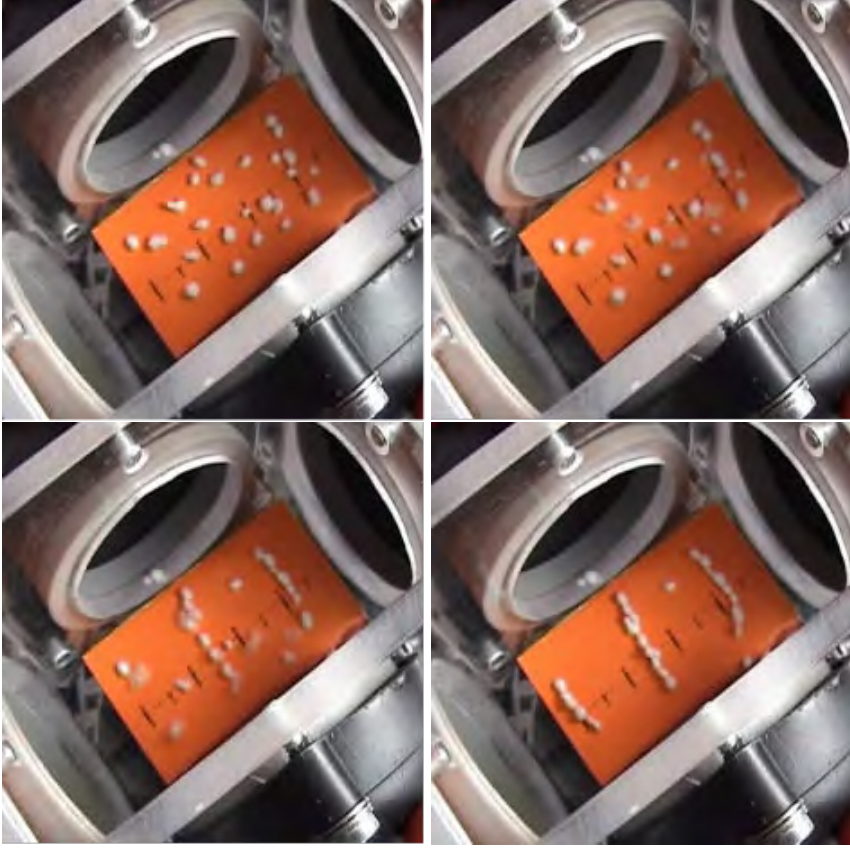


Figure 2.4: Sequence of four snapshots of the process of particle concentration. The first photo shows the initial situation with randomly placed particles, the second and third show the process of separation and the last photo shows the final position of the particles after approximately 0.12s.

displacement versus time using various starting positions is given in Figure 2.5. Given the node to node distance of 0.013 m and a total time of 0.12 s, in which the particles were moving, shows that the maximum particle acceleration is approximately 5 m/s^2 . For a particle mass of $3.4 \times 10^{-6} \text{ kg}$, the maximum force on the particle using Newtons second law results in a force of $1.6 \times 10^{-5} \text{ N}$. The maximum (primary) acoustic force F_{max}^{rad} is given by

$$F_{max}^{rad} = \frac{p_{max}^2 V_p \kappa_a \pi}{2\lambda} \left[\frac{5\rho_p - 2\rho_a}{2\rho_p + \rho_a} - \frac{\kappa_p}{\kappa_a} \right] \quad (2.30)$$

with V_p the particle volume in $[\text{m}^3]$, subscript p for the particle and a for air.

Given the maximum force calculated, from equation 2.30 the maximum pressure p_{max} was calculated to be 7×10^2 Pa and the corresponding p_{rms} is then 5×10^2 Pa. Comparing this result to a regular decibel sound level scale L_p being

$$L_p = 10 \times 10 \log \frac{p_{rms}^2}{p_{ref}^2} = 20 \times 10 \log \frac{p_{rms}}{p_{ref}} \quad (2.31)$$

the acoustic pressure level had a maximum L_p of 148 dB in the standing wave field between the speakers (reference acoustic pressure p_{ref} is 20×10^{-6} Pa). This value of L_p seems a good approximate, since the amplifier was set to full power with a maximum input voltage of 10 V. Note, however, that the calculated pressure was highly dependent on the estimated time of movement, which in this case was rather inaccurate. All input and output parameters are summarised in Table 2.2.

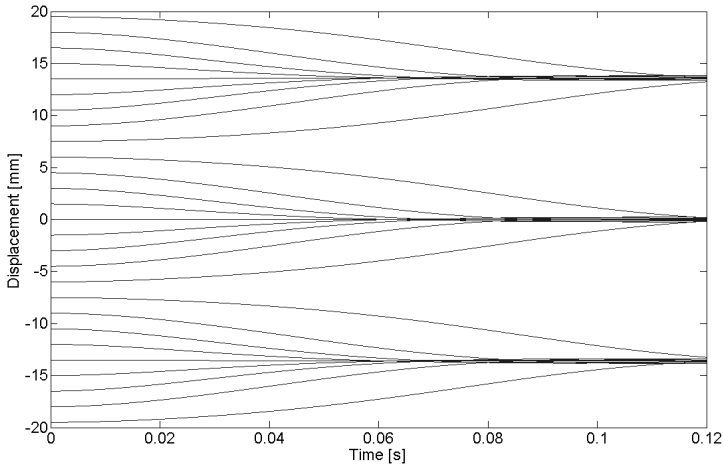


Figure 2.5: Particle displacement versus time in the acoustic pressure field. The value on the y-axis at time 0 represents the initial position of the particle. Particles are driven to three locations in 0.12s.

A consolidated explanation of the principles of acoustic separation was given in this chapter and demonstrated on polystyrene particles in air using four simple piezoelectric speakers and an audio amplifier. Although various eigenfrequencies and nodal lines were expected, only one eigenmode could be determined, a limitation mainly attributed to the frequency response of the speakers used. Basic

Table 2.2: Input and output parameters with corresponding values

Input parameters	Value
Particle material	polystyrene
Density [kg/m ³]	100
Bulk Modulus [Pa]	15×10 ⁶
Particle radius [m]	2×10 ⁻³
Medium	air
Density [kg/m ³]	1.2
Speed of sound [m/s]	343
Eigenfrequency [Hz]	12.6×10 ³
Wavelength [m]	2.7×10 ⁻²
Output parameter	Value
Particle acceleration [m/s ²]	5
Acoustic force [N]	1.6×10 ⁻⁵
Acoustic Pressure [Pa]	7×10 ²
Sound pressure level (SPL) [dB]	148

analytical calculations gave more insight into the pressures and accelerations associated with this demonstrator separation process, providing a comprehensible basis for continuation of the study with water and suspended particles.

3. MODEL OF THE PIEZOELECTRIC TRANSDUCER

Abstract

Design of ultrasonic equipment is more frequently facilitated with numerical models. These numerical models, however, need a calibration step, as usually not all characteristics of the materials used are known. Characterisation of material properties combined with numerical simulations and experimental data can be used to acquire valid estimates of the material parameters. In our design application, a finite element (FE) model of an ultrasonic particle separator, driven by an ultrasonic transducer in thickness mode, is required. A limited set of material parameters for the piezoelectric transducer were obtained from the manufacturer, thus preserving prior physical knowledge to a large extent. The remaining unknown parameters were estimated from impedance analysis with a simple experimental setup combined with a numerical optimisation routine using 2D and 3D FE models. Thus, a full set of physically interpretable material parameters was obtained for our specific purpose. The approach provides adequate accuracy of the estimates of the material parameters, near 1%. These parameter estimates will subsequently be applied in future design simulations, without the need to go through an entire series of characterisation experiments. Finally, a sensitivity study showed that small variations of 1% in the main parameters caused changes near 1% in the eigenfrequency, but changes up to 7% in the admittance peak, thus influencing the efficiency of the system. Temperature will already cause these small variations in response, thus requiring a frequency control unit when actually manufacturing an efficient ultrasonic separation system.

This chapter was published as
H. Cappon and K.J. Keesman (2012) Numerical modelling of piezoelectric transducers using physical parameters. IEEE transactions on Ultrasonics, Ferroelectrics and Frequency Control, Vol. 59, No 5, pp 1023-1032

3.1 Introduction

Currently available acoustic separators use piezoelectric transducers to generate the acoustic field needed for the separation process. In order to gain insight into the characteristics of the transducer and the effect of design parameters on the separation efficiency, a numerical model of the transducer is needed before modelling the entire separator. Confidence in the transducer model can be gained by calibration against experimental results and validation against prior physical knowledge (see [44] for details on model calibration and validation).

The separator model needs to provide acoustic pressure profiles in order to predict acoustic forces on the particles and resulting particle trajectories during the separation process. The pressure profile, which is assumed to change in two dimensions only, can be obtained from a 2D finite element (FE) model. Thus, the piezo transducer model needed is also a (2D) finite element model. Therefore, the aim is to obtain a valid finite element model of the piezoceramic with a realistic frequency response at the first thickness mode for the design of a new acoustic separator and with physically interpretable parameters. Because the model needs to be extended to a separator model at a later stage, the current model was made using Comsol as a generic FE solver instead of using dedicated piezoceramic modelling software. Seven known characteristics, out of a total of eleven parameters, were derived from manufacturer's specifications, one was directly derived from the experimental data, and the remaining three were estimated with numerical optimisation in the frequency band of interest (near 2 MHz). Secondly, a numerical sensitivity analysis of the material parameters on the frequency response indicated that there is a need for control of the driving frequency in a separation unit to maintain maximum efficiency. The measured admittance of the piezoceramic is used as the basis for the calibration process and the sensitivity analysis.

3.2 Background

The most important characteristic of piezoelectric material is the capability to convert an electrical potential to mechanical displacement and vice versa. The electro-mechanical conversion is done with high efficiency, thus explaining the application of piezoceramics as sensors and actuators. Moreover, the ability to mechanically drive systems at high frequencies (up to MHz range) explains its wide use as transducers in, for instance, medical monitoring equipment.

A piezoelectric transducer consists of a piezoelectric ceramic material, often

Lead-Zirconate-Titanate (PZT), between two electrodes of just a few microns thick, generally made of silver or gold. The piezoceramic can be cut in any arbitrary shape, but rectangular and circular plates are commonly used. The piezoceramic material has a predefined orientation allowing the device to operate in thickness mode or in shear/radial mode. In thickness mode the direction of the electrical current is parallel to the mechanical motion, in case of shear operation these directions are perpendicular. For ultrasonic acoustic resonators the thickness mode is mainly applied; the piezoceramic material used is of crystal class 6-mm.

The frequency which induces the largest vibration amplitude is the first eigenfrequency (in thickness mode) and the characteristic vibration pattern at this frequency is called an eigenmode. Therefore, the thickness of the piezoceramic is tuned to offer the best electro-mechanical energy transfer possible. The eigenfrequencies associated with the eigenmodes can be found by measuring the response of the piezoceramic to frequency sweeps: the voltage across and the electrical current through the piezoceramic are measured during the sweep. Such a response measurement is typically done with an impedance analyzer. Eigenfrequencies occur when the measured impedance, defined as $Z = \frac{V}{I}$ is minimal, or more precisely when the real part of the (complex) impedance is minimal. In practise, it is easier to find the maximum of the inverted impedance, which is the admittance $Y = \frac{I}{V}$. Due to dissipation in the piezoceramic, I and V are not in phase, which can be described by using complex variables, so that the real part of the admittance is a measure for the energy transfer from electrical current to mechanical displacement and the maximum real admittance corresponds to an eigenfrequency.

With more demanding and precise applications, like positioning devices in Micro Electro-Mechanical Systems (MEMS), also the use and application of numerical models has become widespread in transducer analysis. In cases where the mechanical displacement (velocity / acceleration) or even the mode shape of the piezoceramic is important, calibration measurements include laser-Doppler interferometry, thus characterising the shape, frequency and magnitude of displacement across the piezo surface or its edges. A difficult task in this calibration process is accurate control of the boundary conditions, because small errors will distort the measurement of the micrometer scale perturbations [52].

The alternative method for calibration is electrical, using an impedance analyser. Boundary conditions can be controlled relatively easy, because the measurement procedure is more robust. By manufacturing various predefined transducer shapes the main material parameters of a piezoelectric material can be determined following a standard procedure, like the ANSI/IEEE standard [1]. This standard,

however, was recently withdrawn, because its 1D mono-modal characterisation was lengthy, incomplete for today's 3D multi-modal demands and applications, and the specimens needed were expensive and difficult to handle [40, 48]. Practical limitations and errors in characterisation with this standard were investigated by Ebenezer and Sujatha [22]. A similar type of standard EN50324 [2] is still in use.

New methods for piezoelectric characterisation have been proposed and applied successfully by various researchers using a combination of impedance measurements and Finite Element simulations [39, 42, 48, 49, 61, 69]. The main advantage of this technique is that any transducer shape can be modelled and analysed. Unfortunately, the characterisation was not fully satisfactory in many cases, due to non-linearities at low and high frequencies [42], the inability to use the characteristics in practise without any modifications [69], physical interpretation of complex (damping) parameters [48] and large deviations from manufacturer's specifications [49]. Nevertheless, the combination of experimental and numerical techniques currently seems the best alternative to sequential one-dimensional characterisations. For this reason, this method is also applied in the current research.

The characterisation done here is limited to the area of interest, namely the first thickness mode of the piezoceramic near 2 MHz, needed to drive an ultrasonic separator. This means that transversal modes and non-linear behaviour at lower frequencies are not of interest; they have been calculated and results are shown, but the response is less important for practical use. The main difference with previous research is firstly that the piezoceramic plate does not necessarily have a shape specified by earlier standards, thus creating a more generic and practical approach and secondly that seven out of eleven material parameters specified by the manufacturer were implemented in the FE code directly and left unmodified. One parameter, the attenuation, was derived from experiments and the remaining three parameters, not specified beforehand and thus unknown, were optimised to match the experimental data. This approach thus avoids, to a large extent, the well-known problems in numerical optimisation, that is the existence of local minima and the computational costs for estimation problems with more than 5–7 parameters.

3.2.1 Piezo modelling basics

The main characteristic of piezoceramic materials is the ability to convert electrical potential or voltage, denoted by V_e , to 3D mechanical displacement \mathbf{u} and vice versa. In order to construct proper models for piezoceramic materials, the

basic constitutive equations which relate electric potential to displacement and displacement to electric potential should be known.

In material mechanics the basic quantities used in the constitutive equations are:

- Stress, denoted by \mathbf{T} with the unit $[\text{N/m}^2]$,
- Strain or relative elongation, denoted by \mathbf{S} which is dimensionless.

For piezoelectric materials these are expanded with

- Electric field intensity, denoted by \mathbf{E} with the unit $[\text{V/m}]$,
- Electrical displacement, denoted by \mathbf{D} with the unit $[\text{N/Vm}]$.

Strain can be expressed in terms of the three-dimensional displacement \mathbf{u} as [48]:

$$\mathbf{S} = \beta \mathbf{u} \quad (3.1)$$

with the first-order differential operator β defined as:

$$\beta = \begin{bmatrix} \frac{\partial}{\partial x} & 0 & 0 \\ 0 & \frac{\partial}{\partial y} & 0 \\ 0 & 0 & \frac{\partial}{\partial z} \\ \frac{\partial}{\partial y} & \frac{\partial}{\partial x} & 0 \\ 0 & \frac{\partial}{\partial z} & \frac{\partial}{\partial y} \\ \frac{\partial}{\partial z} & 0 & \frac{\partial}{\partial x} \end{bmatrix}. \quad (3.2)$$

The electric field intensity in turn can be expressed by the gradient of the electric potential V_e as

$$\mathbf{E} = -\nabla V_e. \quad (3.3)$$

In the description of linear piezoceramic material behaviour the following *stress-charge* relations apply, given in matrix notation as,

$$\mathbf{T} = \mathbf{c}_E \mathbf{S} - \mathbf{e}^T \mathbf{E} \quad (3.4)$$

and

$$\mathbf{D} = \mathbf{e} \mathbf{S} + \epsilon_S \mathbf{E} \quad (3.5)$$

with c_E the stiffness matrix (6 by 6) at constant electric field, e the dielectric constants matrix (3 by 6) and ϵ_S the permittivity matrix (3 by 3) at constant mechanical strain.

In this paper the *strain-charge* relation is used instead [17], because the material parameters of the manufacturer were specified as such. The *strain-charge* relation is given by

$$S = s_E T + d^T E \quad (3.6)$$

and

$$D = dT + \epsilon_T E \quad (3.7)$$

with s_E the compliance matrix (6 by 6) at constant electric field, d the piezoelectric coupling matrix (3 by 6) and ϵ_T the permittivity matrix (3 by 3) at constant mechanical stress.

Devices used as piezoelectric transducers are usually of the 6-mm crystal class, which implies that there are ten governing parameters (matrix elements) in the constitutive relations and the other matrix elements are covered by symmetry or zeros. Five parameters, s_{11} , s_{12} , s_{13} , s_{33} and s_{44} , are located in the compliance matrix [48]

$$s_E = \begin{bmatrix} s_{11} & s_{12} & s_{13} & 0 & 0 & 0 \\ s_{12} & s_{11} & s_{13} & 0 & 0 & 0 \\ s_{13} & s_{13} & s_{33} & 0 & 0 & 0 \\ 0 & 0 & 0 & s_{44} & 0 & 0 \\ 0 & 0 & 0 & 0 & s_{44} & 0 \\ 0 & 0 & 0 & 0 & 0 & 2(s_{11} - s_{12}) \end{bmatrix} \quad (3.8)$$

three parameters, d_{13} , d_{15} and d_{33} , in the coupling matrix

$$d = \begin{bmatrix} 0 & 0 & 0 & 0 & d_{15} & 0 \\ 0 & 0 & 0 & d_{15} & 0 & 0 \\ d_{13} & d_{13} & d_{33} & 0 & 0 & 0 \end{bmatrix} \quad (3.9)$$

and two, ϵ_{11} and ϵ_{33} , in the permittivity matrix

$$\epsilon_T = \begin{bmatrix} \epsilon_{11} & 0 & 0 \\ 0 & \epsilon_{11} & 0 \\ 0 & 0 & \epsilon_{33} \end{bmatrix}. \quad (3.10)$$

In our case seven parameters were known from the manufacturer's specifications and the three remaining needed to be estimated.

Finally the free, undamped mechanical behaviour of this system is described by Newton's second law:

$$\beta^T \mathbf{T} = \rho \frac{\partial^2 \mathbf{u}}{\partial t^2} \quad (3.11)$$

with ρ the density of the piezoceramic material, and by

$$\nabla \cdot \mathbf{D} = q_e \quad (3.12)$$

with q_e the surface charge, which means that the piezoceramic contains only free surface charges on the electrodes, because the piezoceramic itself is an insulator [41]. Damping can be introduced by a mechanical loss factor η_m added to the stiffness matrix as $\bar{c}_{Eij} = c_{Eij} + i\eta_m$ for each of the non-zero elements ij of \mathbf{c}_E .

With the given equations the dynamics inside the piezoceramic can be described with a set of four partial differential equations, three for displacement vector \mathbf{u} and one for potential V_e

$$\rho \frac{\partial^2 \mathbf{u}}{\partial t^2} - \beta^T (\mathbf{c}_E \beta \mathbf{u} + \mathbf{e}^T \nabla V_e) = 0 \quad (3.13)$$

$$\nabla \cdot (\mathbf{e} \beta \mathbf{u} - \epsilon_S \nabla V_e) = q_e \quad (3.14)$$

with $\mathbf{c}_E = \mathbf{s}_E^{-1}$, $\mathbf{e} = \mathbf{d} \mathbf{s}_E^{-1}$ and $\epsilon_S = \epsilon_T - \mathbf{d} \mathbf{s}_E^{-1}$.

3.2.2 Boundary conditions

In order to solve the set of partial differential equations on a 2D-domain, four boundary conditions are needed. Let us, for instance, consider a rectangular piece of piezoceramic material with two electrodes, which is subjected to an electric AC potential with varying frequency $V_e = V_0(\omega)$ on the upper electrode. The lower electrode is grounded. Consequently, this case may be considered as a quasi-static one: the frequency varies, but the vibration of the transducer is in steady state. In such a case, the following boundary conditions apply:

- On the lower boundary (electrode): $V_e = 0$;
- On the upper boundary (electrode): $V_e = V_0(\omega)$;
- On all boundaries: $\mathbf{n} \cdot \mathbf{T} = 0$;
- On the side boundaries (edges): $\mathbf{n} \cdot \mathbf{D} = 0$.

3.3 Materials and Methods

The calibration method is based on a combination of experiments and numerical calculations using the FE model, implemented in Comsol version 3.5a. Subsequently, a sensitivity study was performed using the final FE model and varying all material parameters of the FE model.

3.3.1 Experiments

A plate of piezoceramic material (SPC-140) including electrodes was obtained from SonoSep Technologies, manufacturer of US separators. The size of the PZT was $22.5 \times 13.5 \times 0.983$ mm including two $10 \mu\text{m}$ electrodes. The impedance analyser used was a SinePhase 16777k USB analyser. The piezoceramic was placed upright on a sheet of foam in order to minimise the influence of the boundary conditions on the results. The piezo was stabilised by the electrode wires of the analyser (Figure 3.1). Impedance measurements were done in a range from 1.5-2.5 MHz, knowing this to be the range of application, while applying an average voltage of 200 mV between the electrodes.

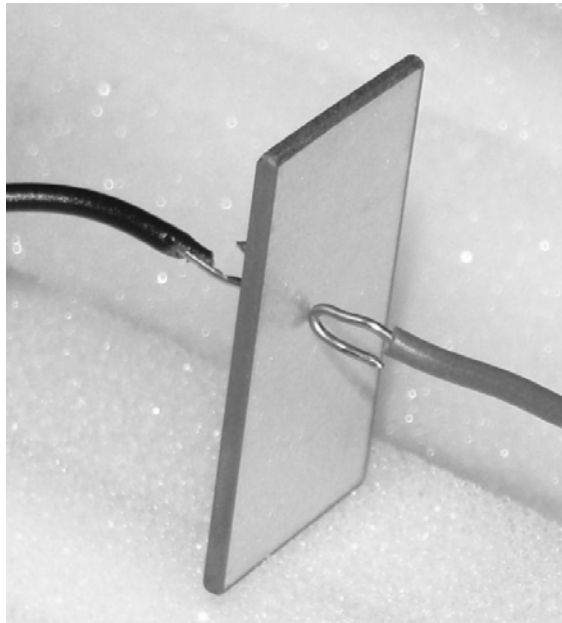


Figure 3.1: Setup for impedance analysis on a plate of piezoceramic material SPC-140.

3.3.2 Finite element model

Numerical simulations for the model calibration step were performed using the partial differential equation and finite element solver, Comsol version 3.5a, coupled to Matlab version 7.7.0. Each of these programs was applied for a different purpose. Comsol was used for the calculation of the admittance and structural deformation and Matlab was applied for the pre- and post-processing, sensitivity analysis and parameter optimisation routine.

One half of the piezo element, cut along the largest dimension, was modelled with one-sided symmetry using 392 triangular 2D elements. All remaining boundaries of the piezo element were free to move, similar to the experiments, and a voltage of 200 mV was applied to the upper electrode, while the lower electrode remained grounded. A second 3D quarter piezo model with 3030 prism elements was made in order to study the influence of the largest dimension on the results.

Material parameters of the SPC-140 piezoceramic were obtained from SonoSep Technologies, according to the values given in Table 3.1. The parameters were assumed to be correct and the remaining unknown parameters were estimated.

3.3.3 Optimisation routine

For the parameters given in Table 3.2, a non-linear least-squares optimisation algorithm was run, using the parameterised 2D FE model in Comsol. The objective function was defined as the sum of squared differences between experimental and simulated admittance magnitude, where the differences were defined as

$$F = |Y_{exp}(f)| - |Y_{sim}(f)| \quad (3.15)$$

with F the residual vector, Y_{exp} the measured admittance and Y_{sim} the simulated admittance in the frequency range from f_{min} to f_{max} .

In our application, we used a least squares large-scale optimisation algorithm that at each iteration minimised the squared 2-norm of the vector $F - J\Delta b$ with $J = \frac{\partial F_i}{\partial b_j}$, the Jacobi matrix, and $\Delta b = b^{(i+1)} - b^{(i)}$ the estimate of the solution for the current iteration. Hence, given the estimate at iteration i , being $b^{(i)}$, and Δb , the new estimate $b^{(i+1)}$ can be calculated. In fact, this is an iterative linear solution using a first-order approximation of the non-linear estimation problem [44]. This implies that an ordinary least squares estimated solution Δb can be found from

$$\Delta b = (J^T J)^{-1} J^T F. \quad (3.16)$$

Table 3.1: Material constants of piezo material SPC-140. The subscripts with numbers, e.g. d_{31} , indicate the coupling in direction 3 with the value in direction 1. For example: a mechanical displacement in z -direction (3) results in a voltage change in x -direction (1)

Parameter	Value	Unit	Description
s_{11}	11.7×10^{-12}	$\frac{m^2}{N}$	elastic constant 11
s_{33}	14.7×10^{-12}	$\frac{m^2}{N}$	elastic constant 33
d_{13}	-60×10^{-12}	$\frac{m}{V}$	charge constant 13
d_{33}	200×10^{-12}	$\frac{m}{V}$	charge constant 33
d_{15}	265×10^{-12}	$\frac{m}{V}$	charge constant 15
$\frac{\epsilon_{33}^T}{\epsilon_0}$	800	-	relative permittivity 33 direction with $\epsilon_0=8.85419$ $\times 10^{-12} \frac{F}{m}$
$\frac{\epsilon_{11}^T}{\epsilon_0}$	680	-	relative permittivity 11 direction
k_p	0.50	-	coupling factor p
k_{33}	0.60	-	coupling factor 33
k_{31}	0.25	-	coupling factor 31
Q	350	-	quality factor
N_t	2100	Hzm	frequency constant in thickness mode
$\tan \delta$	10×10^{-3}	-	dielectric loss factor

In order to obtain the accuracy of final estimate \mathbf{b}^* , an estimate of the covariance matrix of \mathbf{b}^* can be obtained from

$$Cov[\mathbf{b}^*] = \sigma^2 (\mathbf{J}^T \mathbf{J})^{-1} \quad (3.17)$$

with variance σ^2 defined by

$$\sigma^2 = \frac{\mathbf{F}^T \mathbf{F}}{n - p} \quad (3.18)$$

and with \mathbf{J} and \mathbf{F} the final Jacobi matrix and estimated residual vector,

Table 3.2: Material parameters of piezo material SPC-140 to be estimated and predefined range and parameter step for full factorial design of experiments [first value:step size:last value].

Parameter	Range	Unit	Description
s_{12}	[-5:0.2:-4] $\times 10^{-12}$	$\frac{m^2}{N}$	elastic constant 12
s_{13}	[-5:0.2:-4] $\times 10^{-12}$	$\frac{m^2}{N}$	elastic constants 13
s_{44}	[4:0.2:4.2] $\times 10^{-11}$ [4.0:0.2:5.0] $\times 10^{-11}$	$\frac{m^2}{N}$	elastic constant 44

respectively. Hence,

$$Cov[\mathbf{b}^*] = \frac{\mathbf{F}^T \mathbf{F}}{n - p} (\mathbf{J}^T \mathbf{J})^{-1} \quad (3.19)$$

with n the number of function evaluations, in our case the number of numerical samples (length of $\mathbf{Y} = 4001$), and p the number of estimated parameters, in our case three. $Cov[\mathbf{b}^*]$ is a symmetric matrix with the squared estimated standard deviation of the solution \mathbf{b}^* on the diagonal and which satisfies the Cramer-Rao inequality (see e.g. [44, 6]).

Note that the result of the minimisation depends on both the frequency range, specifically the values of \mathbf{Y}_{exp} and \mathbf{Y}_{sim} , as well as the frequency step applied, i.e. the final number of function evaluations n .

3.3.4 Initial estimate

To reduce the computational costs of the numerical optimisation and to avoid local minima, to a large extent, initial estimates of the three parameters in vector \mathbf{b} were obtained from two full factorial designs of experiments (DOE): each parameter was varied with fixed steps in a predefined range and the peak of the admittance curve was compared with experimental data. The first series included parameters s_{12} and s_{13} each with six steps and s_{44} in two steps (72 simulations). This series showed that s_{44} seemed not very sensitive to variation, which was further investigated with a second DOE varying s_{44} in six steps as well [4:0.2:5] $\times 10^{-11}$. The DOE ranges and parameter steps are given in Table 3.2.

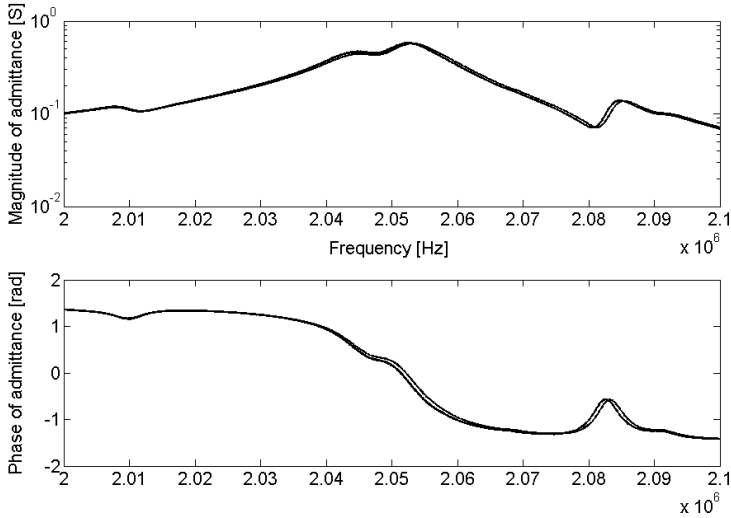


Figure 3.2: Admittance Bode plot for the piezoceramic. Nine measurements with a frequency sweep from 2.0-2.1 MHz with 100 Hz intervals on a single new specimen.

3.4 Results

3.4.1 Experiments

The experiments and simulations were the basis for the piezo model calibration process. Figure 3.2 shows the admittance curves versus frequency for nine measurements on a single specimen. Except for one measurement (also shown in Figure 3.2), the curves are quite reproducible. There was no reason, however, to discard the outlying measurement. Two close peaks in the magnitude of the admittance occur, namely at 2.045 MHz and at 2.052 MHz. The peak corresponds to the maximum real admittance, which means that the maximum power P of the system is reached $P = V_{rms} * I_{rms} = V_{rms}^2 * Y$, with $_{rms}$ indicating the root-mean-square of the harmonic signal V and I .

The width of the peak at half height is a measure for the attenuation of the system, denoted by the quality factor $Q = \frac{\Delta f}{f_c}$, where Δf the peak width at half the height and f_c the frequency of the peak. The higher Q , the better the performance of the system. The average Q factor in nine experiments was 129, based on estimates of the SinePhase software version 2.3. The attenuation or loss can have a mechanical, electrical or electro-mechanical origin. The analyser does not discriminate between the different types of loss.

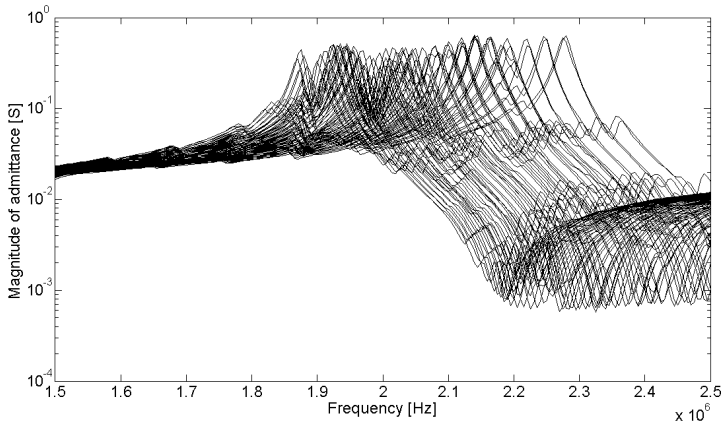


Figure 3.3: Absolute value of the admittance versus frequency for a full factorial DOE varying s_{12} (6 values), s_{13} (6 values) and s_{44} (2 values).

3.4.2 Simulations

Apart from the three parameters in the numerical optimisation, also the quality factor (attenuation) needed to be adjusted, because the peak in the simulations was too narrow and too high. Attenuation was modelled as mechanical loss with a loss factor $\eta_m = \frac{1}{Q}$. It is known that specified quality factors in data sheets are usually theoretical maximum values, which are seldom reached in practise. A Q of 129, as measured, instead of the specified 350, indeed gave better results.

The DOE involved three parameters, s_{12} , s_{13} and s_{44} , each of which was varied with six different values. The admittance curves of the first $6 \times 6 \times 2$ DOE are shown in Figure 3.3. This figure shows that peak frequency varies significantly with s_{12} and s_{13} and further optimisation is justified.

The sum of squared differences between the simulated and experimental signal (residual) was taken as a measure for the goodness-of-fit, similar to the optimisation routine. Figure 3.4 shows the sum of squares of the residuals versus s_{12} and s_{13} , indicating two minima in the DOE. The parameter values associated with these minima were taken as starting values for the optimisation. The influence of s_{44} was negligible in comparison to the other two parameters, which can also be derived from the sensitivity analysis below.

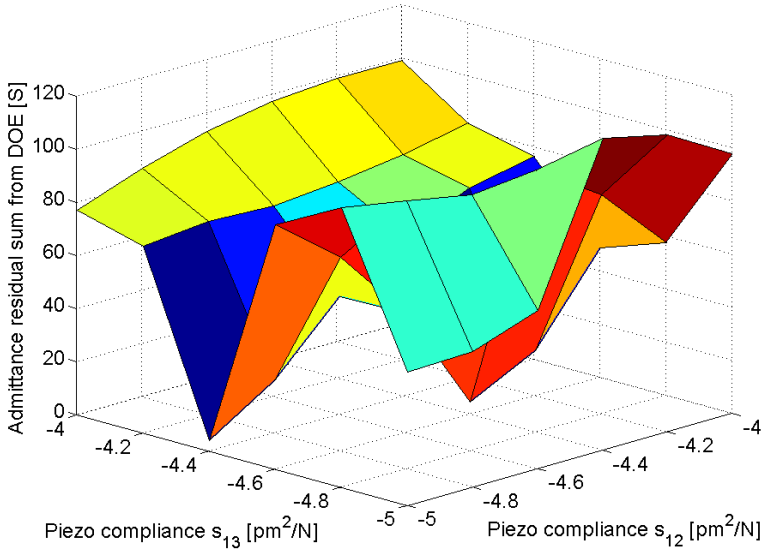


Figure 3.4: Residual sum of squared differences between simulated and experimental admittance (z-axis) versus s_{12} (x-axis) and s_{13} (y-axis).

The results of the optimisation routine following the DOE are given in Table 3.3. This table provides the following results:

- the initial estimated value before optimisation based on the DOE. Two initial estimates were used;
- the value of the estimated parameters;
- the estimated standard deviation of the solution.

The final parameter values in Table 3.3 appeared to be independent of the initial estimate.

Given the standard deviation, which is near 1% for each parameter, one can conclude that the estimated solution is accurate enough to be used for future simulations. The sensitivity study in section 3.4.3 will show once more that parameter s_{44} is rather insensitive to variations considering the thickness mode.

The fitted admittance curve for the three estimated parameters and the new quality factor is shown in Figure 3.5 and 3.6. The double peak seen at resonance near 2.05 MHz in the experiments could not be found in the simulations. Simulations

Table 3.3: Material constants of piezo material SPC-140 estimated with a least squares optimisation routine

Parameter	Initial estimates	Final value	Standard deviation	Multiplication factor
s_{12}	-5.0 / -4.4	-4.88	0.017	$\times 10^{-12}$
s_{13}	-4.4 / -4.6	-4.44	0.005	$\times 10^{-12}$
s_{44}	4.5 / 4.5	5.00	0.011	$\times 10^{-11}$

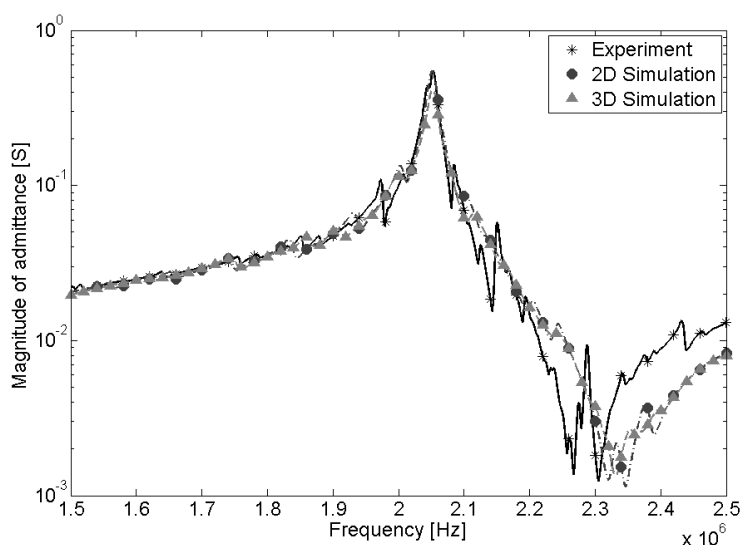


Figure 3.5: Admittance amplitude plot obtained with a least squares optimisation routine with 2D simulations. The theoretical quality factor Q needed to be reduced from 350 to the measured value of 129 to obtain the correct peak height. The 3D analysis was added for comparison and shows small differences with the 2D results.

over a larger frequency range showed no additional higher peaks, which verifies that the peak shown is the eigenfrequency searched for. In addition to the 2D analysis, a 3D analysis was added for comparison. The 3D simulation results (Figs. 3.5 - 3.6) were quite similar to the 2D results, justifying that subsequent analyses can be made with a 2D model. Figure 3.7 shows the vertical acceleration pattern in the 3D (quarter) transducer model at the eigenfrequency of 2.05 MHz, verifying the characteristic shape of the first thickness mode.

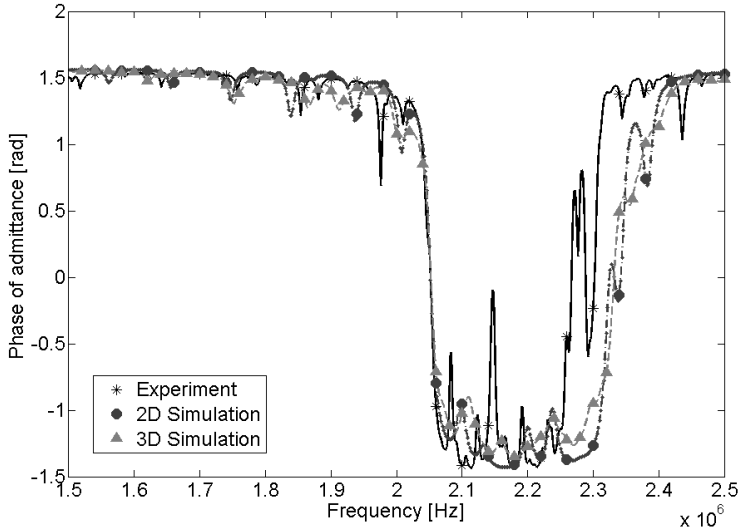


Figure 3.6: Admittance phase plot obtained with a least squares optimisation routine with 2D simulations. The 3D analysis was added for comparison and shows small differences with the 2D results.

3.4.3 Sensitivity study

In order to obtain insight into the sensitivity of the FE model on the piezo material parameters, each of the parameters was varied independently by $\pm 1\%$. The response of this variation on the shift in eigenfrequency and magnitude of the admittance peak is shown in Table 3.4. These results show that parameter changes of 1% result in frequency changes of less than 1%, which, however, still corresponds to 20 kHz. For a frequency controller, this frequency shift is small, but for the efficiency of a resonator it is substantial, because the admittance decreases rapidly with minor frequency shifts. In some cases the frequency changes are small (ϵ_{11} , d_{15} and Q). The magnitude of Y changes less than 1% for parameters which have no z-component (direction 3) and over 7% for s_{33} , which means that this piezoceramic characteristic is sensitive to changes in s_{33} . An illustration of the effect of the more sensitive parameters s_{13} and d_{31} on the admittance is shown in Figure 3.8 comparing the sum of residual differences between experiment and simulation. This figure shows a saddle point, indicating that multiple minima will occur and thus multiple solutions will exist if these parameters were included into an optimisation routine. A similar small variation of s_{33} combined with d_{33} did not show multiple minima.

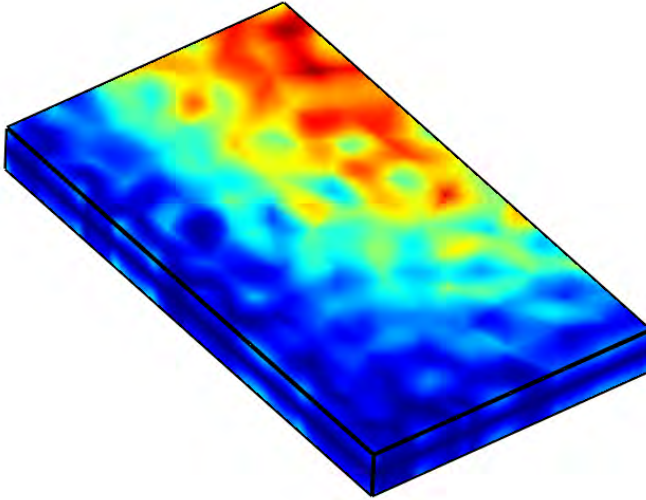


Figure 3.7: 3D acceleration pattern of the quarter piezoceramic at the eigenfrequency of 2.05 MHz, verifying the first thickness mode.

3.5 Discussion

On the basis of the material parameters given for SPC-140 and the formulae stated in the EN50324 standard at least s_{12} could have been estimated in advance, assuming one has the standard at hand. Nevertheless, the value obtained thus, $-11 \frac{pm^2}{N}$, did not even provide any reasonable starting value for optimisation. Moreover, for determination of s_{44} and s_{13} another set of characterisation measurements is needed. Therefore, the full unknown set of three compliance parameters was taken as a basis for characterisation.

If all ten parameters of the piezoceramic were taken as input for the optimisation routine, no consistent solution was to be expected, because multiple parameters have similar effects on the admittance. Figure 3.9 shows the eigenfrequency of the admittance resulting from a $6 \times 6 \times 3$ DOE with s_{12} , s_{13} and s_{33} , with s_{33} varying between 14.6 and 14.8 $\frac{pm^2}{N}$. The figure shows that a similar peak location or eigenfrequency can be obtained by multiple sets of parameters, taking into account only three out of ten. Thus as the amount of unknown parameters increases many more possible optimal solutions will appear. Table 3.5 shows the result of

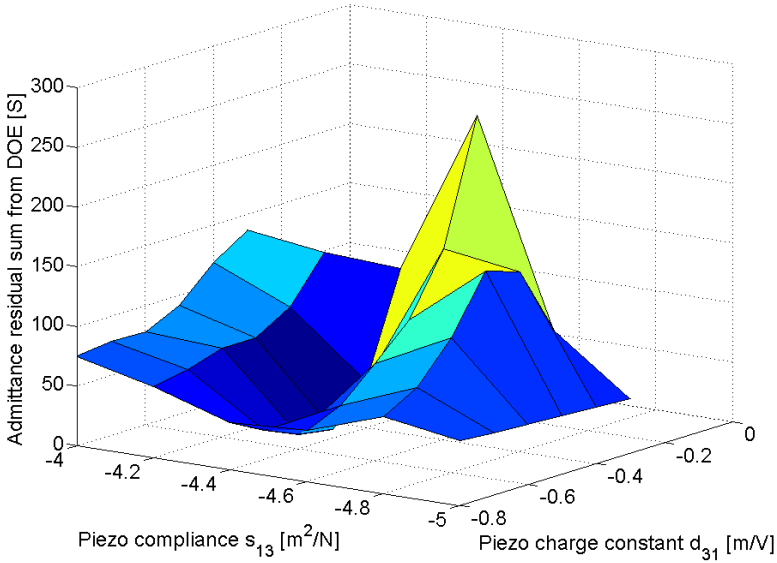


Figure 3.8: Residual sum of squared differences between simulated and experimental admittance (z-axis) versus s_{13} (x-axis) and d_{31} (y-axis).

a full 10 parameter optimisation with starting values derived from manufacturer data and results from the previous optimisation. The deviations from manufacturer data are small, although d_{15} , being an insensitive parameter (see Table 3.4), deviated near 5%. This result gives trust in the manufacturer data. Nevertheless, a 10 parameter optimisation takes several days to compute, while three parameters are optimised in only a few hours.

In this study an appropriate fit was obtained for the admittance peak, whereas the maximum impedance (or minimum admittance) peak at 2.32 MHz was not similar to the experimental peak. Piranda et al. [61] recommended to use both the admittance and the impedance peaks for material characterisation. In our case taking into account both peaks meant that at least one more material parameter needed to be changed: either ϵ_{33} needed to increase or d_{33} needed to decrease approximately 5% for a good fit. Ebenezer and Sujatha [22] showed that d_{33} was always overestimated by approximately 0.5-5% with a 1D experiment, so that a decrease would be justified, while they showed that ϵ_{33} always gave a perfect fit. Decreasing only d_{33} by 5%, however, meant changing other parameters as well for a decent fit (see Table 3.6 and Figure 3.10). This change was not desirable, because the characteristics given (i.e. $d_{33} = 2 \times 10^{-10}$) were the basis for the

Table 3.4: Sensitivity of admittance peak frequency and magnitude to 1% change in parameter value. The first row of each parameter corresponds to -1% change, the second to +1% change. The shift is calculated as a percentage of the given reference value

Parameter	Frequency [kHz]	Frequency shift [%] (ref: 2051.6 kHz)	$abs(Y)$ [S]	Y shift [%] (ref: 0.5454 S)
s_{11}	2062.6	0.54	0.55	0.21
	2041.0	-0.52	0.54	-0.36
s_{33}	2068.8	0.84	0.58	5.70
	2034.8	-0.82	0.51	-7.19
s_{12}	2047.0	-0.22	0.54	-0.39
	2056.0	0.21	0.55	0.35
s_{13}	2039.0	-0.61	0.52	-4.78
	2064.6	0.63	0.56	3.58
s_{44}	2051.8	0.01	0.54	-0.94
	2051.2	-0.02	0.55	0.85
ϵ_{11}	2051.6	0.00	0.54	-0.08
	2051.4	-0.01	0.55	0.08
ϵ_{33}	2052.2	0.03	0.55	0.14
	2050.8	-0.04	0.54	-0.13
d_{33}	2049.8	-0.09	0.52	-3.87
	2053.2	0.08	0.57	3.99
d_{15}	2051.4	-0.01	0.55	0.11
	2051.6	0.00	0.54	-0.10
d_{31}	2052.0	0.02	0.55	1.74
	2051.0	-0.03	0.54	-1.71
$\frac{1}{Q}$	2051.6	0.00	0.55	1.00
	2051.6	0.00	0.54	-0.98

Table 3.5: Result of optimisation with 10 parameters showing the initial values, derived from the previous optimisation, the final values and the deviation from the initial value.

Parameter	Initial value	Final value	Difference with initial value	Multiplication factor
s_{11}	11.70	11.79	-0.8%	$\times 10^{-12}$
s_{33}	14.70	14.68	0.1%	$\times 10^{-12}$
s_{12}	-4.88	-4.97	-1.8%	$\times 10^{-12}$
s_{13}	-4.44	-4.41	0.7%	$\times 10^{-12}$
s_{44}	5.00	4.57	8.6%	$\times 10^{-11}$
d_{33}	2.00	2.01	-0.5%	$\times 10^{-10}$
d_{15}	2.65	2.78	-4.9%	$\times 10^{-10}$
d_{31}	-0.60	-0.60	0.0%	$\times 10^2$
ϵ_{11}	6.80	6.73	1.0%	$\times 10^2$
ϵ_{33}	8.00	7.99	0.1%	$\times 10^2$

current approach. Moreover, the separator to be made will be operated near resonance (maximum admittance) and not anywhere near anti-resonance (maximum impedance).

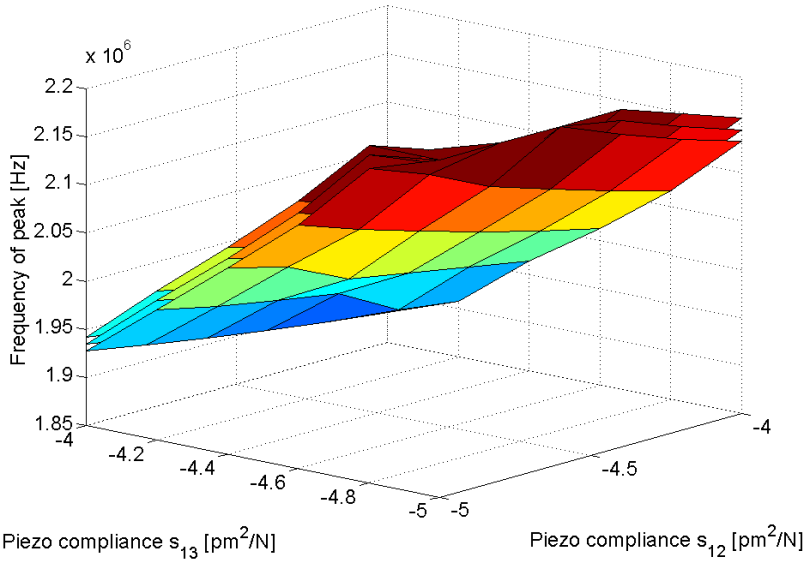


Figure 3.9: Eigenfrequency (peak location) of the admittance (z-axis) versus s_{12} (x-axis) and s_{13} (y-axis) at three different values of s_{33} (the three stacked layers). The figure was obtained using a $6 \times 6 \times 3$ full factorial DOE. The figure shows that the set of three parameters is not unique at a given eigenfrequency.

Table 3.6: Material constants of piezo material SPC-140 estimated with a least squares optimisation routine after decreasing d_{33}

Parameter	Value	Multiplication factor
d_{33}	1.90	$\times 10^{-10}$
Q	1.51	$\times 10^2$
s_{12}	-4.62	$\times 10^{-12}$
s_{13}	-4.55	$\times 10^{-12}$
s_{44}	5.00	$\times 10^{-11}$

3.6 Conclusion

As a first step in ultrasonic separator modelling, a numerical model of an SPC-140 piezoceramic was established using the material parameters specified by the manufacturer complemented, to preserve prior physical knowledge, with estimated characteristics of the remaining unknowns using an optimisation routine.

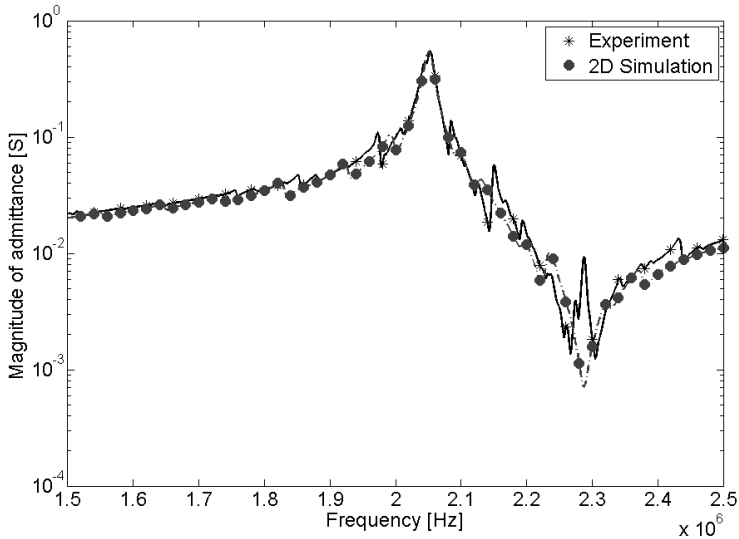


Figure 3.10: Admittance amplitude plot obtained with a least squares optimisation routine with 2D simulations after decreasing d_{33} by 5%. This implied increasing quality factor Q as well.

The optimisation routine gave consistent results for multiple starting values obtained from a full factorial design of experiments. Limiting the optimisation to a minimum amount of parameters is essential in preventing the occurrence of multiple minima with an increasing amount of unknown parameters to be estimated, resulting in unrealistic numerical models. Using manufacturer data as known initial values for a larger scale optimisation requires much more computational power, while showing little improvement of the result.

The quality factor specified by the manufacturer ($Q=350$) was much higher than measured and implemented ($Q=129$). The sensitivity analysis showed that small changes (1%) to the material parameters can also change the eigenfrequency with approximately 1%, which is about 20 kHz, and can cause changes up to 8% in the calculated peak admittance. Such sensitivity calls for precise frequency control in an ultrasonic separation unit to maintain maximum efficiency.

4. MODEL OF AN ULTRASONIC SEPARATOR

Abstract

Our final aim is to apply acoustic separation technology for the recovery of valuable particulate matter from wastewater in industry. Such large scale separator systems require detailed design and evaluation in order to optimise the system performance at the earliest stage possible. Numerical models can facilitate and accelerate the design of this application. Therefore, a finite element (FE) model of an ultrasonic particle separator is a prerequisite. In our application the particle separator consists of a glass resonator chamber with a piezoelectric transducer attached to the glass by means of epoxy adhesive. Separation occurs most efficiently when the system is operated at its main eigenfrequency.

The aim of the paper is to calibrate and validate a model of a demonstrator ultrasonic separator, while preserving known physical parameters and estimating the remaining unknown or less certain parameters to allow extrapolation of the model beyond the measured system. A two-step approach was applied in order to obtain a validated model of the separator. The first step involved the calibration of the piezoelectric transducer. The second step and subject of this paper, involves the calibration and validation of the entire separator using non-linear optimisation techniques.

The results show that the approach lead to a fully calibrated 2D model of the *empty* separator, which was validated with experiments on a *filled* separator chamber. The large sensitivity of the separator to small variations indicated that either such system should be made and operated within tight specifications to obtain the required performance or the operation of the system should be adaptable to cope with a slightly off-spec system, requiring a feedback controller.

This chapter was published as
H. Cappon and K.J. Keesman (2012) Numerical modeling, calibration and validation of an ultrasonic separator. IEEE transactions on Ultrasonics, Ferroelectrics and Frequency Control, Vol. 60, No 3, pp 614-621

4.1 Introduction

The principle of acoustic separation has already been investigated by various studies [60, 35, 33, 36, 65, 57] and is in use in commercially available acoustic separators for fluid suspensions, like the BioSep from Applikon (Metrohm-Applikon B.V., Schiedam, The Netherlands). Numerical studies of acoustic separators have also been performed by various authors [36, 56, 37, 25, 55]. However, to our knowledge, none of them present a step-wise strategy for obtaining a calibrated and validated model, which can be applied in a numerical design process and performance optimisation.

Optimising the design of a separator is important when larger volumes with high efficiency need to be processed. Experimental optimisation with changes made to a series of prototypes is an extensive and expensive method, providing little insight into the main parameters influencing the separation process. In this context, numerical models are a cost effective way of understanding, improving and optimising systems. Therefore, the aim of the paper is to calibrate and validate an FE model of an existing separator preserving the known parameters of the system and estimating the unknown parameters, similar to the approach presented earlier [11], while simultaneously gaining a thorough understanding of the parameters which are important for the design of a novel separation device.

The piezoelectric transducer in an ultrasonic separation system acts both as an actuator and as a sensor. The response of both the mechanical structure as well as the coupled fluid layer in the separation chamber affect the electrical properties of the transducer and therefore influence the resonance frequencies of the system. These eigenfrequencies occur when the impedance, the ratio of voltage (V) and current (I), defined as $Z = V/I$ is minimal, or more precisely, when the real part of the (complex) impedance is minimal. In practise, it is easier to find the maximum of the inverted impedance, which is the admittance $Y = I/V$. Due to dissipation in the material, I and V are not in phase. Hence, in what follows, complex variables are used. Measured and simulated electrical admittance at different frequencies were used for model calibration and validation.

Characterisation and validation of the SPC-140 piezoelectric transducer itself was performed in a previous study [11]. Consequently, the current focus is on the separation unit model with the transducer as is.

4.2 Materials and Methods

4.2.1 Device description

An ultrasonic resonator cuvette is one of the simplest physical representations of an ultrasonic separator (Figure 4.1). This device was built by SonoSep Technologies and was used to demonstrate the principle of ultrasonic particle separation, in our case resulting in enhanced sedimentation of suspended starch. The aim was to use this physical separator for calibration and validation of an FE separator model, which is to be modified at a later stage to support novel designs.

This resonator is a rectangular, beam shaped enclosure made of borosilicate glass driven by a piezoelectric transducer. The wall unto which the transducer is glued is called the matching layer. The wall opposite to the matching layer, across the cavity with the fluid, is called the reflector. In case the reflected wave matches the incoming wave, a standing wave is created. In such case the acoustic pressure across the cavity will consist of (fluid) velocity nodes and anti-nodes in which the suspended particles will concentrate and agglomerate depending on their physical properties [30]. The piezoelectric transducer was protected with an aluminium cover, which was also glued to the cuvette.

In order to model the geometry of the cuvette the main dimensions of the cuvette were measured with a pair of sliding callipers. The dimensions are shown in Table 4.1, noting that the matching layer between the transducer and the fluid could not be measured accurately because of the aluminium cover. The actual thickness of the matching layer was verified with the manufacturer, as were the dimensions of the piezoelectric transducer. The thickness of the epoxy adhesive layer between the transducer and the glass was estimated by the manufacturer to be near $50 \mu\text{m}$. The electrodes of the transducer were cut in half along the vertical axis and the two half adjacent transducers thus created were electrically connected in series. The end electrodes were connected to the amplifier and the remaining two electrodes were interconnected, creating a unidirectional current inside the two halves. This arrangement resulted in a higher impedance, allowing higher operating voltages for a given current.

The piezoelectric transducer is driven by a frequency controller (Applikon ADI1015) which maintains the eigenfrequency of the system within a given frequency bandwidth. The controller aims to maximise the real output power at constant voltage, thus searching for maximum real electrical admittance.

Table 4.1: Main dimensions of the cuvette

Dimension	size [mm]
Outer height	70
Cavity height	67
Cavity width (right-left)	27
Cavity depth (fore-aft)	20
Side wall thickness	3.2
Matching layer thickness	4.25
Reflector layer thickness	3.2
Transducer height	44
Transducer width	23
Transducer thickness	0.965

4.2.2 Experimental approach

For the calibration and validation of the FE model admittance measurements were performed with the separator in both empty and water filled conditions. In the empty condition the side walls and reflector have little influence on the measurements, because the air in the cavity of the separator cannot adequately transfer the acoustic energy through the cavity. Water on the other hand is perfectly capable of transferring this acoustic energy and thus the reflector and side walls will affect the measurements.

Admittance measurements were performed with a SinePhase 16777k impedance analyser, using both an empty separator and a filled one. Frequency sweeps were in the range of 0.5 - 3 MHz with 250 Hz steps and 1.95 - 2.05 MHz with 25 Hz steps, thus focusing on our domain of interest, which are the main operating frequencies of the separator near 2 MHz. The quality factor of the main eigenfrequency in the system was estimated from the highest peaks found, using the software (version 2.3) provided with the analyser. The temperature of the water in the filled separator was measured with a 0.2K scale thermometer, before and after each admittance measurement to ensure thermal stability.

The material parameters of glass and water were known. However, the material properties and thickness of the adhesive layer between piezoceramic and glass were unknown. Moreover, the dimensions of the system were of large influence at high ultrasonic frequencies (near 2 MHz), as will be shown, and not all dimensions could be easily measured and implemented into the model. Therefore, optimisation of the thickness of matching layer and epoxy adhesive layer was done with admittance measurements on the empty separator, while using the

filled separator for model validation.

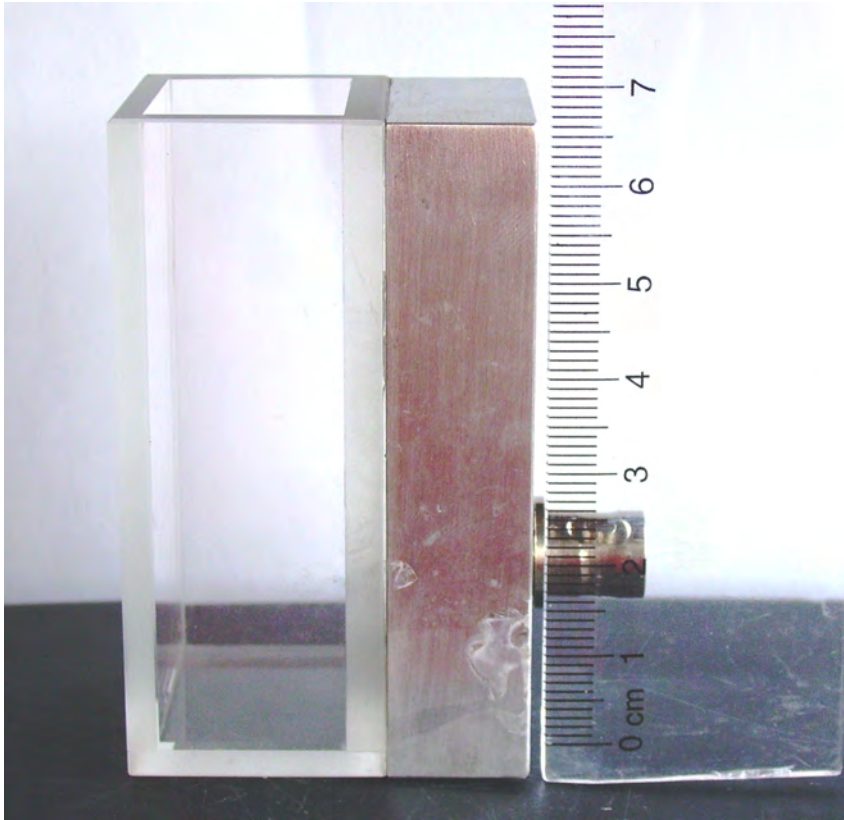


Figure 4.1: The borosilicate cuvette, a basic non-flow separation device, with a BNC power connector on the right side.

4.2.3 Numerical model

A 2D numerical model of the separator was developed with the finite element solver Comsol (Comsol Inc. Burlington MA, USA), version 4.1. The model was set up in top view, as shown in Figure 4.2, and consists of three components: the piezoelectric transducer, an epoxy adhesive layer and a borosilicate glass cuvette. The aluminum cover was excluded from the model. The assembly is a symmetrical system, apart from the electrical connection between the two transducer halves, these are connected in series. So structurally the model is symmetrical, but electrically it is not. In the Comsol solver one needs to apply the feature of boundary similarity to 'connect' the electrodes in series.

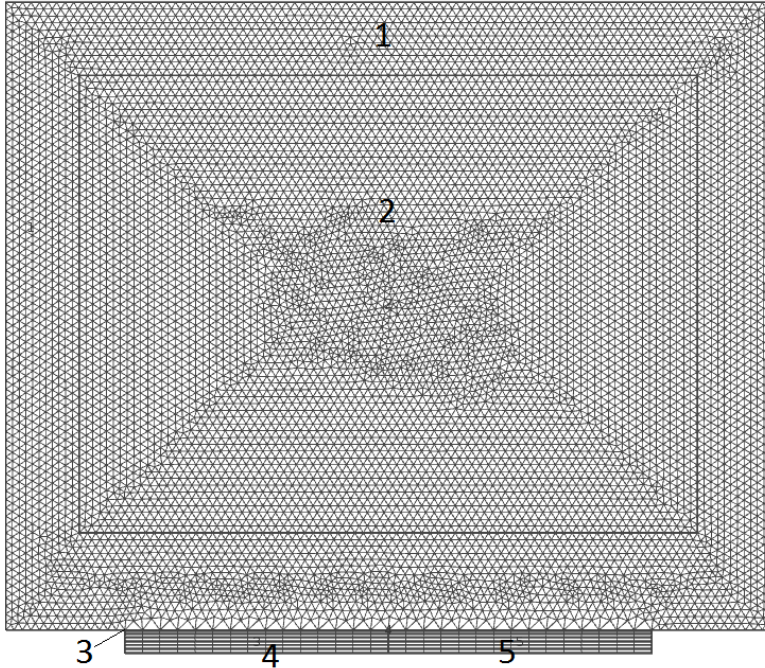


Figure 4.2: Finite element model of the separator, top view. The five numbered areas are 1) glass cuvette, 2) water, 3) adhesive layer, 4) and 5) piezo halves.

Furthermore, the model was set up using two coupled domains: a piezoelectric domain for the electro-mechanical vibration and a pressure acoustics domain for the sound propagation in the fluid. The piezoelectric transducer, the epoxy adhesive layer and the cuvette were assigned to the piezoelectric domain. Glass and epoxy adhesive were modelled as an anisotropic, decoupled (non-electric) material. In the case of a water filled cuvette a sound propagating fluid in the pressure acoustics domain was implemented. The coupling between the two domains across the boundary was as follows:

- The acoustic pressure of the water was modelled as distributed force (force per unit length) on the inner glass walls of the separator, thus having continuity in pressure;
- The mechanical acceleration of the glass walls was similar to the acoustic acceleration of the water inside the separator, thus having continuity in acceleration;

- The outside area of the transducer and the separator radiate into the surrounding air having a specific impedance $z_{air} = \rho_{air}c_{air}$ with ρ_{air} the density of air (1.25 kg/m³) and c_{air} the speed of sound in air (343 m/s).

The material properties of the SPC-140 piezoceramic were taken from a prior characterisation [11]. The elastic (E) modulus and density of borosilicate glass were 63 [GPa] and 2230 [kg/m³], the Poisson ratio was 0.20. The adhesive layer was modelled using material parameters from Epo-Tek 301 epoxy adhesive, provided by Cease et al. [16] with an elastic modulus of 3.67 [GPa], a density of 1080 [kg/m³] and Poisson ratio 0.358. The quality factor Q (an inverse measure for attenuation) was initially set to 25, derived from Hill et al. [36]. Note that the E-modulus of the epoxy adhesive is much smaller than the modulus of the glass (63 GPa) and the piezoelectric transducer (68 GPa) [11]. The adhesive layer was modelled as 0.040 [mm] thick epoxy, being an initial estimated value.

4.2.4 Calibration and validation strategy

The calibration and validation process is summarised in the flow chart of Figure 4.3.

In order to study the influence of epoxy characteristics on the system's response, the unknown parameters, being epoxy layer thickness, Young's or E-modulus and damping were varied in a rectangular grid (indicated in Figure 4.3 by DOE - design of experiments). Moreover, the thickness of the matching layer was known up to 0.05 mm accuracy and could not be measured, introducing another unknown parameter, which was varied as well on a fixed interval. Finally, the attenuation of the piezoelectric transducer will be influenced by the surrounding structure, so that the Q-factor found in our previous study [11] is likely to change as well. Thus five parameters are used in the calibration step as indicated in Table 4.2.

Given the model responses related to the different parameter combinations, the most sensitive parameters were selected for calibration of the empty separator model. The non-linear least squares optimisation routine applied to estimate these parameters was similar to the one in our earlier study of the transducer [11]. In summary, the objective function was defined as the sum of squared differences between experimental and simulated admittance magnitude, while a least squares large-scale optimization algorithm was used, updating the parameter estimation vector \mathbf{b} at each iteration. The accuracy of the solution was determined from the covariance matrix of the estimated solution vector. The validation step encom-

passes the comparison of the model response with the experimental data from a filled separator, while keeping parameters fixed.

In the Comsol simulations similar frequency sweeps as in the experiments were performed. Typically, these 1.8-2.4 MHz frequency sweeps with 2 kHz steps required 6 minutes on an Intel Core i5 3.1 GHz CPU with 3 Gb of RAM. Finally, the admittance was calculated at the (electrically hot) boundary of the piezo transducer as $Y = I/V$. As Comsol software calculates the electric current through each FE element, the current was integrated across all boundary elements to calculate the (overall) admittance of the piezo transducer.

4.3 Results

4.3.1 Experiments

The results of the experimental admittance measurements are shown in Figure 4.4. Two main peaks can be seen at 1.99 and 2.29 MHz. The quality factor Q of the first main peak was estimated to be 360, the Q of the second 129.

For the validation the admittance of the filled separator was measured at three different water temperatures: 19.0, 19.2 and 20.2 °C. As the water was heated by the surrounding (higher) room temperature, it can be assumed that the temperature of the entire system was thermally stable during each experiment. Moreover, the system hardly heated itself during the (low voltage) impedance measurement, which was verified by the temperature taken before and after each run. As can be seen from Figure 4.5, the slight changes in temperature caused frequency shifts of several kHz.

4.3.2 Calibration

The calibration of the FE model was performed with admittance measurements of the empty separator, because it involves fewer variables than a filled separator. Applying the material properties and geometry as in Table 4.1 and the initial values from Table 4.2, resulted in the admittance curve for the 2D model of the empty system as shown in Figure 4.6. These results show that the model produces two peaks at almost the right location, but that the height of the peaks is incorrect.

Changes were then made to the parameters shown in Table 4.2, to find out which of these are responsible for any of these discrepancies. The results of these variations are shown in Figures 4.7 to 4.11. These figures show that the epoxy E-modulus and the epoxy layer thickness are responsible for changes in the position

of the second peak: higher stiffness or smaller thickness result in lower eigenfrequencies. Secondly, the matching layer thickness is responsible for the position of both peaks: a larger thickness means a lower eigenfrequency. The epoxy Q-factor accounts for the height of the second peak, whereas the transducer Q-factor accounts for the height of the first. These results show that two largely independent parameter groups can be distinguished: stiffness and thickness determine peak positions, whereas Q factors determine peak height, which is to be expected for linear dynamic systems. Note that the model is very sensitive to changes in epoxy adhesive layer thickness and the matching layer thickness, because small changes of 10 μm and 0.05 mm, respectively, result in a eigenfrequency shifts of 10 and 20 kHz.

Table 4.2: *Parameter grid for model calibration*

Parameter	Initial value	Grid points [start:step:stop]	Calibrated value	Standard deviation	Unit
Epoxy E-modulus	3.664	2.0:0.5:5.0	-	-	GPa
Epoxy Q	25	25:25:150	20	1.1	-
Epoxy thickness	40	30:5:50	45	<1‰	μm
Transducer Q	129	100:50:400	322	29	-
Matching layer thickness	4.25	4.15:0.05:4.30	4.255	<1‰	mm

Based on these results two separate optimisation runs were performed: one to position the peaks using the epoxy layer thickness and the matching layer thickness and the second to acquire the right admittance magnitude of both peaks. Optimisation focussed on the two peaks of interest, thus limiting the frequency ranges to 1.95-2.05 MHz and 2.25-2.35 MHz. The epoxy E-modulus was kept constant, because it will counteract the epoxy layer thickness. The calibration results are given in Table 4.2 (column 4 and 5) and the admittance plots are shown in Figure 4.12. Note that the adhesive layer thickness and the matching layer thickness changed very little during the calibration, while still showing large model improvement. The large change in the transducer Q-factor was needed to obtain the correct response of the first eigenfrequency at 1.99 MHz. The minor thickness changes, with corresponding small standard deviations (Table 4.2), and the results of the variations in Figure 4.9 and 4.11 indicate high sensitivity of the admittance to the layer thicknesses.

4.3.3 Validation

The validation step encompasses the comparison of the model response, using the fixed (Table 4.1) and calibrated (Table 4.2) parameter values, with the experimental data from a filled separator. Dimensions of the cavity and the reflector were measured and were kept constant during the validation. The temperature of the water in the model was set equal to the experiments. Because there were slight eigenfrequency differences seen between experiments and simulations, the influence of cavity width and water temperature was also evaluated. Variation of the cavity width and water temperature showed that small inaccuracies (50 μm in width and 0.1°C, see Figure 4.13) caused frequency shifts of several kHz. A good fitting model was obtained with a cavity width of 19.95 mm instead of 20.0 mm (Figure 4.14). This is within the accuracy of the sliding calipers used to measure the dimensions. Note that not all eigenfrequencies are equally well matched, which will be discussed in the next section. The pressure profiles of the water filled separator in Figure 4.15 show the typical nodal lines which cause the ultrasonic agglomeration of particles.

4.4 Discussion

Several studies have shown the potential of numerical models in understanding the influence of various parameters on the system response. Some have clearly shown, mostly with 1D models, that the influence of the adhesive layer is substantial and needs to be taken into account in the models [36, 8]. This conclusion is further supported by this study using 2D models, while even identifying the large influence of the adhesive layer thickness and its material characteristics.

The results showed that the approach led to a successfully calibrated 2D model of the complete separator. In the validation step, some differences remain between the physical device and the model causing eigenfrequency shifts (see Figure 4.14). These differences are mainly attributed to small inaccuracies and non-linearities in the physical device, whereas the model is fully linear (except for the characteristics of water implemented in the Comsol software, i.e. non-linear behaviour of density, viscosity and thus speed of sound as a function of temperature). An example of a non-linearity in the physical device is caused by the borosilicate bottom of the cuvette, which reflects ultrasonic waves as well and which is not covered by a 2D model. Additionally, the 2D model assumes 2D waves, whereas 3D waves occur in reality. The earlier modelling study of the piezoelectric transducer, optimized to the thickness mode only, already showed

that the transducer is not fully linear [11], because its geometry is far from the ideal sample assumed in the standards. Therefore, it was most unlikely from the beginning that the full model would perfectly fit the experimental data, because for the whole separation unit even more possible non-linearities were introduced.

Even though the numerical approach was successful, the sensitivity analysis on the piezo transducer and the results of the DOE in this study show that very small changes to the input parameters, like the epoxy adhesive layer thickness or even the water temperature, will dramatically change the system response. This means that either such system should be made and operated within tight specifications to obtain the required performance or the operation of the system should be adaptable to cope with a slightly off-spec system, requiring a feedback controller to find and maintain the eigenfrequency, as is currently done with Applikon's ADI1015.

It would be interesting to validate the model also with a half filled separator, because a half filled system shows the intermediate state of an empty separator and a filled one, thus showing the increasing influence of the water level on the impedance as the separator fills up. A distinction between impedance caused by the matching layer and impedance caused by the water and the other walls will further help understanding the system. In that case, however, one would need a full 3D model. An empty separator modelled in 3D already contains over 9 million elements, because a fine mesh is needed for the high frequency acoustics. Hence, a 3D FE model of a (half) filled separator could not be solved and thus a 3D model with these dimensions is, as yet, not an option.

4.5 Conclusions

A numerical calibration and validation procedure was successfully applied to 2D FE models of an empty and filled acoustic separator, while preserving known physical and geometrical properties. The model of an empty separator was first calibrated to estimate the unknown system parameters and then, with all parameters fixed, validated with measurements on a water filled model. The accuracy and the sensitivity of the model indicates that system optimisation can be done numerically to a large extent. Nevertheless, given the sensitivity of the model (and the physical device) to changes in temperature or slightly off-spec dimensions, an optimised system would still require a frequency controller to maintain an eigenfrequency at which the separation efficiency will be maximum.

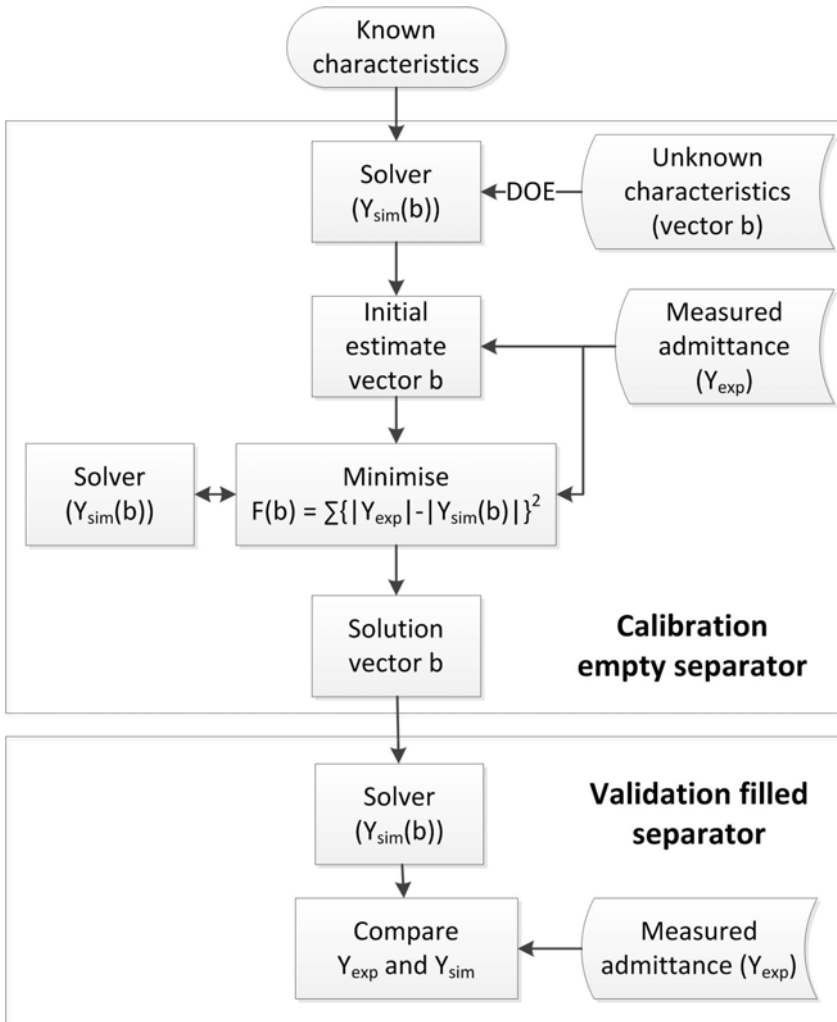


Figure 4.3: Flow chart of the numerical calibration and validation process.

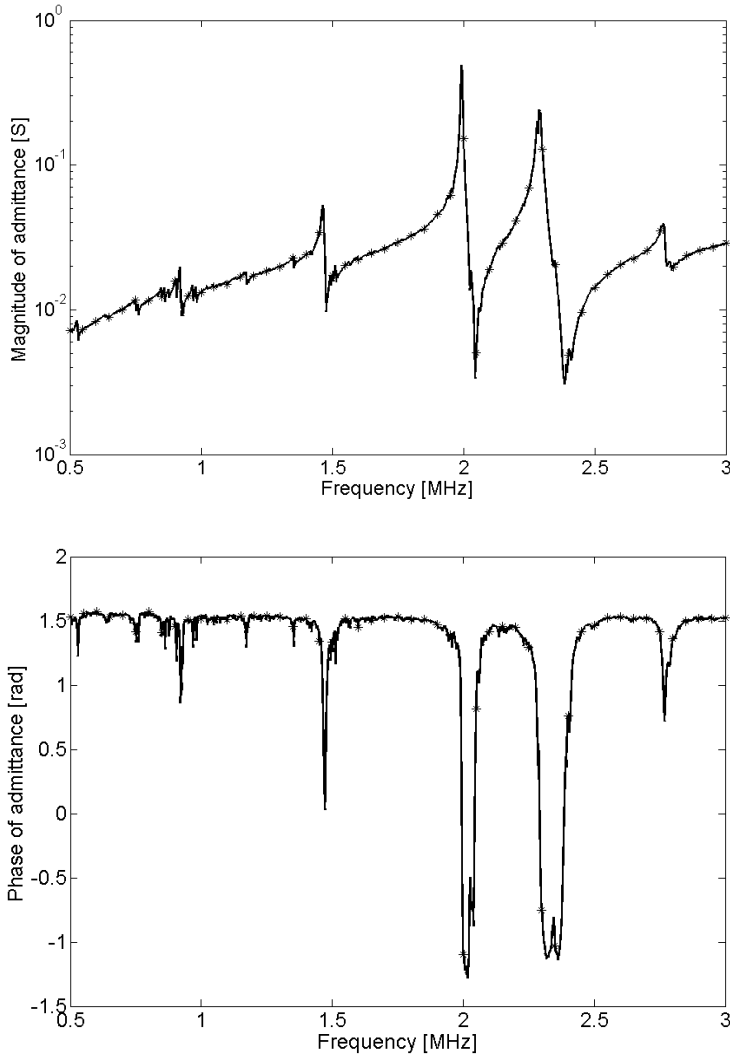


Figure 4.4: Admittance curve, magnitude and phase, measured on an the empty separator from 500 to 3000 kHz. The first main peak at 1.99 MHz is caused by the matching layer of the separator, the second at 2.29 MHz is the (shifted) eigenfrequency of the piezoelectric transducer.

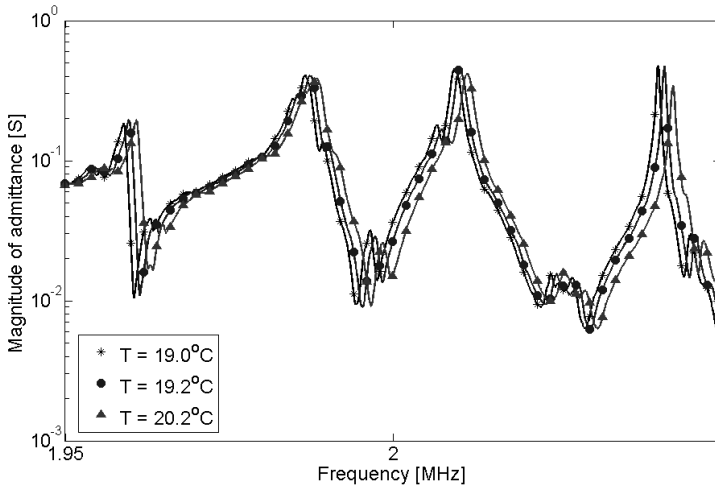


Figure 4.5: Admittance curve (magnitude) measured on the water filled separator from 1950 to 2050 kHz at three different temperatures.

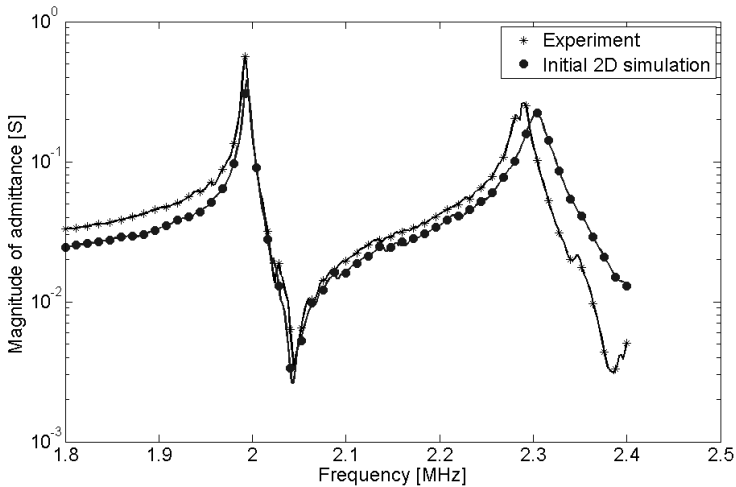


Figure 4.6: Experimental and simulated admittance curve of the empty separator based on the initial 2D model.

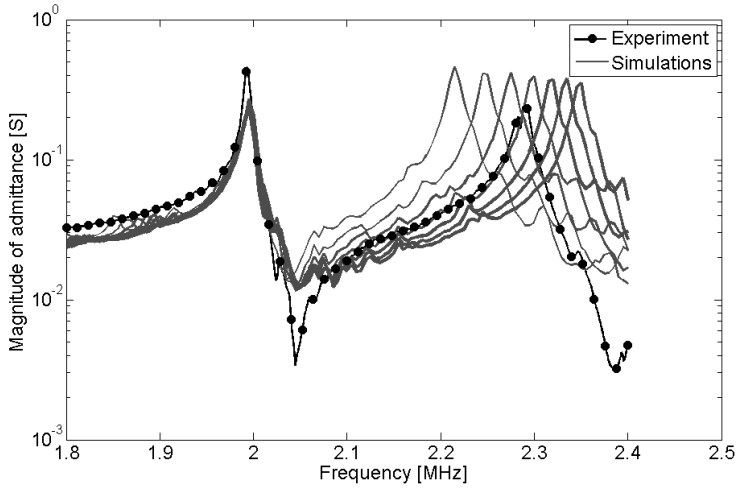


Figure 4.7: Model frequency response while varying epoxy E-modulus from 2.0 to 5.0 GPa in 0.5 GPa steps; increasing stiffness means shifting the second peak to the right (with increasing line thickness).

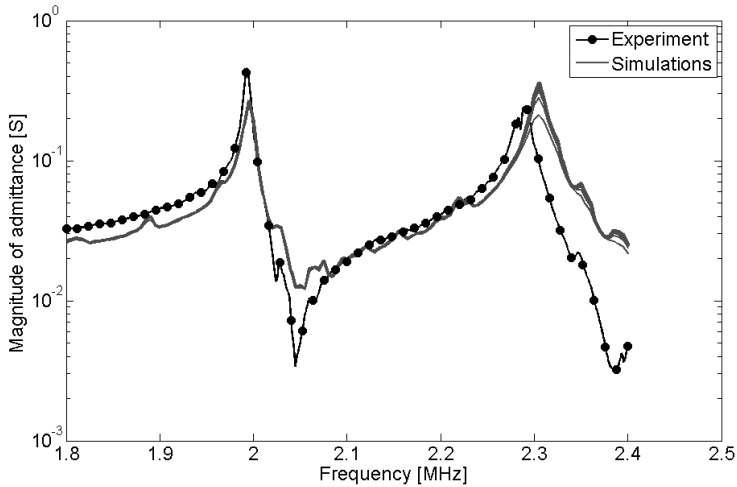


Figure 4.8: Model frequency response while varying epoxy quality factor from 25 to 150 in 6 steps; higher Q means higher (second) peak (with increasing line thickness).

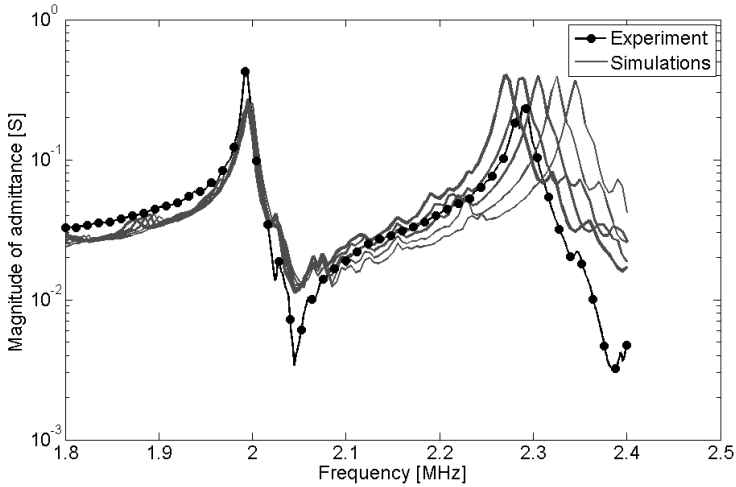


Figure 4.9: Model frequency response while varying epoxy adhesive thickness from 30 to 50 μm in 5 μm steps; increasing thickness means shifting the second peak to the left (with increasing line thickness).

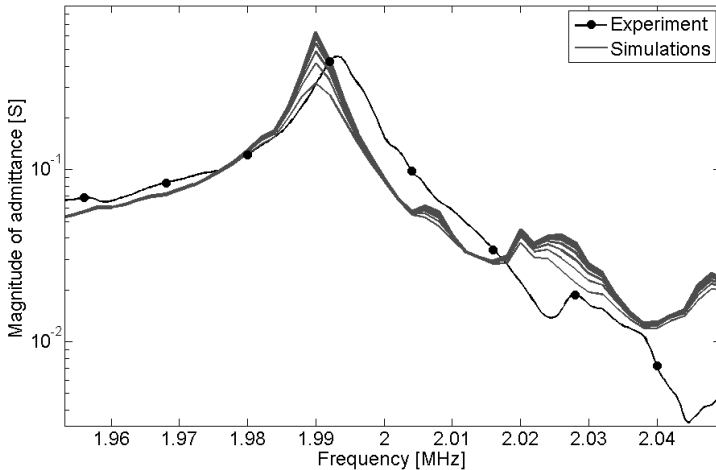


Figure 4.10: Model frequency response while varying the transducer Q -factor from 100 to 400 in 6 steps; increasing Q means higher (first) peak (with increasing line thickness).

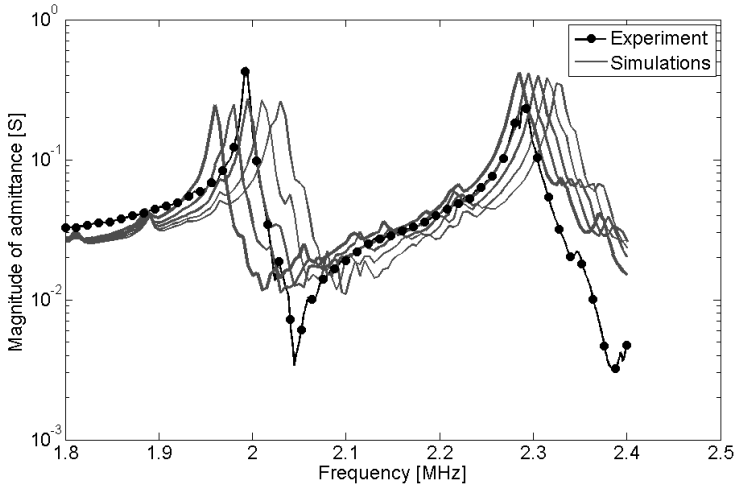


Figure 4.11: Model frequency response while varying matching layer thickness from 4.15 to 4.30 mm in 0.05 mm steps; increasing thickness means a general peak shift to the left (with increasing line thickness).

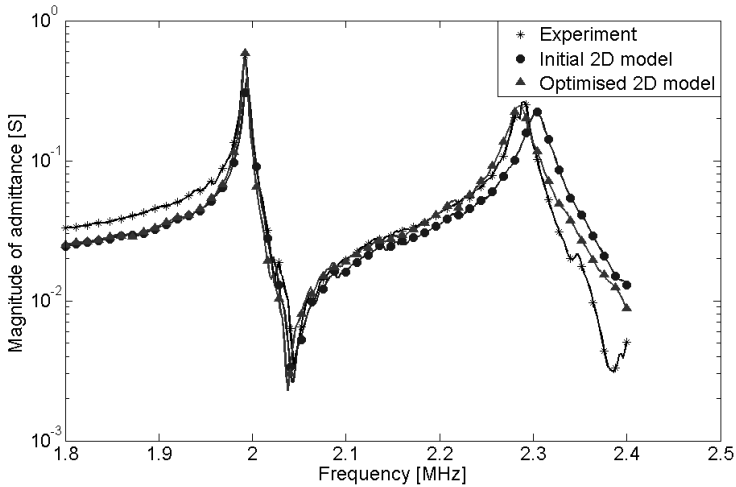


Figure 4.12: Experimental and simulated magnitude of admittance of an empty separator. The simulated signal before and after calibration of the 2D model is shown.

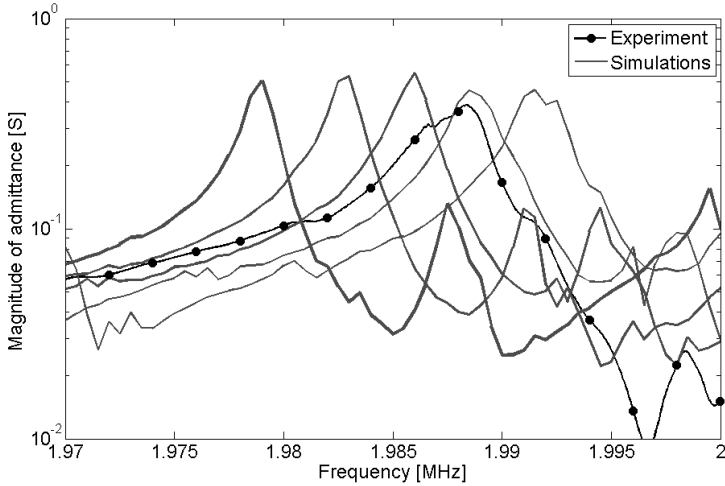


Figure 4.13: Simulated magnitude of admittance of a water filled separator with varying channel width from 1.99 to 2.01 mm in 50 μm steps; increasing channel width means a peak shift to the left (with increasing line thickness).

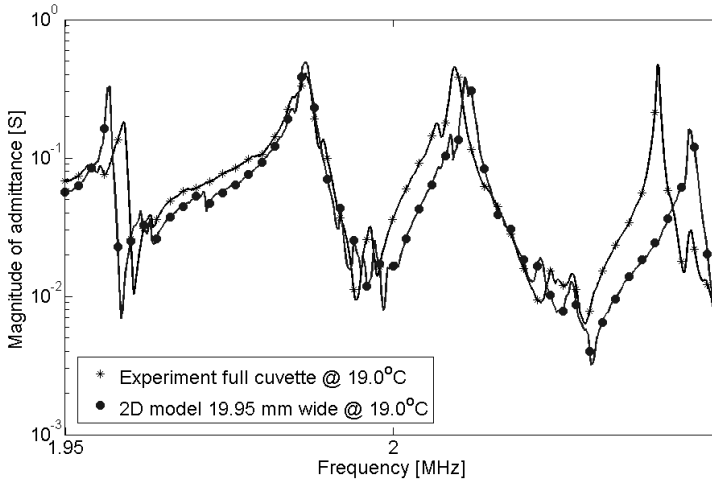


Figure 4.14: Experimental and simulated magnitude of admittance of a water filled separator showing four eigenfrequencies.

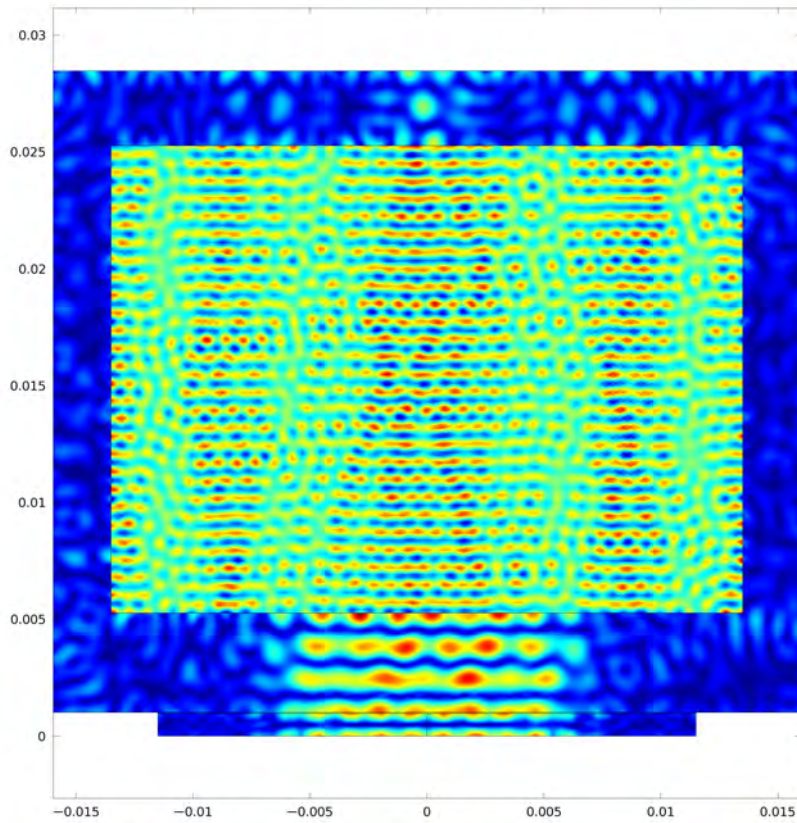


Figure 4.15: Simulated pressure profile in a 2D separator (top view) showing the typical nodal and anti-nodal pressure lines causing acoustic particle separation.

5. BASIC DESIGN FOR AN INDUSTRIAL SEPARATOR

Abstract

This study presents the process of obtaining a basic design for an industrial scale acoustic separator based on flow characteristics inside the separation chamber, on acoustic analysis within the chamber and calculated particle trajectories combining these two analyses. Adequate criteria for subsequent optimisation were evaluated. Results showed that positioning the piezoelectric transducer surfaces perpendicular to the flow direction and introducing chamber partitioning with multiple flow lanes to enforce laminar flow, resulted in high particle retention. The average particle displacement was found to be related to acoustic pressure in the fluid, showing large retention at peak pressures above 1 MPa or average pressures above 0.5 MPa for small ($10\ \mu\text{m}$), near buoyant ($1100\ \text{kg/m}^3$) particles at a flow speed of 3.5 cm/s, thus providing comprehensible criteria for subsequent optimisation.

This chapter was published as

H.J. Cappon and K.J. Keesman (2013) Design basis of industrial acoustic separators. In: Proceedings of the IEEE UFFC International Ultrasonics Symposium, Prague, 20-25 July

5.1 Introduction

Acoustic liquid-solid separation of suspensions has been studied over the last decades by various researchers [60, 35, 36, 57]. The most recent studies focus on miniaturising the separation system in order to sense or characterise the particles trapped [51]. The larger scale application of acoustic separation is limited to one commercial device, namely BioSep from Applikon (Metrohm-Applikon B.V., Schiedam, The Netherlands), which is capable of processing up to 200 L/day. BioSep applies ultrasound enhanced sedimentation by which particle agglomeration is enhanced by the ultrasonic field thus improving the settling characteristics of the particles. Other large scale applications (>200 L/day) have remained out of sight for a number of reasons:

1. Energy consumption - generating a standing wave at high ultrasonic frequencies (above 1 MHz) capable of catching particles requires a quickly alternating current at several volts, resulting in significant heat loss even at high Q factors [31];
2. Investment cost - the acoustic properties of the system are at best when its components are manufactured with high precision of fractions of wavelengths, which is comparable to fractions of mm [35, 23];
3. Advanced process control - control is needed to save energy, while maintaining system's performance, as minor changes to the circumstances (temperature, flow rate, particle properties, concentration) affect the separation.

Nevertheless, the separation efficiency of these larger systems is quite good (95% or higher at moderate energy consumption) [15]. Furthermore, there is no or little deterioration of quality of the filtered (biological) products [26], which also make them applicable as filters for biological cells or sludge particles [45]. Moreover, internals are not needed, so that pore blocking or clogging does not occur. Lastly, high value of the filtered particulate matter and/or the remaining fluid contributes to the feasibility of this separation process. Improving the efficiency of the system by optimisation will eventually make the technique attractive for industrial operation.

Experimental optimisation with changes made to a series of prototypes is an extensive and expensive method for system improvement. Numerical models, on the other hand, are a cost effective way of understanding, improving and optimising systems, whereas they may take quite some time for development and validation in order to be predictive. However, even in a numerical optimisation

study one needs to have at least some basic idea on what the separator should look like. Therefore, the aim of the paper is to provide the background of the choices to be made in the basic design process using a finite element (FE) model, and to identify adequate criteria for optimisation.

For any model to be predictive, model validation is required. The materials and material parameters used in the current FE model are based on earlier work performed on characterisation of an existing separator, including the piezoelectric transducer thereof [11, 14]. This knowledge provided confidence in the model needed for the current design update and subsequent optimisation.

5.2 Materials and methods

Basically, the separator to be designed consists of at least one piezoelectric transducer connected to a resonance chamber, with at least one inlet and one outlet. In a sequenced batch system, the inlet feeds the water with particulate matter into the chamber, the outlet contains the purified water, while the particles are retained within the resonance chamber. These particles can periodically be removed from the resonance chamber by draining either through the inlet or outlet, while directing the flow to a storage tank with a valve, or through a separate outlet. In a continuous flow-through system the concentrate and filtrate flows are split right after separation [34]. Several attempts have been made to make industrial continuous systems by applying frequency sweeps, frequency stepping or multiple transducers [55, 33]. The difficulty of process control combined with relatively low efficiency and high energy consumption do not contribute to a feasible solution for continuous, large scale (>200 L/day) processing. We therefore aimed at batchwise processing in this study.

Given these basic requirements, there are still numerous possible designs for an acoustic separator. In addition to that, there are numerous design parameters that can be varied during the design process. In this study, a step wise numerical approach was taken in order to obtain the best design possible. To start with, the flow direction and positioning of the piezoelectric transducer were studied. Secondly, the flow patterns, which are best suited for separation were evaluated. Thirdly, the acoustic properties were studied, thereby searching for suitable optimisation criteria at the final stage of the design process.

5.2.1 Transducer positioning and flow direction

The first step involved the location of the piezoelectric transducer with respect to the resonance chamber and the flow direction. A theoretical 2D square shaped resonator with one inlet and outlet was considered throughout this study. The assumed depth of the system is 20 mm. The resonator (Figure 5.1) consisted of two opposite, parallel transducers (1.016 mm thick) with a glue layer (0.04 mm) and a wall/matching layer (3.25 mm). The resonator chamber had a height and width of 30.5 wavelengths (app. 2.3 cm). The transducers combined with the chamber created a homogeneous acoustic pressure field at an eigenfrequency near 1.95 MHz. A parabolic shaped inlet flow with constant average flow rate u_{in} of 6 ml/s was applied from the bottom or the side edges, resulting in a maximum flow speed of 19.5 mm/s in the centre. In separators using ultrasound enhanced sedimentation, like BioSep, the flow is parallel to the transducer surface, which is bottom to top. The drag forces on the particles are then perpendicular to the main acoustic forces. The flow can also be chosen perpendicular to the transducer surface, from left to right, so that the primary acoustic forces counteract the particle drag forces. In fact, this approach was applied by Hawkes [34] in the h-shaped continuous separator, in which particles were kept from entering the upper outlet by means of acoustic forces. Logically speaking, the latter option, with the flow perpendicular to the transducer surface, is the better one, which will be verified here. An option which was simulated, but not shown here, is having the flow at a non-perpendicular angle with the transducer surface, which would result in a ultrasound enhanced layered separator.

5.2.2 Flow lane design

In a theoretical resonator (Figure 5.1) with the flow direction perpendicular to the transducer surface the inlet and outlet coincide with the transducers themselves, which is physically impossible. This means that the inlet and outlet need to be positioned at the top or the bottom of the chamber (in our 2D case) and that the flow direction needs to bend within the resonator. Calculating the flow within such chamber, using 5 mm wide inlet and outlet, resulted in a flow pattern which is far from uniform and even introduces an eddy current in the square shaped resonator (Figure 5.2). This can be solved by either lengthening the chamber between inlet and outlet, which will make the separator quite long and deteriorate the acoustic field, or by introducing multiple channels or flow lanes with adequate flow splitting. Splitting can be done by making multiple inlets and applying a series of valves before each inlet, but a better solution would be to make the geometrical

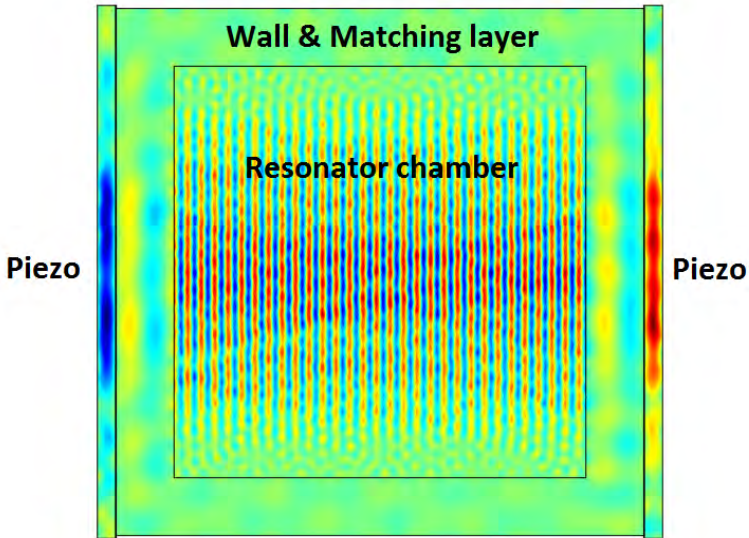


Figure 5.1: Side view of the model of the resonator chamber with two piezo transducers on the left and right. The transducers create the acoustic pressure field shown inside the chamber.

design such that the flow is split automatically, by incorporating partitions inside the chamber. The effect of various partition positions on the flow was evaluated by varying the position of individual partitions with a numerical Design of Experiments (DOE) study using a rectangular grid of the factors and calculating the resulting flow inside each lane.

5.2.3 Optimisation criteria

The ultimate aim is to retain as many particles as possible. This requires optimisation of the flow field and the acoustic field. Simulating particle displacement with peak acoustic pressures above, for instance, 1 MPa requires high computational efforts (near 2 hrs for 3s simulated time with Intel Core i5 3.1 GHz CPU and 3Gb RAM). Thus, optimising the shape of the resonator with combined acoustic-flow criteria is much faster than using a particle displacement criterion. Resonance can be detected by calculating or measuring the impedance or admittance of the piezoelectric transducer (see [11, 14]). At a given eigenfrequency, the acoustic pressure increases linearly with increasing voltage, but the admittance remains

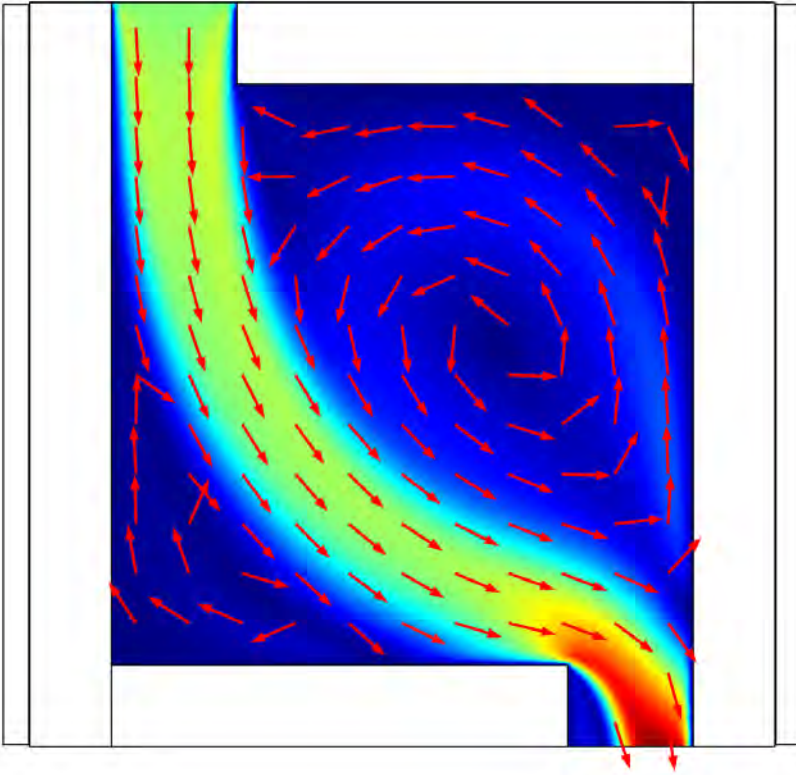


Figure 5.2: An example of a resonator chamber with short-circuiting flow pattern causing eddy currents

constant. Hence, average particle displacement was compared to the average (across the cross-sectional area of the chamber) absolute acoustic pressure in the chamber and to the (absolute) peak acoustic pressure at the eigenfrequency. For this purpose 25 equally distributed particles were released at the inlet and their (horizontal) positions at time 0 and after 1 s of simulated time were calculated and related to the pressure calculated, while stepping the voltage from 0 to 3 V with 0.5 V steps.

5.3 Results

Simulations determining particle displacement were performed in Comsol 4.3a using three sequential studies:

1. Frequency domain analysis incorporating the piezoelectric and acoustic field simulation. The eigenfrequency of the system was found here;
2. Stationary flow study calculating the flow inside the resonator chamber;
3. Time dependent particle tracing study calculating the particle trajectory using the calculated flow field of step 2, drag forces, gravity and acoustic forces at the eigenfrequency determined in step 1.

The frequency domain analysis resulted in a maximum acoustic pressure of 1.2 MPa at 1.955 MHz with an input voltage of 2V for the square shaped resonator. The average particle displacement, after 1s, of 25 particles released at the inlet was calculated. Results showed an average particle displacement of 13 mm in case of flow parallel to the transducer surface and 1.3 mm with the flow perpendicular to the surface. This result verified the idea that a flow direction perpendicular to the transducer surface retains the particles better.

In order to obtain a steady laminar flow inside the resonator, flow splitting was incorporated using multiple flow lanes. If equal length and perfectly aligned partitions inside the resonator are used, there will be a preferred flow path (Figure 5.3 left), but positioning the partitions more precisely on the basis of the DOE, gives the pattern as shown in Figure 5.3 (right). The associated flow shape inside the channels with aligned and adapted partitions is shown in Figure 5.4.

The dependency of the flow pattern at rates ranging from 1-5 ml/s is shown in Figure 5.5. Although a fully developed flow is only seen at 1 ml/s, no reverse flows or eddies occur. This observation indicates that a longer channel will ensure fully developed, laminar flow.

Combining the acoustic field at 10 V input with the flow patterns in the channels, while releasing particles at the inlet at time 0, resulted in the particle trajectories shown in Figure 5.6 (left) after 1s simulated time. The result without ultrasound is shown in Figure 5.6 (right). Although this is a non-optimised system with low voltage (10V) and relatively high flow rate (4 ml/s) a clear difference in particle retention can be observed.

Maximum particle retention incorporates an ideal flow field inside the resonance chamber and high peak or average pressure throughout the resonator. Optimising

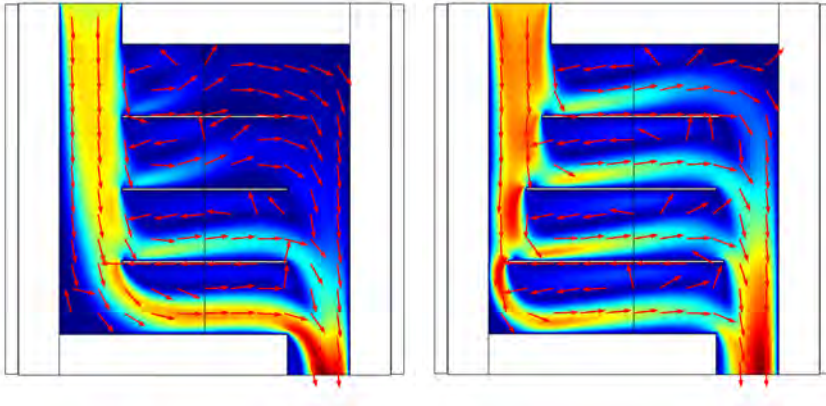


Figure 5.3: Preferred flow path inside a chamber with multiple, equally sized flow lanes (left) and inside a chamber applying geometrical flow splitting, resulting in almost equal flow in each lane (right).

the flow field, assuming an equally distributed acoustic pressure field, means that each lane should have an equal flow rate. Therefore, a good optimisation criterion is the minimisation of the sum of differences in flow rate between lanes.

In order to obtain a relevant optimisation criterion for the acoustic field, related to particle filtering, the calculated average and peak pressure inside the chamber were related to the average particle displacement, while varying the voltage in 0.5 V steps. Figure 5.7 shows the relationship between particle displacement and these pressure norms. Note that a peak acoustic pressure above 1 MPa or an average absolute acoustic pressure above 0.5 MPa corresponds to low particle displacement. Thus, at constant voltage, the criterion for the optimisation of the acoustic field is the acoustic pressure: the resonator chamber's shape should be such that the pressure is maximised. Because the average absolute acoustic pressure provides more insight into the entire pressure field, instead of a possibly localised peak pressure, this criterion will be used for optimisation.

5.4 Conclusions and discussion

The basic design of an acoustic separation unit was investigated in this study, using a series of numerical simulations based on a design of experiments approach (DOE). This resulted in choices in the positioning of the piezoelectric transducer surfaces perpendicular to the flow direction and in chamber partitioning by introducing multiple flow lanes to obtain laminar flow. The average particle dis-

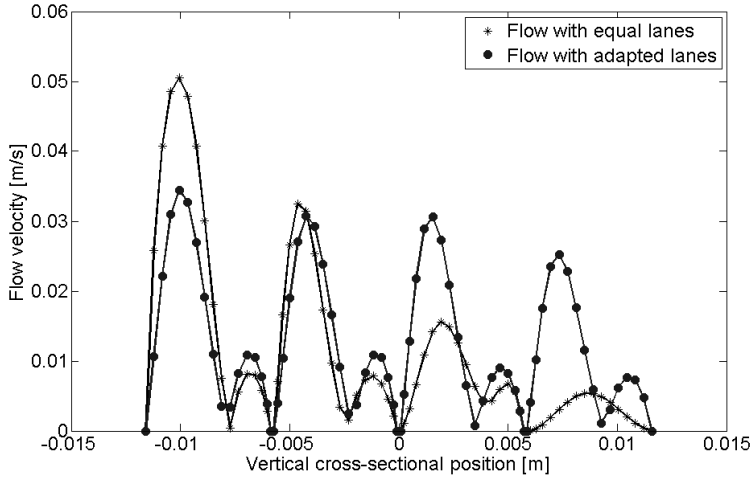


Figure 5.4: Flow pattern with aligned and adapted partitions inside the chamber at 4 ml/s.

placement was found to be related to acoustic pressure, showing large retention at pressures above 1 MPa or average absolute pressures above 0.5 MPa (for 10 μm , 1100 kg/m^3 particles and a flow speed of 3.5 cm/s), thus providing a comprehensible criterion for subsequent optimisation.

Manufacturing the best design found in this study will be difficult to realise, because it is not possible to reproduce the exact numerical dimensions. Therefore, the final design needs to be checked (numerically) on its robustness, meaning that small changes in the design should not affect the performance to a large extent. A sensitivity study with the most influencing parameters can be used to cover this last issue before manufacturing.

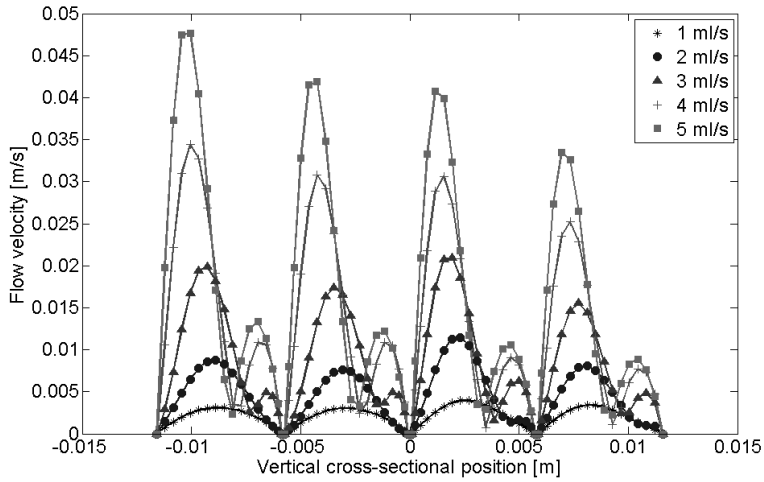


Figure 5.5: Flow pattern with adapted partitions and flow rates from 1-5 ml/s

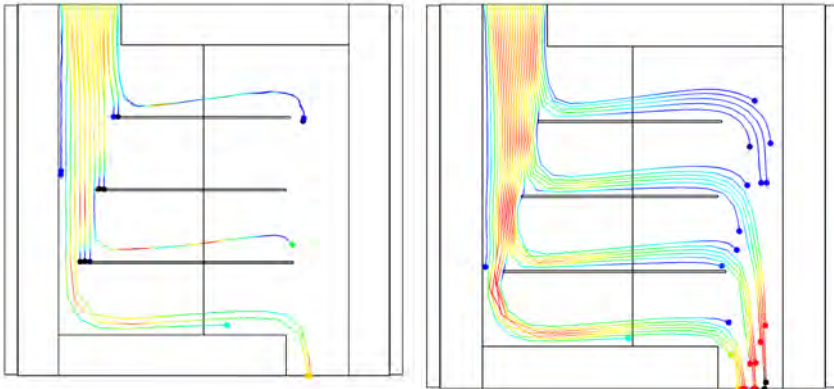


Figure 5.6: Particle trajectories of the combined acoustic field and flow simulations with ultrasound (left) and without ultrasound (right).

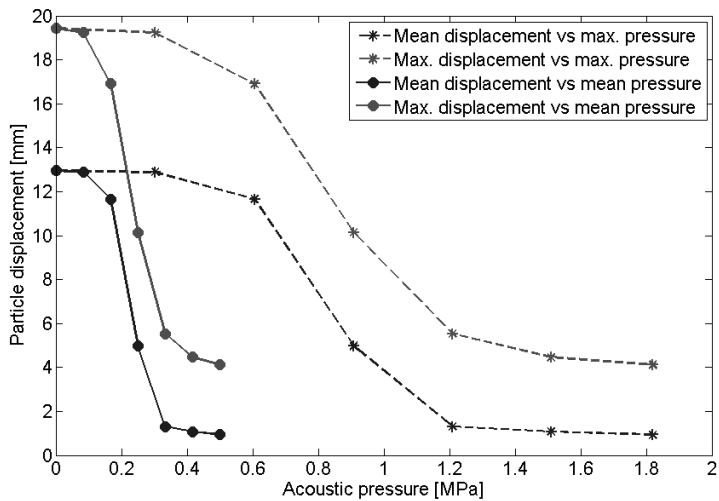


Figure 5.7: Particle displacement versus acoustic pressure norms in a square resonator chamber. With peak acoustic pressure above 1 MPa or average acoustic pressure above 0.5 MPa particle displacement clearly decreases.

6. INDUSTRIAL SCALE SEPARATOR DESIGN

Abstract

The aim of the present study is to optimise a basic ultrasonic standing wave separator design with respect to separation efficiency, throughput and energy consumption. The study involved more than 300 finite element model simulations in which acoustics, flow characteristics, particle retention and energy demand were evaluated. The methodology, using a design of experiments approach, showed that it was possible to improve system performance based on acoustic pressure profiles, separation efficiency and flow robustness. Compromising the energy consumption and aiming for maximum separation efficiency with a laminar stable flow up to 5 ml/s resulted in a separator with inner dimensions of 70 mm length, 20 mm width and 28.5 mm height using two transducers perpendicular to the direction of flow and three parallel flow lanes with 9.5 mm height each and operating at approximately 1.95 MHz.

6.1 Introduction

Acoustic separation technology applies ultrasonic acoustic standing waves (USW) to retain particulate matter in specific locations within a resonance chamber. When suspensions are fed into the chamber, the system is able to separate the solids from the liquid, thus forming a filter [34, 38, 31]. Recent USW research has focused mainly on miniaturising the separation system for particle detection, characterisation and manipulation [51, 29]. The only larger-scale (up to 4 l/h), commercial device, aimed at filtering biological material and called BioSep (Metrohm-Applikon B.V., Schiedam, The Netherlands), has already been around for over a decade. Widespread usage of large-scale USW separators is limited by various drawbacks, like high energy demand and heat development, limited throughput and investment cost. On the other hand, the potential of separating high value (biological) components without deterioration of quality [26] offers various potential applications, like harvesting (neutral buoyant) algae [9] and retention of biological flocs in waste water treatment [45]. Instead of building many prototype separators and testing these in practise, separator improvement aiming at a higher performance of such systems can also be established by applying numerical models to support the study of the characteristics of acoustic devices and therefrom proposing changes for improvement.

A basic design study, finding the most important design considerations for system improvement, was performed in [12], setting the basis for the current study. Therefore, the aim of the present study is to optimise this basic design to a USW separator with high separation (retention) efficiency, high throughput and preferably low energy consumption. This design study involves finite element (FE) model simulations of acoustics, flow characteristics, particle retention and energy demand.

6.2 Materials and methods

6.2.1 Methodology

Particle retention simulations require large amounts of CPU time and since optimisation generally requires many simulations, optimising to maximum particle retention is a very time consuming process. Since the results of the acoustics and flow simulations are fed into the particle retention simulations, optimisation with respect to acoustics and flow was assumed to be an appropriate procedure for maximising particle retention. After the optimisation, the particle retention

efficiency was evaluated numerically, thus verifying this methodology.

6.2.2 Basic configuration

Our basic design composed of a resonance chamber with two transducers facing each other on either side of the chamber. The flow inside the chamber is perpendicular to the faces of the transducers, which means that the flow needs to be bent inside the chamber to achieve this. For appropriate particle retention a laminar flow needed to be pursued, which was established by splitting the chamber into various flow lanes. Equally sized lanes proved to provide an unequal flow regime and therefore, geometrical changes were introduced to equalise the flow in each lane (see [12] for the pre-study), resulting in a three-lane system as shown in Figure 6.1. This basic configuration was evaluated by experiments, showing promising results.

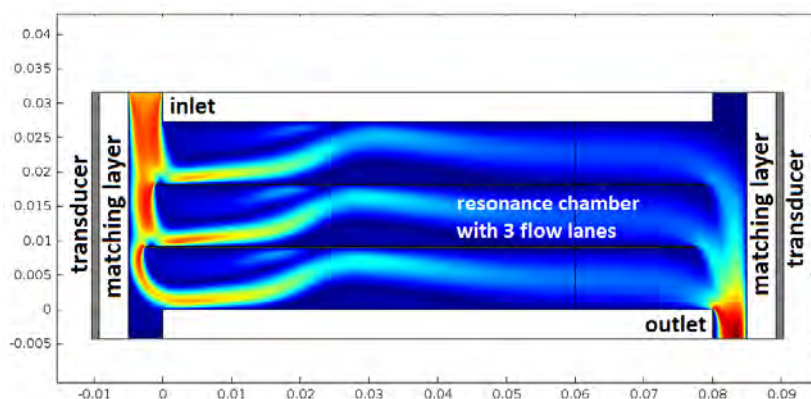


Figure 6.1: Example of the 2D resonator FE model consisting of two transducers on either side of the resonator, an inlet (top left) and outlet (bottom right) and three flow lanes with equalised flow velocity

6.2.3 FE model

The 2D (side view) FE model consisted of three components: the piezoelectric transducers, glass walls, which also serve as matching layer, and a resonance chamber with flow dividers making up three flow lanes (see Figure 6.1). Four in- and outlets were modelled of which only two were used. The full geometry of the basic configuration model was described by a minimum number of eight

parameters: separator length, separator depth (20 mm), flow lane height (3 lanes), flow divider thickness (0.15 mm), in/outlet width (5 mm), matching layer thickness, epoxy glue thickness (40 μm) and transducer thickness (1.035 mm). The particle properties were set to 10 μm diameter and 1100 kg/m^3 density and a bulk modulus of 4.5 GPa.

The full analysis of the model consists of three steps:

1. Stationary flow analysis with flow rates of 1-5 ml/s. At the inlet the flow speed is specified, the outlet has zero pressure;
2. Frequency domain analysis of the piezoelectric transducers with a fixed voltage of 10V AC per transducer and coupled to the filled resonance chamber to find the eigenfrequency of the system. The admittance was calculated with the transducers parallel connected;
3. Time dependent particle tracing analysis, combining step 1 and 2, to determine the particle trajectories at the eigenfrequency found.

The first two steps require different FE meshes. The stationary flow analysis runs easily with a coarse triangular mesh with an element size of 1 mm inside the resonator chamber. However, the second step (frequency domain analysis) requires a mesh with the largest element size being a fraction of the wavelength, near 0.15 mm in that same chamber. In the third step, the result of the second step is projected onto the mesh of the first and the particle trajectory is then calculated. Unfortunately, a 1 mm mesh is too coarse for the projection of the results of the second step. Therefore, the first mesh was refined to a maximum of half a wavelength element size for proper projection on the second mesh.

The piezoelectric transducers (1.035 mm thick) and the glue layer (40 μm thick) were divided into 15 and 10 elements along their thickness, respectively. The matching layers elements were set to a maximum element size near 0.5 mm. The models acquired in this way for steps 1-3 contained up to 350.000 elements for a 10 cm long separator system.

The acoustic model was set up using two coupled domains: a piezoelectric domain for the electro-mechanical vibration and a pressure acoustics domain for the sound propagation in the fluid. The piezoelectric transducer, the epoxy adhesive layer and the separator were assigned to the piezoelectric domain. Glass and epoxy adhesive were modelled as an anisotropic, decoupled (non-electric) material. The coupling between the two domains across the boundary was as follows:

- The acoustic pressure of the water was modelled as distributed force (force per unit length) on the inner glass walls of the separator, thus having continuity in pressure;
- The mechanical acceleration of the glass walls was similar to the acoustic acceleration of the water inside the separator, thus having continuity in acceleration;

Simulations were run with Comsol 4.3a on an Intel Core i5 3.1GHz CPU with 3Gb RAM (and 1Gb assigned swap space). Flow analysis simulations lasted less than a minute, while particle trajectory simulations took up to 12 hours for 5 seconds of simulated time. These 5 seconds were sufficient to obtain a stable particle displacement (see section 6.3 for details).

6.2.4 Design criteria and variables

The basic design still involved many parameters that could be used to improve the efficiency. Earlier studies showed the influence of resonance chamber size, matching layer thickness and even glue layer thickness [36, 14]. The size of the chamber and the thickness of the matching layer (between transducer and water) can be varied rather easily before manufacturing, whereas a fixed thickness of the glue layer is more difficult to realise in reality. Thus, decision variables for system optimisation are the resonator chamber size (i.e. length of the flow path and lane height) and matching layer thickness. Table 6.1 provides the ranges for each of the decision variables.

The eigenfrequency of the entire system is mainly influenced by the eigenfrequency of the transducer and the thickness of various layers in the system (epoxy glue, glass and water). An adequate transducer model was obtained earlier [11]. The transducers used for prototyping were off-the-shelf Noliac NCE41 1 mm thick transducers, which are different from the modelled SPC140 transducers used in [11]. The new design was tuned with respect to the NCE41 transducers. The eigenfrequency of the NCE41 transducers was measured to be near 1.95 MHz and thus the thickness of the transducer model was chosen such that its eigenfrequency corresponded to the measured eigenfrequency (thickness 1.035 mm).

The acoustic responses of the resonator were evaluated using frequency sweeps between 1.82 and 1.97 MHz with 5 kHz steps to find the eigenfrequencies of the system. The voltage on the transducers was 10 V. In order to study the en-

tire resonance field, the absolute acoustic pressure, averaged over the entire (2D modelled) chamber was taken as a resonance criterion function and is given by:

$$|\bar{p}| = \frac{\sum(|Re(p_i)|A_i)}{\sum A_i} \quad (6.1)$$

with p_i the pressure in [Pa] and A_i the area of each element i in the FE model of the resonance chamber in [m²].

However, high (local) peaks in the acoustic pressure field may cause high average values, which does not necessarily mean that the separation is optimal. In our previous study we found that maximum absolute acoustic pressures above 1 MPa and averaged absolute pressures above 0.5 MPa adequately trapped particles of 10 μ m and 1100 kg/m³ at a flow speed of 20 mm/s. Hence, in addition to function 6.1 and as an alternative criterion function, the 2D area with absolute pressure above 1 MPa was calculated as a fraction of the total 2D chamber area and is given by:

$$AR = \frac{\sum A_{i(|p|>1MPa)}}{\sum A_i} \quad (6.2)$$

Secondly, not only the pressure is of importance, but also the power, which is linearly related to the admittance at constant voltage:

$$P = V^2 Re(Y) \quad (6.3)$$

with P power in [W], V voltage in [V] and Y admittance in [S].

The criterion functions to evaluate the flow are the maximum flow speed U_{max} and the relative difference of flow speed U_r in each lane, where U_r is defined as:

$$U_r = \sum_{[i,j]} |U_{imax} - U_{jmax}| \frac{h_{lane}}{h_{ref}} \quad (6.4)$$

with U_{max} the maximum flow speed in a lane, h_{lane} the height of the flow lane and h_{ref} a reference height of 5 mm, with $[i, j] \in \{[1, 2]; [1, 3]; [2, 3]\}$. The multiplication by $\frac{h_{lane}}{h_{ref}}$ was used to compensate for different flow lane heights.

Consequently, the aim for the acoustic simulations is to find a high pressure area ratio AR and a low (real) admittance $Re(Y)$ for fixed voltage, whereas the aim for the flow simulations is to obtain a low maximum flow velocity U_{max} and a low flow velocity difference U_r .

6.2.5 Simulation strategy

Simulations were run with Comsol 4.3a coupled with Matlab R2012b. Comsol provides the FE modelling environment and Matlab an easy environment for pre- and post-processing of the numerical data. Two sets of simulations were run using a Design of Experiments (DOE) approach in order to determine a good starting point for subsequent design improvement. The first set was a full-factorial DOE with two factors: the resonator chamber length and matching layer thickness (rectangular grid, 7×10 simulations, second column in Table 6.1). This set provided too little insight into the entire design space (Section 6.3). Therefore, a second larger series was launched, being a (multiple) randomly sampled Latin Hypercube DOE with three factors: chamber length, matching layer thickness and flow lane height. This series resulted in 180 simulations randomly covering the entire design space (column 3, Table 6.1), adding up to a total of 250 simulations.

Table 6.1: Ranges of factors (LH = Latin Hypercube; FF = Full Factorial; Ac. = Acoustic domain; Fl. = flow domain)

Factor	Range				Units
	Ac. FF	LH Ac. + Fl.	Fl. FF	Combined LH	
Separator length	35-65	30-100	30-100	70-75 / 80-85	[mm]
Matching layer thickness	2.75-5.0	2.5-4.5	-	2.9-3.1 / 4.15-4.25	[mm]
Flow lane height	-	5-10	5-10	8.5-9.5	[mm]
Number of simulations	70	180	48	12	-

Within the factor ranges of Table 6.1 the flow patterns were also evaluated using a constant flow of 3 ml/s. First, a full factorial DOE with two factors, separator length and lane height (8×6 grid) was conducted (column 4). Subsequently, also the 180 simulations of the previous DOE were evaluated with respect to flow (column 3).

The best starting points at various resonance chamber sizes were taken from the DOE's and fed into a new, more narrow DOE of 12 simulations (Latin Hypercube, last column in Table 6.1). Initially, a formal optimisation procedure (minimum search algorithm) was implemented. However, the response surfaces appeared to be extremely irregular, so that this algorithm (and others) ended up in local minima and provided no improvement.

The acoustic simulations together with the flow simulations determined the main dimensions of the separator to be made, which needed to be small, robust and efficient. Robustness of the model was checked by introducing small variations to the parameters of the model and evaluating the influence on the selected criterion functions. Changes were made to the separator length (0.5 mm), matching layer

thickness (0.05 mm) and flow lane height (0.1 mm). Finally, particle retention was evaluated with particle tracing simulations through comparison of the maximum and average travelled distance of 25 particles, released at the inlet going with the flow, with and without ultrasound.

6.3 Results

The variables related to resonator size, i.e. separator length, flow lane height and matching layer thickness, were changed within the limits provided in Table 6.1. This resulted in 262 simulations in all for the acoustics, and 240 simulations for the flow conditions.

6.3.1 Acoustics

Figures 6.2, 6.3 and 6.4 show the relation between the averaged absolute pressure $|\bar{p}|$ and separator length, matching layer thickness and flow lane height, respectively. Figure 6.2 shows that the pressure tends to decrease with increasing separator length. This effect, although rather small, is mainly caused by attenuation of the water ($\alpha = 0.87 \text{ dB/m @ } 20^\circ\text{C}$) inside the separator, indicating that short separators have a preference, from an acoustic point of view. Figure 6.3 shows that the matching layer thickness is of large influence on the pressure obtained. If the matching layer thickness is near $2n + \frac{1}{2}$ wavelengths, then resonance occurs. In this case the eigenfrequency is not always 1.95 MHz, so that resonance is not always detected at exactly the same thickness (see Figure 6.3). Nevertheless, a matching layer thickness of 3.0 or 4.25 mm seems quite appropriate. According to Figure 6.4 the height of each flow lane does not really seem to matter to the acoustic properties of the system, which gives way to decoupled optimisation with respect to flow.

Good separation is expected, when a large area of the separator has high acoustic pressure. Figure 6.5 shows the area ratio AR versus the real admittance, which is a measure for the power P at a fixed voltage. The best separation is obtained with a very high AR whereas low energy consumption is obtained at low admittance. The two encircled points with a high average absolute pressure, over 1.5 MPa and AR larger than 0.5, both resulted from small separators, only 35 mm long. The chance of obtaining a laminar flow pattern inside these separators is small. A separator (indicated by a square box in Figure 6.5) with 1.15 MPa average absolute pressure and an AR of 0.49, which should be sufficient for particle trapping,

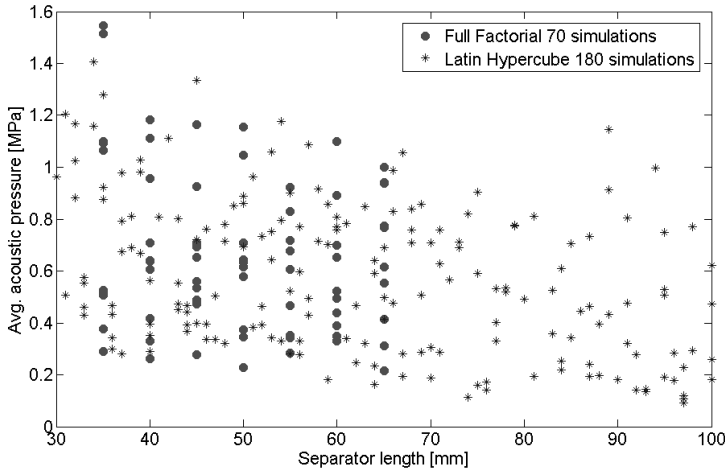


Figure 6.2: Relation between the averaged absolute pressure and separator length

had a length of 89 mm. It is expected that this separator will also show good flow characteristics.

Considering energy efficiency, a high area ratio with low admittance is the best solution. Dividing the ratio AR by the real admittance $Re(Y)$ and plotting the result versus the average absolute acoustic pressure leads to Figure 6.6. The highest (encircled) point in this scatter plot was obtained with a 56 mm long separator, which had adequate flow characteristics, but a high maximum flow velocity of 15 mm/s at 3 ml/s flow rate. Note that this system has an average absolute pressure of 0.6 MPa, which means it should be able to trap the particles easily [12].

6.3.2 Flow characteristics

Now that the acoustic properties of the system are analysed, the next step is to evaluate the flow characteristics. A total of 228 simulations in two DOE series (columns 3 and 4, Table 6.1) were performed at flow rates of 3 ml/s. The evaluation was based on the maximum flow velocity U_{max} inside the separator flow lanes and the velocity difference criterion U_r . Figures 6.7, 6.8 and 6.9 show the dependency of these performance indicators on separator length and flow lane height. Figure 6.7 shows that the lower bound on U_{max} generally decreases with increasing separator length. At separator lengths above 70 mm there is almost no further decrease, indicated by the lower dashed lines, which means that the flow

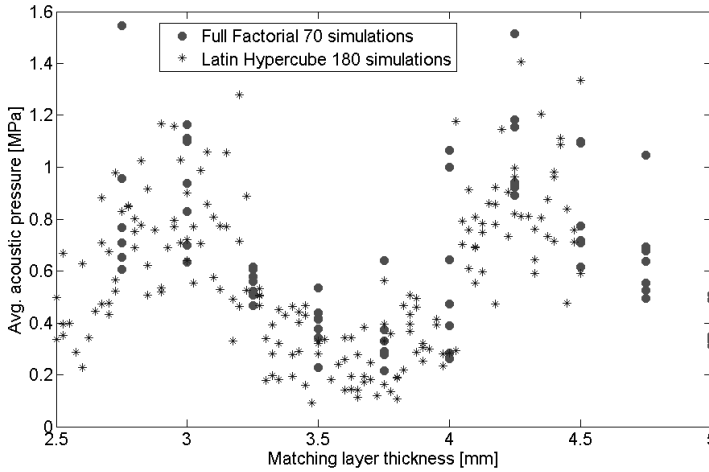


Figure 6.3: Relation between the averaged absolute pressure and matching layer thickness

inside the separator was fully developed. With smaller flow lane height, the flow development was quicker, which means that a shorter separator length with fully developed flow, down to 40 mm length, is then possible (see the dashed upper bound on U_{max}). However, if the flow rate increases the length needed for fully developed flow will also increase. Moreover, large flow lane heights mean lower flow velocities and thus easier particle trapping.

Figure 6.8 shows that the maximum flow velocity U_{max} decreases with increasing flow lane height, which was a result of increasing separator cross-sectional area for a fixed flow rate. Also, high values of U_{max} were found at high flow lane heights due to short separators with undeveloped flow showing high local flow peaks.

The 3D surface in Figure 6.9 shows the dependency of (relative) flow lane differences U_r on separator length and lane height, based on a full factorial DOE of 48 simulations. This figure shows a minimum at approximately 70 mm separator length and 9 mm flow lane height. Generally speaking, the total separator length needs to be larger than 60 mm and the flow lanes larger than 9 mm in order to have adequate laminar flow, even at higher flow rates up to 5 ml/s.

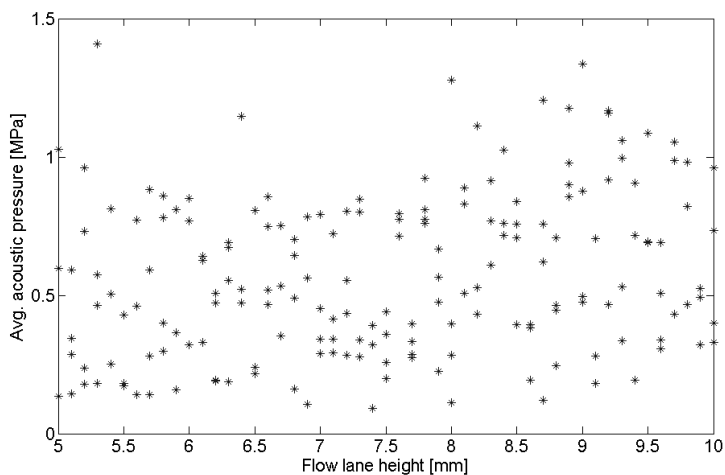


Figure 6.4: Relation between the averaged absolute pressure and flow lane height (180 simulations)

6.4 Compromised design

The best results of all simulations are summarised in Table 6.2, showing the corresponding best performing criterion in bold. The best acoustic results - apart from the very short (35 mm) separators - were obtained with a separator length of 56 mm (low energy) and 89 mm (high pressure) with a corresponding flow lane height of 5.0 and 6.4 mm, respectively. The flow velocity in these chambers was still relatively high, 15 and 11 mm/s, whereas the overall minimum went down to 7 mm/s. The flow characteristics, however, are best at larger flow lane heights around 9 mm and larger separator lengths above 60 mm. Because the flow is independent of the matching layer thickness, the matching layer thickness is chosen to best fit the acoustics related criteria. A good matching layer thickness is around 3 or around 4.25 mm (see Figure 6.3), contributing to high pressure.

Narrowing down the DOE to a separator length of 70-75 mm or 80-85 mm, the matching layer thickness to 2.9-3.1 or 4.15-4.25 mm and the flow lane height to 8.5-9.5 mm (last column Table 6.1), a separator with good acoustic and flow characteristics was found with a length of 70 mm, matching layer thickness of 4.2 mm and a lane height of 9.5 mm (resonator chamber dimensions: 70×20×28.5 mm). The average pressure reached was 1.24 MPa at 1.95 MHz and the area

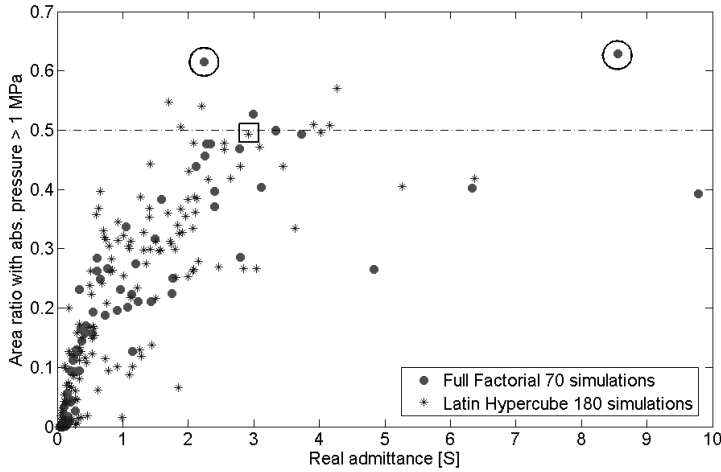


Figure 6.5: Area ratio with pressure above 1 MPa versus real admittance Y

ratio AR was 0.56, but the admittance $Re(Y)$ was 5.71 S^{-1} , meaning that this separator has very good characteristics, but is not energy efficient, which limits its application to recovery of high value particles.

Table 6.2: Optimal separator designs based on different criteria, shown in bold

Separator length [mm]	Matching layer [mm]	Lane height [mm]	f_{eig} [MHz]	$ p $ [MPa]	$Re(Y)$ [S]	AR [-]	U_{max} [mm/s]	U_r [mm/s]
35	4.25	8.0	1.945	1.51	8.6	0.63	12	3.6
35	2.75	8.0	1.920	1.54	2.2	0.62	12	3.6
62	3.275	9.2	1.925	0.47	0.22	0.09	8	0.5
87	4.375	10.0	1.880	0.73	0.92	0.31	7	0.7
89	4.2	6.4	1.960	1.15	2.92	0.49	11	4.7
56	4.125	5.0	1.965	0.60	0.18	0.20	15	5.8^2
51	4.4	10.0	1.895	0.96	2.30	0.42	9	4.4^3
Final design								
70	4.2	9.5	1.950	1.24	5.71	0.56	8	0.9

Robustness of this optimal design was checked by introducing small changes to the nominal factor values and evaluating the changes in the selected criteria. The three factors were varied in three steps each, including combined variations, thus resulting in 27 variations. As small eigenfrequency shifts were expected, the frequency sweeps were narrowed down to 1.92-1.97 MHz with 1.0 kHz steps. Table

¹Such admittance will result in unrealistically high currents in practise; see Discussion.

²Configuration with a high area to admittance ratio.

³Configuration with a high average pressure in one x -position, see Discussion, section 6.5.

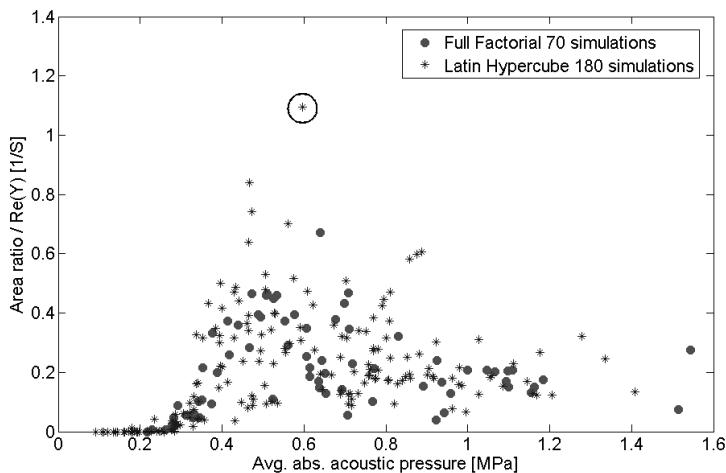


Figure 6.6: Area ratio divided by $Re(Y)$ versus average absolute pressure

6.3 shows the influence of individual changes of the factors and the maximum effect of combined changes to the selected criteria. Appendix A shows the results of all 27 variations and indicates that the effect of these variations may be quite large, up to 147% (the maximum $Re(Y)$ found is 14.08 S). Overall, the average pressure and area ratio remained high, with a calculated minimum of 1.04 MPa and 0.42, respectively, for a separator with 70.0 mm length, 4.15 mm matching layer thickness and 9.4 mm flow lane height. The changes in separator length and matching layer thickness mainly affect $Re(Y)$ and thus the energy requirement of the system. The flow characteristics hardly change, although U_r is sensitive to small changes in terms of percentage.

6.4.1 Particle tracing

For the new nominal design, with a separator length of 70 mm, matching layer thickness of 4.2 mm and a lane height of 9.5 mm and operated at 1.95 MHz, a particle tracing simulation was performed. The flow patterns inside this separator are shown in Figure 6.10 at various flow rates, from 1-5 ml/s. U_{max} is 20 mm/s at 5 ml/s, which means that particles should be retained when the average absolute pressure is above 0.5 MPa [12]. The maximum and average horizontal distances travelled by the 25 particles with and without ultrasound were taken as an evaluation criterion. The particle retention in this separator at 5 ml/s is 100%, already established after two of the five seconds simulation time. Table 6.4 shows

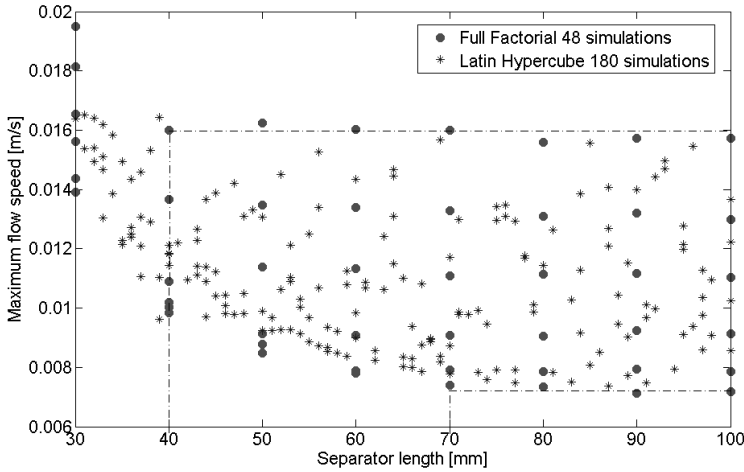


Figure 6.7: Maximum flow velocity versus separator length

the particle displacements with and without ultrasound, indicating that the new design is able to trap all particles.

6.5 Discussion

This study provides a detailed numerical procedure to develop an ultrasonic separator based on a selected basic design using predefined criteria like acoustic pressure, flow velocity and energy consumption with a preset input voltage of 10 V. The best performing system chosen in this study is based on maximum separation efficiency, compromising on energy consumption. Lowering energy consumption by reducing the input voltage will compromise on particle retention efficiency. The best design (Table 6.2) was chosen to retain suspended particles (near neutral buoyant, 10 μm diameter, 1100 kg/m^3). This is not necessarily the optimal design because of the discrete optimisation procedure based on the DOE schemes in Table 6.1. Other separation targets, like ultrasound enhanced sedimentation, may result in different optimal designs.

The model used for the current design process was based on earlier validated models of the transducer and ultrasonic separator. Validation of the best performing design found here should still be performed by actually building and testing the separator. In fact, the construction should be done with similar transducers and materials for the model to be valid. It is likely that the transducer charac-

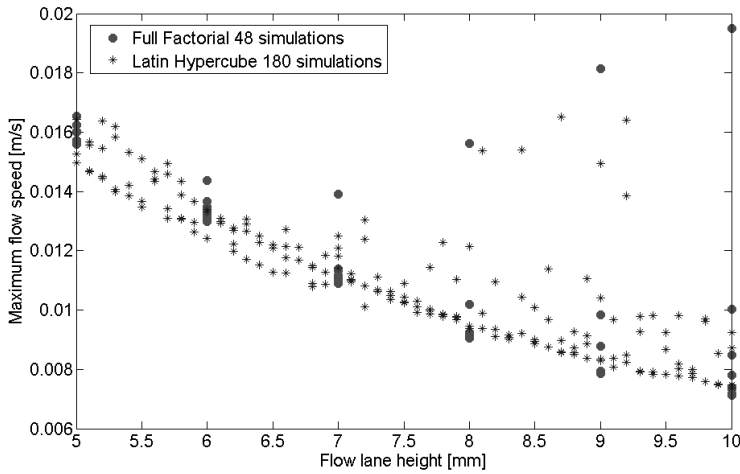


Figure 6.8: Maximum flow velocity versus separator lane height

teristics are not exactly similar and the material and geometrical properties will deviate from the properties provided, resulting in a sub-optimal separator. The only way to really validate the model in such case is to build the separator, characterise it and implement the findings in the model, thus detailing the model in an iterative manner. Without this iteration the efficiency of the built separator will not be as good as the current best design found in this study, although we assume that the insights provided here will help improving existing systems. Since the ultimate aim was not on model building and validation, but on presenting an efficient separator design procedure, such iteration is beyond the scope of the paper.

The results show large variations in calculated admittance. High admittance will induce extreme and practically unrealistic electrical currents, requiring operation at a lower voltage. This issue can be partly solved by connecting the transducers in series, decreasing the admittance to a quarter of the values given. Secondly, actual manufacturing is likely to introduce additional inaccuracies, lowering the admittance even further. Finally, appendix B shows that the most energy efficient operation will not occur at the main eigenfrequency, where high pressure and high admittance are found, but at a frequency with lower admittance and yet adequate average absolute pressure for particle trapping. For the new nominal design this implies a frequency shift from 1.95 MHz to approximately 1.935 MHz, where $Re(Y)$ drops from 5.71 to 0.18 S and the power from 571 (at 10 V) to 28 W (at 12.7 V). Figure 6.11 shows the frequency dependency of power at 10 V input, minimum power (required for 0.5 MPa average absolute pressure) and the

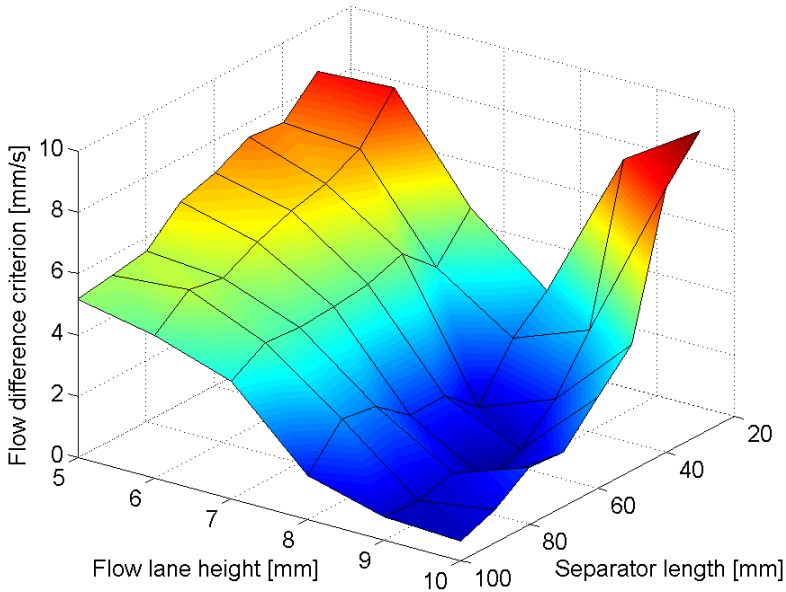


Figure 6.9: Flow lane criterion versus separator length and flow lane height based on a full factorial DOE of 48 simulations

average absolute pressure for the nominal design at 10 V input.

Average absolute acoustic pressures above 0.5 MPa are able to retain the small-sized particles of $10\ \mu\text{m}$ used here. Such pressure fields have high local pressure peaks above 1 MPa. In practise, peak pressures above 1 MPa may induce other (non-linear) effects in the fluid, like acoustic streaming or even cavitation [28], which were not taken into account in these simulations. Real world experiments will indicate whether these phenomena will occur.

The criteria chosen for separator performance determine the solution (see Table 6.2). If average pressure, real admittance, area ratio or flow characteristics are used as individual evaluation criteria, large differences between the 'best systems' will be found. In fact, the ultimate aim of a separator is to trap each particle between inlet and outlet. Hence, if each particle encounters a single boundary with high pressure along its trajectory, the particle will not be able to travel beyond this boundary (if the flow speed is not too high). This pressure boundary then serves as a wall. Consequently, searching along the length of a separator for one or several boundaries perpendicular to the flow with uniform high pressure

Table 6.3: Sensitivity of responses to changes in the factors, changing one factor at a time. The last row shows the maximum deviation found, while changing all factors simultaneously.

Factor	value	$ p $ [MPa]	$Re(Y)$ [S]	AR [-]	U_{max} [mm/s]	U_r [mm/s]
Design basis	[mm]	1.24	5.71	0.56	8	1.0
Separator length basis = 70 mm	69.5	1.49 (+20%)	11.10 (94%)	0.59 (6%)	8 (1%)	1.0 (20%)
	70.5	1.08 (-13%)	14.08 (147%)	0.48 (-14%)	8 (0%)	0.9 (3%)
Matching layer thickness basis = 4.2 mm	4.15	1.24 (0%)	7.78 (36%)	0.52 (-7%)	8 (0%)	0.9 (3%)
	4.25	1.09 (-12%)	10.48 (84%)	0.50 (-10%)	8 (0%)	1.0 (15%)
Lane height basis = 9.5 mm	9.4	1.41 (13%)	2.90 (-49%)	0.57 (2%)	8 (1%)	1.0 (22%)
	9.6	1.24 (0%)	5.12 (-10%)	0.53 (-6%)	8 (0%)	1.1 (24%)
Simultaneous changes	-	[-16,20]%	[-63,147]%	[-14,7]%	[-1,1]%	[-6,34]%

Table 6.4: Particle displacement results at various flow rates in the final design. A maximum displacement of 66 mm and average displacement of 63 mm indicates that no particles are trapped.

Flow (ml/s)	Maximum displacement [mm]	Average displacement [mm]
3 (no sound)	53	43
3 (sound)	0	0
4 (no sound)	66	63
4 (sound)	44	11
5 (no sound)	66	63
5 (sound)	20	3

should also provide us with an adequate solution. Although theoretically correct, such criterion was not found to be robust, as small changes to the dimensions resulted in large changes to local pressure minima, which in turn deemed the separator unsatisfactory. Furthermore, changes in local minima do not necessarily mean that particles will not be trapped. In that sense such a logical, though local criterion, is not adequate for our evaluation of the designs.

The separator designed by the procedure presented in this study are highly sensitive to small changes (see Table 6.3), which will definitely occur during manufacturing. This means that the efficiency found numerically will, in general, not be reached in reality. The results from Table 6.2 compared to those in Table 6.3 indicate that even the worst 'best separator' performs better than the separators found in the initial sets of DOE's. Further numerical optimisation, however, is not useful, as it will easily end up in a local minimum and will only tighten the

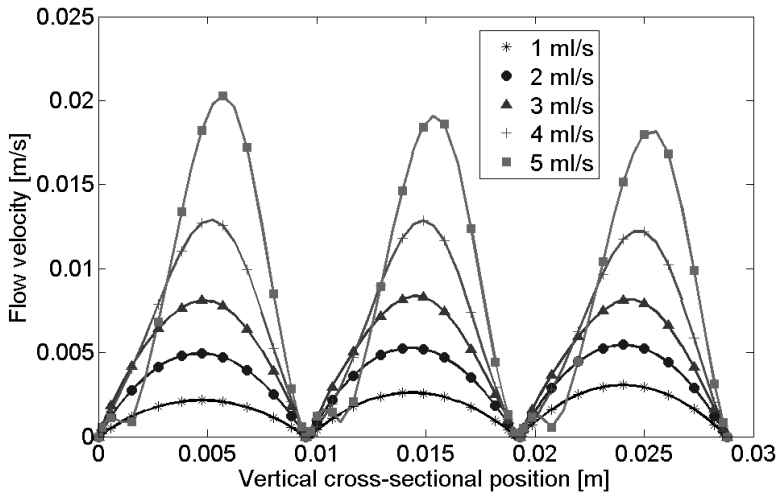


Figure 6.10: Flow velocity profile inside each lane at flow rates of 1-5 ml/s (left: lower lane, right: upper lane)

specifications of the dimensions even further, most likely beyond sensible accuracy.

6.6 Conclusions

A methodology for separator design was presented, based on a pre-selected basic configuration with the transducers perpendicular to the direction of the flow and the flow divided into three parallel lanes. It was shown that it is possible to improve system performance based on a set of relevant criteria, like energy consumption, separation efficiency and flow robustness. Compromising the energy consumption and aiming for maximum particle retention with a laminar stable flow up to 5 ml/s (i.e. >400 l/day) provided a separator with chamber dimensions of 70 mm length, 20 mm width and 28.5 mm height (i.e. a volume of approximately 0.04 l) and to be operated at 1.935 MHz. The full factorial based sensitivity study, with variations up to 10% , showed that high pressure levels and associated particle retention could be maintained, proving the robustness of the design procedure.

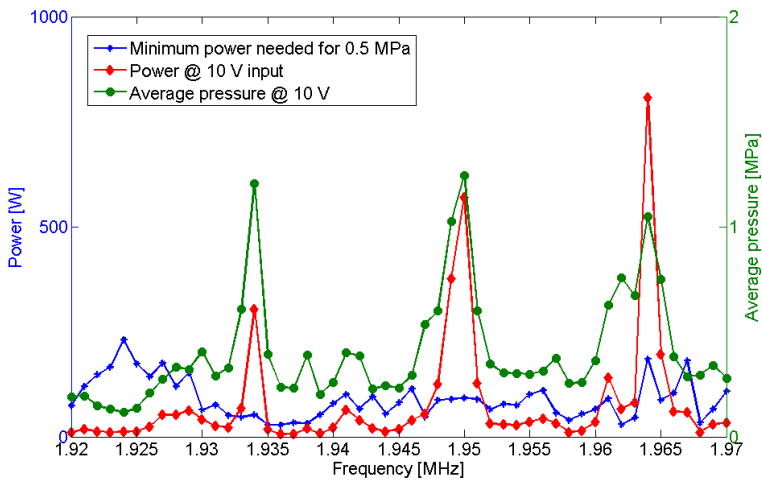


Figure 6.11: Frequency dependency of the minimum power required to obtain 0.5 MPa average pressure and the power at 10 V input (on the left y-axis) and average absolute pressure (on the right y-axis) for the new nominal design.

7. INDUSTRIAL SCALE SEPARATOR EVALUATION

Abstract

This study presents the evaluation of a new ultrasonic particle filter, which was designed in a combined numerical-experimental approach. The particle filter is a three channel glass device of 70×28×20 mm with four in/outlet ports. It was operated in sequenced batch mode - 150 s of filtering followed by a 20 s backwash with filtrate, which removed the collected particles from the separator as concentrate. The separation efficiency was evaluated at three flow rates ranging from 1 to 3 ml/s, using a stock suspension of insoluble potato starch of 1 g/l (1000 ppm). Concentrations of stock, filtrate and concentrate were measured using a turbidity meter and significant effects of particle concentration were measured at both outlets of the process. The maximum filtration efficiency and concentration efficiency were 54% and 76%, respectively. The performance found was lower than obtained in the model based design study. The deviation in performance is mainly a result of (i) the pulsation of the feed pumps, (ii) differences between the model and the actual prototype, (iii) the limited power supply used and (iv) (too) small particles occurring in the starch suspension.

This chapter was submitted to Separation and Purification Technology as
H.J. Cappon, K.J. Keesman, Experimental evaluation of a model-based design of an acoustic separator

7.1 Introduction

The increasing need for water and material reuse drives the innovation of technology. One of the new technologies being investigated for water purification and recycling or constituent recovery is ultrasonic particle separation, which is the subject of the current study. In this technique, mainly known from cell and particle harvesting in biotechnology [20, 31, 9, 55] and standing wave particle manipulators [29, 18, 25], high frequency ultrasound (MHz range) is used to concentrate suspended particles in water. This technique is especially interesting for harvesting or removal of particles or cells with an almost neutral buoyancy with respect to the surrounding liquid [30].

The aim of this study is to experimentally evaluate a model-based ultrasonic particle separator design with respect to particle retention and flow characteristics. The design of the separator was presented in [13] and was geometrically optimised to laminar flow and maximum particle retention at minimal energy consumption. This separator is meant to operate at a frequency of 1.95 MHz and at flow rates up to 5 ml/s (18 l/hr) with a separation efficiency near 100%. Although numerical evaluations pointed out that it should adequately trap near neutral particles, with a diameter of 10 μm (and larger) and a density of 1100 kg/m^3 , experimental evaluations are needed to evaluate the actual performance. Given the tight specifications for manufacturing these separators and the sensitivity to various factors, like temperature, particle size and driving voltage, a lower efficiency is expected from a real-world system. This study quantifies the prototype separator efficiency from experimental data.

7.2 Materials and Methods

7.2.1 Experimental setup configuration

The prototype separator designed in [12, 13] has a resonance chamber of 70 mm length, 28.5 mm height and 20 mm width. It was constructed using borosilicate glass (4.2 mm thick) and two neighbouring NCE41 transducer strips (40 \times 10 \times 1 mm) at both ends (Figure 7.1). Each of the two sets of transducers were connected in series in order to have higher resistance (higher voltage, but lower current). In the resonator chamber two flow dividers were implemented, which divide the flow (almost) equally between the three flow lanes. The inlets and outlets were 3D printed from ABS and the flow dividers were made of PVC sheets (0.15 mm thick). These ABS and PVC parts were glued to the borosilicate body with epoxy

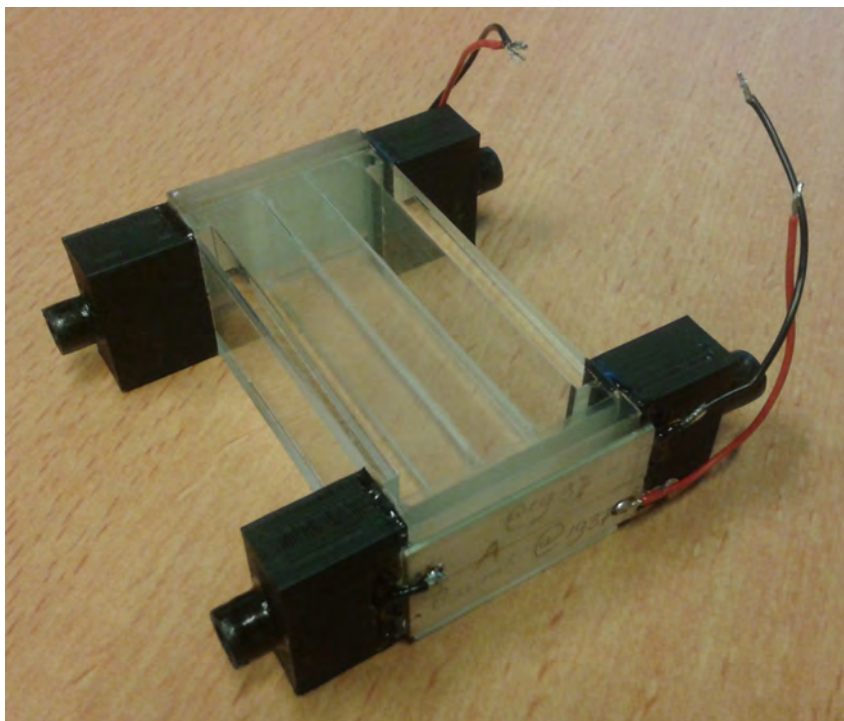


Figure 7.1: Prototype separator for experimental evaluation

adhesive. The total volume of the separator was measured to be 49 ml.

The entire experimental setup is shown in Figure 7.2. The separator has four outlet/inlet ports, numbered 1 to 4. Port 1 (inlet) and port 4 (outlet) were used for the normal filtering operation. A suspension of 1.0 g/l (1000 ppm) starch was prepared and continuously stirred in a 1 l beaker. This suspension is fed into the chamber through port 1 by a digital Masterflex LS pump (ColeParmer Inc.). The filtrate was collected from port 4 in a sample beaker and particles were retained in the resonance chamber during filtering. During the backwash, port 4 was used as inlet and port 2 as outlet, thus using the filtrated fluid to rinse the concentrated fluid from the resonance chamber into a separate sample beaker. The backwash pump (digital Masterflex LS) was connected to port 2, drawing the suspension from the chamber.

The flow rate of this setup was calibrated before the experiment took place. From previous experiments it was already known that the flow is not fully stable. The three rolls in the LS pump head cause periodic fluctuations in the flow pattern and high associated fluid accelerations, which become increasingly disturbing

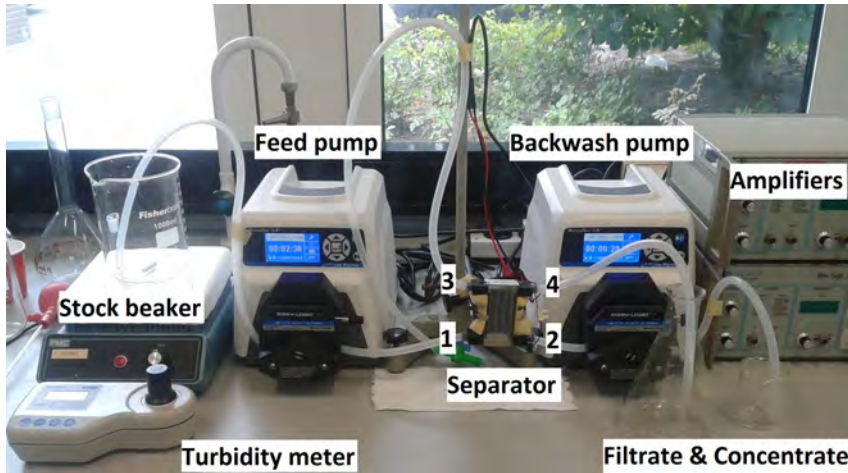


Figure 7.2: The experimental setup used to test the separator (center) with ports numbered 1-4. The bottom power amplifier was used in this evaluation.

at increasing flow rates. Therefore, a piece of hose was connected to port 3, suspended vertically and filled with some (5 cm) feed suspension. It was plugged at the end in order to act as an air-fluid damper, reducing the fluctuations partly.

All four transducers were connected in series and fed by a Biosep ADI1015 frequency amplifier (Applikon B.V., Schiedam, the Netherlands). The separator was operated at a power output of approximately 10 W, which was the maximum possible, given this setup. This power level is far below the power needed for proper separation, which was numerically estimated to be near 30 W¹. Before starting the experiments the operating eigenfrequency of the filled separator was determined with a SinePhase Z-Check 16777k impedance analyser (SinePhase Instruments GmBh, Hinterbrühl, Austria).

7.2.2 Concentration calibration

From previous experiments [15] it was known that the concentration of starch is linearly related to the turbidity of the suspension. Therefore, turbidity was used as a measure for the concentration. Turbidity was measured using a portable Martini Instruments MI415 turbidity meter. Before starting the experiments four 10 ml samples were taken from the stock solution and the turbidity was measured trice

¹The amplifier is able to deliver a maximum voltage of approximately $12.5 V_{rms}$ and a maximum current of 1.5 A, so that the maximum power output of the amplifier is near 20 W. Due to the low admittance, the maximum current could not be reached.

for each sample in order to determine the accuracy of the turbidity measurement. Then, a second sample was diluted by adding 40 ml of demineralised water, followed by sampling and measuring another 4 samples trice. This procedure was repeated twice in order to obtain a concentration-turbidity curve. Also, a blank of demineralised water was measured trice to confirm that the curve passes through the origin.

7.2.3 Batch mode operation

The separator was operated in sequenced batch mode, meaning that suspension was fed through the separator for 150 s while the ultrasound was switched on. Then, the ultrasound and the feed pump were paused for 30 s. After 5 s of the pause, the chamber was backwashed with filtrate during 20 s at a flow rate of 2.5 ml/s, so that the entire chamber (49 ml) was drained. During the remaining 5 s of the pause the filtrate and concentrate beakers were replaced by empty ones. Three flow rates were applied ranging from 1.0-3.0 ml/s in 1.0 ml/s steps.

7.2.4 Sampling and efficiency

At the end of a complete filter run with three batches, there were three samples of filtrate and three samples of 50 ml concentrate ². The turbidity of each sample was measured trice, resulting in nine measurements for each stream. Efficiency of filtration ϵ_f and concentration ϵ_c was calculated as the ratio of the difference between the concentrations of filtrate (port 4) / concentrate (port 2) and the stock solution (port 1), respectively, with respect to the stock solution, and given by

$$\epsilon_f = \frac{[S] - [F]}{[S]} \quad (7.1)$$

$$\epsilon_c = \frac{[C] - [S]}{[S]} \quad (7.2)$$

with $[S]$ the concentration of the stock suspension, $[F]$ the concentration of the filtrate and $[C]$ the concentration of the concentrate.

²The first sample is smaller, because some concentrate is used to fill up the outlet hose first.

Table 7.1: Test matrix of the experimental runs performed and the amount of samples taken per input/output port. The turbidity of each sample taken was measured three, resulting in nine measurements per port per experimental run.

Run no.	Flow rate [ml/s]	Type	no. of samples		
			Stock	Filtrate	Concentrate
1	1	Blank	3	3	3
2		Run US 1	3	3	3
3		Run US 2	3	3	3
4	2	Blank	3	3	3
5		Run US 1	3	3	3
6		Run US 2	3	3	3
7	3	Blank	3	3	3
8		Run US 1	3	3	3
9		Run US 2	3	3	3

Preceding to the runs with ultrasound, a blank run was performed for each of the flow rates (see test matrix in Table 7.1). The blank is used to determine whether separation also takes place without the use of ultrasound, simply because the separator is positioned upright and some gravitational settling of the starch may take place. After the blank, two filter runs with ultrasound were performed on each of the flow rates.

7.3 Results

With the impedance analyser the eigenfrequencies of both transducer sets on either side of the filled chamber and the transducer sets in series were determined (Figure 7.3). The maximum admittance of the transducers in series was 64 mS at an eigenfrequency of 1942 kHz, which implies that the maximum power P_{rms} applied can be 10 W (of which 8.8 W is real power) at 12.5 V_{rms} ($P_{rms} = V_{rms}^2 Y = (12.5)^2 * 64 * 10^{-3} = 10$ W). In the separation experiments, the separator was operated at this eigenfrequency, although it is known that, from an energy consumption point of view, this most likely is not the optimal frequency [13].

Concentration and turbidity are linearly related ($R^2 = 0.99$), so that turbidity and concentration are interchangeable when calculating the efficiency. The results of the various runs are shown in figures 7.4 to 7.6 using a 95% confidence interval for each bar. The results of all runs are given in appendix C. The associated

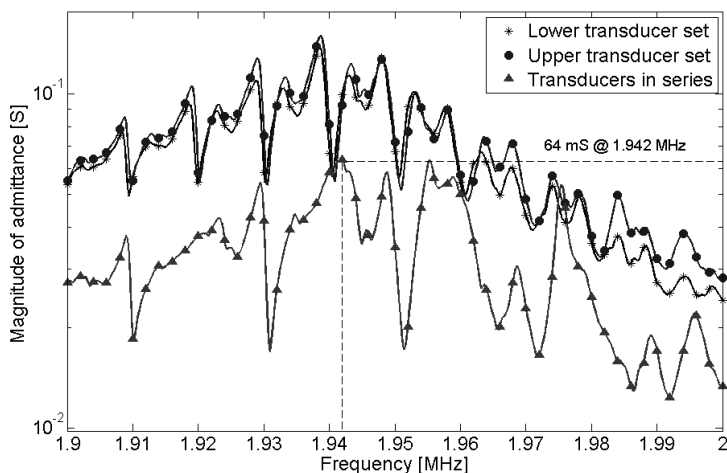


Figure 7.3: Magnitude of the measured admittance versus frequency for each individual transducer set at each end of the separator as well as both sets connected in series.

Table 7.2: Concentration and filtration efficiency in % as compared to the stock solution with the associated significance (Student T-test using a 95% confidence interval). Only the numbers in *italics* show non-significant differences.

Flow rate:	1 ml/s		2 ml/s		3 ml/s	
Efficiency [%]:	ϵ_c	ϵ_f	ϵ_c	ϵ_f	ϵ_c	ϵ_f
Blank	-15 (0.000)	7 (0.004)	14 (0.003)	-7 (0.041)	-1 (<i>0.556</i>)	-1 (<i>0.797</i>)
Run 1	44 (0.000)	52 (0.000)	67 (0.000)	15 (0.001)	16 (0.002)	7 (0.039)
Run 2	57 (0.000)	54 (0.000)	76 (0.000)	21 (0.000)	3 (<i>0.469</i>)	20 (0.000)

filtration or concentration efficiency and the significance level of a Student T-test on each pair of bars is shown in Table 7.2. In all cases, there is significant concentration/filtration performed by the ultrasound with a maximum of 54% on filtration and 76% on concentration.

7.4 Discussion

The evaluation shows that the use of ultrasound in the model-based separator design contributes significantly to the separation of starch particles and water. Starch is a rather sticky substance, which is difficult to separate using conventional techniques and the obtained separation efficiency up to 76% is considerable. Nevertheless, some mismatches between theory and practise remained, many of which can be solved simply by using more dedicated equipment.

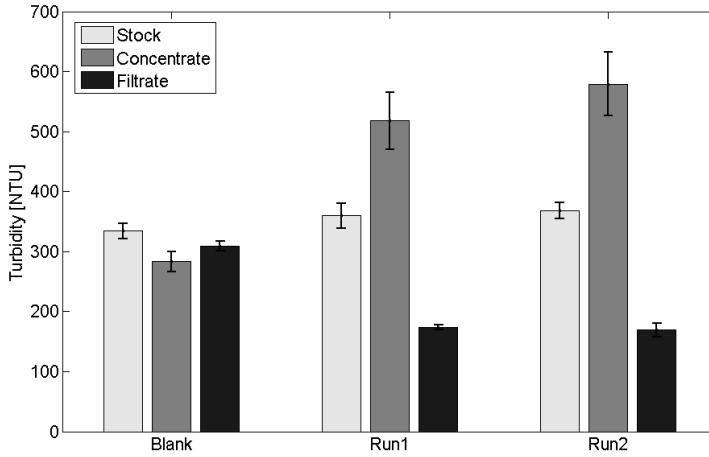


Figure 7.4: Turbidity of stock, concentrate and filtrate for one blank and two ultrasound experiments at a flow rate of 1 ml/s. The error bars indicate the 95% confidence interval.

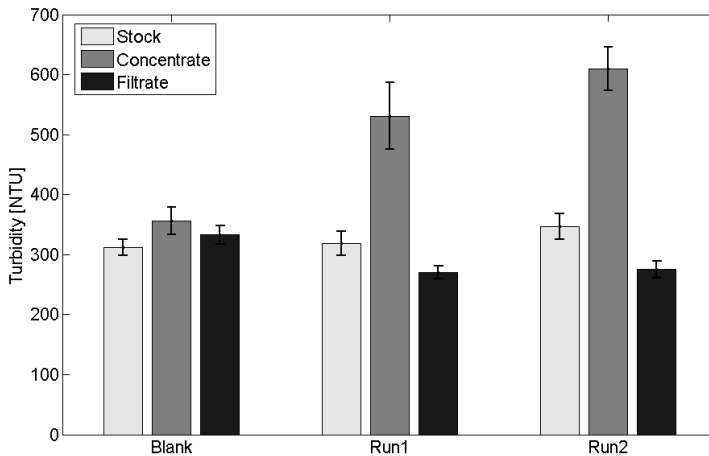


Figure 7.5: Turbidity of stock, concentrate and filtrate for one blank and two ultrasound experiments at a flow rate of 2 ml/s. The error bars indicate the 95% confidence interval.

Firstly, and the main reason for the mismatch, was the pulsation of the peristaltic feed pump. Although outlet 3 was used as a water-air damper, it did not remove

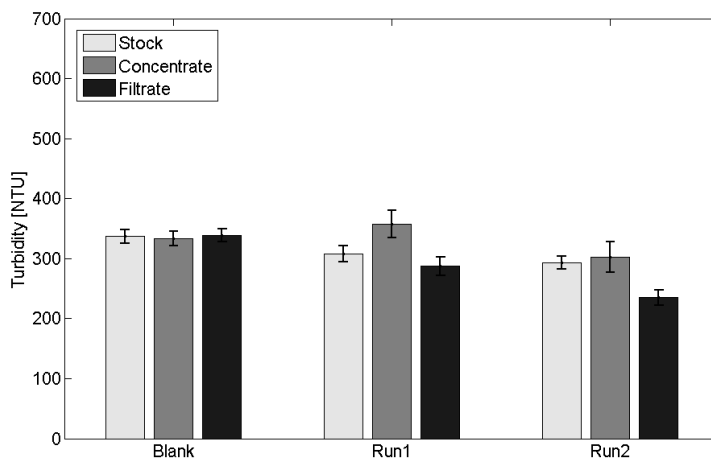


Figure 7.6: Turbidity of stock, concentrate and filtrate for one blank and two ultrasound experiments at a flow rate of 3 ml/s. The error bars indicate the 95% confidence interval.

the pulsation entirely. The high accelerations associated with this cyclic pumping behaviour showed to push trapped and agglomerated particles from their trapped position. This effect increased with higher flow rates, so that flow rates above 3 ml/s were not considered. Therefore, a stable, laminar flow is essential for highly efficient operation of ultrasonic particle filters.

Secondly, the lack of efficiency can be partly attributed to the limited power fed into the separator, which was far below the minimum power needed (8.8 W instead of 24-36 W [13]). Neither the voltage nor the current could be increased, because of the voltage and/or current limitation on the amplifier (12.5 V and 1.5 A). Adding a second amplifier was tried, but did not work properly, because of bad frequency synchronisation between the two. Moreover, the lower efficiency is also related to a low admittance. The simulations presented in the design study [13] showed a minimum admittance of 2080 mS at the main eigenfrequency, with the transducers connected in parallel, as compared to 303 mS seen here in practise (a serial configuration of 64 mS was used here to obtain the maximum power possible). The 2D model did not have two transducers in series on each side as does the physical separator. Theoretically, a prototype separator with a transducer of one piece (and not two halves) would have an admittance of 1212 mS (4×303), which is 60% of the simulated value. This is partly related to the transducer model. The (dedicated, expensive) SPC-140 transducer [11] used in

the model-based design study, was different from the (mass produced) Noliac NCE-41 transducer applied here, although the eigenfrequencies matched. The difference in admittance (0.55 versus 0.47 mS/mm²) already accounts for 15% of the discrepancy. Moreover, the simulation model in the design study did not account for additional mass and damping on the transducers due to soldering and the extra epoxy added between the transducers and the ports.

Finally, the starch suspension used was found to contain many small particles, as well. Figure 7.7 shows the distribution of potato starch particles in the suspension used (measured with a Mastersizer 2000, Malvern Instruments Ltd., Worcester-shire UK). The figure indicates that many particles, about 12%, have a size below the limit of $10\mu\text{m}$, accounting for about 10-30 % of the turbidity of the stock solution (30-115 NTU). Moreover, a quick microscope scan indicated that particles with a size over $30\mu\text{m}$ mainly occurred in the concentrate and not in the filtrate. In order to filter particles smaller than $10\mu\text{m}$, either the flow should be decreased or the power increased. However, if this particle size is consistently present in the water to be treated, it is more beneficial to redesign the separator for higher frequencies, since small particles are more easily caught at higher frequencies.

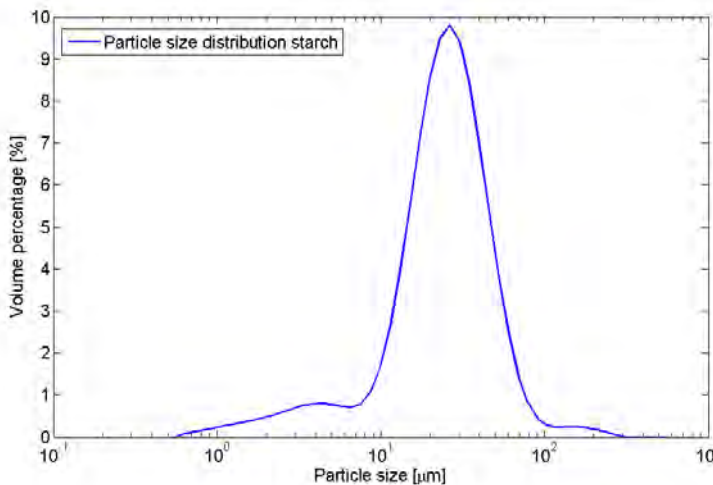


Figure 7.7: Particle size distribution of the potato starch used in the experiments.

Additional simulations with the separator model as given in [13] with particle sizes of 1, 2, 5, 10, 20 and $40\mu\text{m}$, a flow rate of 1 ml/s and a voltage per single transducer of 3.5 V, shows that only particles above $10\mu\text{m}$ are adequately trapped. Table 7.3 shows the average particle displacement of 25 particles released at the inlet after 15 s of simulated time, with and without the application of ultrasound

Table 7.3: Simulated average displacement in mm of 25 particles released at the inlet after 15 s of simulated time as a function of particle size, without and with ultrasound applied.

Particle size [μm]	without US	with US
1	34	34
2	34	34
5	34	25
10	34	3
20	34	0
40	33	0

in the model. This result indicates that particles below $10\mu\text{m}$ were hardly trapped by the ultrasound, supporting the finding that small particles cannot be trapped at the low voltage used, since $10\mu\text{m}$ is the absolute minimum particle size in the most ideal (simulated) circumstances.

In the sequenced batch mode used in this study, the separation efficiency will also be dependent on the duration of the filter runs and the duration of the backwash. The longer the filter run, the more saturated the separator chamber becomes. The backwash was chosen to be an entire volume of 50 ml, although turbidity measurements show that the first part of the backwash contains most of the particulate. The current filter duration of 150 s was chosen on the basis of some trials during which saturation seemed to occur. Particle agglomeration stopped when the flocs inside the acoustic nodes became too large. When acoustic nodes become saturated, the particles simply start to bypass the nodes towards the outlet. If the agglomerated particles become too heavy, they may settle to the bottom taking other agglomerations along. In fact the system then behaves as an acoustically enhanced settler, similar to Applikon's BioSep, used in biotechnology. Optimisation of such a settler can be done with similar models as used for the design evaluated here. The integration of experiments and models can be used to optimise the operational settings [15].

The acoustic separator might also perform well if a continuous mode of operation combined with a quasi-standing wave is used. Introducing a 0.1 kHz frequency shift between the upper and lower transducer set will force particles to the lower end of the separation chamber as done earlier in [67]. In that case the outlet port 2 can be continuously used to withdraw concentrated particles. Such a configuration requires accurate frequency control on both the upper and lower set of transducers, which was not possible with the devices used.

7.5 Conclusions

The evaluation of a new acoustic particle separator was presented in this study. The system was evaluated at three flow rates 1, 2 and 3 ml/s. The maximum filtration efficiency was 54% and the concentration efficiency 76%. The performance found was lower than the 100% that was found in a simulation study [13]. The mismatch was mainly attributed to (i) the pulsation of the feed pump, (ii) modelling discrepancies, (iii) limitations to the power supply and (iv) the small particle size used in these evaluations.

8. FLOW CONTROL IN ACOUSTIC SEPARATORS

Abstract

Acoustic separation is a relatively new method for recovering valuable particulate matter from suspensions. This separation method is mainly used in medical technology, but may well be applicable as water purification and material recovery technique. The key question then is what separation efficiency can be reached and whether this can be realised in an energy-efficient way.

In the current study, a commercially available acoustic separator, named BioSep, which employs ultrasound enhanced sedimentation, was used. With the aim to achieve a high separation efficiency with minimal energy consumption, a model-based open-loop switching control strategy was designed for the BioSep, using a numerical-experimental approach. Firstly, a dynamic BioSep model structure was derived from mass balances and its system properties were studied. Then, the unknown system parameters were estimated from steady state and dynamic experimental data and subsequently, the switching times of the control input were determined. The model with switching control outputs was then validated by experiments. Finally, the control strategy was implemented in the experimental setup and tested using suspended potato starch. Results showed that the optimal control strategy reached a mass separation efficiency of 96%, which was an improvement of 4% with respect to the initial settings, while using less energy.

This chapter was published as

H.J. Cappon, L.A. Stefanova, K.J. Keesman (2012) Concentration based flow control in acoustic separation of suspensions. *Separation and Purification Technology*, Vol. 103, pp 321-327

8.1 Introduction

Separation technology plays an important role in process industry. Solid-liquid separation is a common type of separation used in processing particulate slurries and it has three important functions [62]: i) recycling and reusing both phases of the suspension, ii) recovering the valuable solids (particles) and iii) recovering and cleaning the liquid.

Our final aim is to apply acoustic separation technology for the recovery of valuable particulate matter from waste water in industry. For this type of applications, large scale separator systems require detailed design and evaluation in order to optimise the system performance at the earliest stage possible. Numerical models can aid the design of the acoustic separator system itself [11, 14] as well as enhance its efficiency by adequate process control strategies, the latter being the objective of this study.

In the current study a commercial acoustic separator named BioSep (Applikon B.V., Schiedam, The Netherlands) is used for suspension separation. The main objective is to obtain an optimal switching control strategy for the BioSep in order to achieve a high separation efficiency with minimal energy consumption. Initially, separation efficiency is defined as the difference of particle concentrations measured in the concentrate and filtrate of BioSep. As concentration is linearly correlated to turbidity, turbidity is used to calculate efficiency. The switching control strategy is obtained by formulating a state space model of the separator, identifying the system parameters from steady state analysis and dynamic experiments and finally optimising the control strategy. The optimised strategy thus obtained is validated under real-world conditions in an experimental setup.

8.2 Acoustic separation principle

The principle of acoustic separation is based on the fact that acoustic waves exert forces on solid particles in a liquid or gas [47]. At ultrasonic frequencies, and even more in ultrasonic standing wave fields, these forces become large enough to concentrate particles in acoustic pressure nodes (when the particles are denser and stiffer than the surrounding medium), thus separating the solid and fluid phase to a large extent (see Figure 8.1). The phenomenon has already been investigated by various studies [60, 35, 36, 65, 57, 55] and was also tested in an industrial setting for the removal of suspended particles from cooling water [7]. However, it proved unsuccessful due to the extremely small particles involved. The technique proved successful in lab-scale, commercially available acoustic separators,

like the BioSep from Applikon (Metrohm-Applikon B.V., Schiedam, The Netherlands) used in this study.

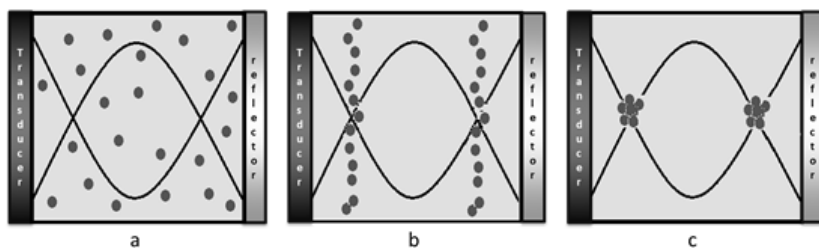


Figure 8.1: Three step acoustic separation principle: a) creation of the ultrasonic standing wave field, b) collection of particles in nodal lines, and c) agglomeration of particles forming clumps, which settle more easily.

The BioSep acoustic separator applies ultrasound enhanced sedimentation as separation technique. The system creates a standing wave in a water filled cavity, called the resonance chamber, which causes the particles to agglomerate and settle at the bottom of the chamber. The system has one inlet at the bottom and two outlets, each of which is driven by a pump: the filtrate is extracted from the top of BioSep, while the concentrate is drawn from the cavity at the bottom, near the inlet. In order to drain the cavity regularly, both the filtrate pump and ultrasound are switched off, while the concentrate pump continues running. It is important to note that the standing wave field does not cover the entire chamber: the top and bottom of the chamber experience little resonance, so that the flow in the actual resonance area is hardly hindered by inlet and outlet flows.

8.3 Materials and Methods

8.3.1 Experiments

Two sets of experiments were performed in order to determine the system properties, which are needed for adequate model based controller design:

1. Determination of the optimal pump rate of both outlet pumps connected to BioSep. A calibrated suspension of 0.83 mg/ml potato starch was fed into BioSep and the turbidity of both outlets (concentrate and filtrate) were measured. Because maximum filtration efficiency is pursued, the optimal pump rates were determined by varying both pump rates from setting 1 to 9,

leading to 81 experiments being evaluated for a certain inlet concentration. After each run the turbidity of both outlets was determined with an off-line turbidity meter. The settings producing the maximum efficiency, defined as the difference between the turbidities of concentrate and filtrate, were used in the subsequent steps. The switching time (sound on/off, filtrate pump on/off) was kept constant at 30 s on and 3 s off.

2. Determination of the steady state and dynamic behaviour of the measured concentrations. Again a calibrated suspension of 0.83 mg/ml potato starch was fed into BioSep and the turbidity at both outlets was determined with a sampling rate of 2 Hz with an in-line turbidity meter during 10 switched runs of 30s on/3s off, resulting in an experimental run of 330 seconds.

The experimental setup used is shown in Figure 8.2, consisting of the following materials: BioSep ADI 1015 (AppliSens), which consists of a control module (ADI 1015) and a resonator chamber (SonoSep ABF100.1); two peristaltic pumps with double-rotor pump head L/S EASY-LOAD MasterFlex 7518-00 (Cole-Parmer Instruments) ; off-line turbidity meter - MI 415 (Martini instruments); on-line turbidity meter, consisting of Turbidity Transmitter Trb 830 (Mettler-Toledo) and a Data Acquisition System (DAQ); measurement chamber for the inline turbidity meter made of ABS; LabVIEW 2010 software (National Instruments); MATLAB R2011a software (MathWorks); magnetic stirrer RCT basic (IKA LaboRtechnic); scale LabStyle 303 (Mettler-Toledo); glass beakers; cylinders; 99% pure insoluble potato starch and distilled water.

8.3.2 Piece-wise linear state space model

In order to obtain a valid dynamic model of the separator system, the chamber of the BioSep is divided into three virtual compartments (see Figure 8.3). The first compartment (C1) includes the upper part of the BioSep's chamber, including the actual resonance area. However, it excludes the volume, which contains the suspended particles held by the acoustic field and the liquid in their near proximity, which is actually the third compartment (C3). This division in the upper part of the chamber is needed in order to have particles migrate from the fluid to the acoustic pressure nodes when the acoustic field is switched on and from the nodes to the fluid when the acoustic field is switched off. The lower part of the BioSep's chamber is the second compartment (C2). Every compartment (C_i) is characterised by its own volume V_i and concentration of suspended particles S_i . The concentrations in the three compartments are chosen to be the system state variables.



Figure 8.2: Experimental setup using a BioSep, two peristaltic pumps and an inline turbidity meter (left) and a zoomed in view of the BioSep resonator chamber (right).

The model is built up with the following features:

1. Biosep has one inlet and two outlets - one for the filtrate and one for the concentrate. There are two pumps, which determine the filtrate flow rate (Q_1) and the concentrate flow rate (Q_2). Addition of these gives $Q_{in} = Q_1 + Q_2$ for the entire system. In the current setup pump 1 switches simultaneously with the acoustic field. This switch is modelled with a digital transducer coefficient α , which can have only two values: 1 (on) and 0 (off);
2. Mass transfer takes place between C1 and C3. This transfer is characterised by a transfer rate coefficient (k_1);
3. When the acoustic field is switched off a reverse reaction of the concentration occurs. Suspended particles from C3 are released to C1, described by a reverse transfer coefficient (k_3);
4. In addition to the reverse reaction, a settling reaction occurs. It is assumed that this reaction takes place between C1 and C2 and characterised by a settling coefficient (k_2);

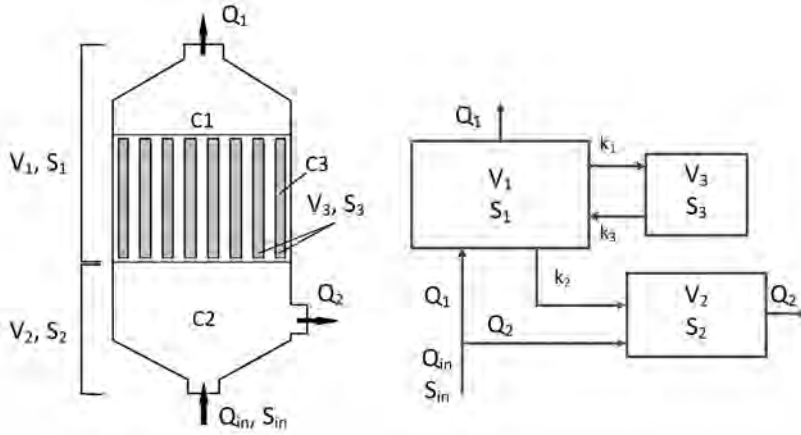


Figure 8.3: Separation model of BioSep using three compartments, one inlet and two outlets for filtrate and concentrate flows.

5. The losses from C1 to C2 due to turbulence or diffusion are also taken into account by introducing a loss coefficient (k_4).

Mass balances are defined for each of the three compartments with fixed volumes. As a result, the following model, which gives the relationship between the system state variables, is obtained:

$$V_1 \frac{dS_1}{dt} = Q_1 S_{in} - Q_1 S_1 - \alpha k_1 S_1 V_1 + (1 - \alpha) k_3 S_3 V_3 - \frac{k_2 S_1 V_1}{Q_1 + k_4} \quad (8.1)$$

$$V_2 \frac{dS_2}{dt} = Q_2 S_{in} - Q_2 S_2 + \frac{k_2 S_1 V_1}{Q_1 + k_4} \quad (8.2)$$

$$V_3 \frac{dS_3}{dt} = \alpha k_1 S_1 V_1 - (1 - \alpha) k_3 S_3 V_3 \quad (8.3)$$

with V_i the compartment volume, S_i the compartment concentration, Q_i the flow rate for $i = 1, 2, 3$, k_j the transfer coefficients with $j = 1, 2, 3, 4$ and α the control switch parameter. These equations can be interpreted as follows:

- Equation 8.1 represents the mass balance over C1. Mass changes $V_1 \frac{dS_1}{dt}$ in C1 are caused by incoming particles from the stock suspension ($Q_1 S_{in}$), outgoing particles from C1 to C3 caused by the acoustic field ($\alpha k_1 S_1 V_1$), incoming particles from C3 when the acoustic field is off ($(1 - \alpha) k_3 S_3 V_3$), outgoing particles from C1 to the filtrate ($Q_1 S_1$) and finally settling of particles from C1 to C2 ($\frac{k_2 S_1 V_1}{Q_1 + k_4}$).

- Mass changes in Equation 8.2 are a result from incoming particles from the stock solution ($Q_2 S_{in}$), outgoing particles from C2 to the concentrate ($Q_2 S_2$) and incoming particles from C1 due to settling reaction ($\frac{k_2 S_1 V_1}{Q_1 + k_4}$).
- The mass changes in the third compartment are defined by equation 3. The mass change is determined by incoming particles from C1 as a result of the ultrasonic field ($\alpha k_1 S_1 V_1$) and outgoing particles from C3 to C1 when the ultrasonic field is switched off ($(1 - \alpha) k_3 S_3 V_3$).

Based on these equations, and under the assumption that all concentrations are output of the separator system, the BioSep model in general state space form becomes:

$$\frac{d}{dt} \begin{bmatrix} S_1 \\ S_2 \\ S_3 \end{bmatrix} = \begin{bmatrix} \frac{Q_1 S_{in}}{V_1} - \frac{Q_1 S_1}{V_1} + \frac{(1-\alpha)k_3 S_3 V_3}{V_1} - \alpha k_1 S_1 - \frac{k_2 S_1}{Q_1 + k_4} \\ \frac{Q_2 S_{in}}{V_2} - \frac{Q_2 S_2}{V_2} + \frac{k_2 S_1 V_1}{V_2(Q_1 + k_4)} \\ \frac{\alpha k_1 S_1 V_1}{V_3} - (1 - \alpha) k_3 S_3 \end{bmatrix} \quad (8.4)$$

$$\mathbf{Y} = \begin{bmatrix} S_1 \\ S_2 \\ S_3 \end{bmatrix} \quad (8.5)$$

Where S_1 , S_2 and S_3 are the state variables, Q_1 , Q_2 and α are the control inputs, S_{in} is the disturbance input and \mathbf{Y} is the system output vector. Since the control inputs Q_1 , Q_2 and α are determined from an optimal switching control strategy, the control inputs are fixed on a interval and thus Equations 8.4 and 8.5 become a so-called piece-wise linear state-space model. The coefficients k_i are not yet known and need to be derived from steady state analysis and/or dynamic experiments.

8.4 Results

8.4.1 Optimal pump rate ratio

The 81 experiments at different pump rates for both outlet pumps result in the landscape shown in Figure 8.4. It shows a maximum when filtrate pump 1 is set to rate 2 (0.46 ml/s) and concentrate pump 2 to rate 5 (1.38 ml/s). These settings are used for the steady state and dynamic analysis, thus fixing Q_1 and Q_2 . However, note that Q_1 will become 0 when the acoustic field is switched off.

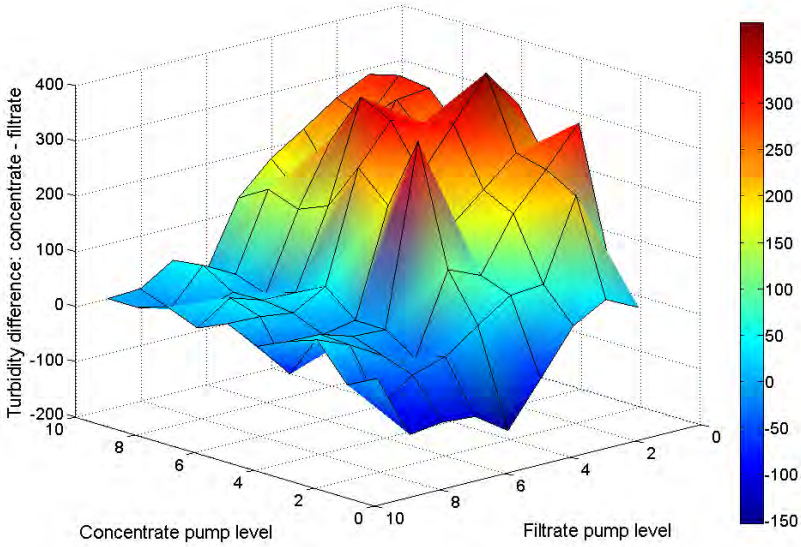


Figure 8.4: Landscape of 81 experiments with nine flow rates for the filtrate pump and concentrate pump.

8.4.2 Steady state analysis

Figure 8.5 shows the changes in the concentrations of interest (S_{in} , S_1 and S_2) over time using averaged data of multiple runs. The acoustic field is switched on for 30 s and off for 3s, thus four cycles are shown. There is a significant difference between S_1 and S_2 , which was also clearly observed in the experiments by visual inspection. Secondly, the turbidity of the stock solution (S_{in}), 0.83 mg/ml potato starch, can be assumed constant. Surprisingly, S_2 also seemed to be constant over time. The expected increase of S_2 during particle release (sound off) was not observed. The slight increase due to particle release is most likely submerged in the measurement noise. S_1 reached its steady state value during the sound-on period, so that this part of the signal could be used for steady state analysis. During the sound-off period no steady state was reached. However, in what follows, it is assumed that the minimum of S_1 on the sound-off interval can be used as a steady state estimate.

Given the steady state values for S_{in} , S_1 and S_2 (denoted by the index ss), and the equation $\frac{dS_1}{dt} = \frac{dS_2}{dt} = 0$, three parameters k_1, k_2 and k_4 can be estimated

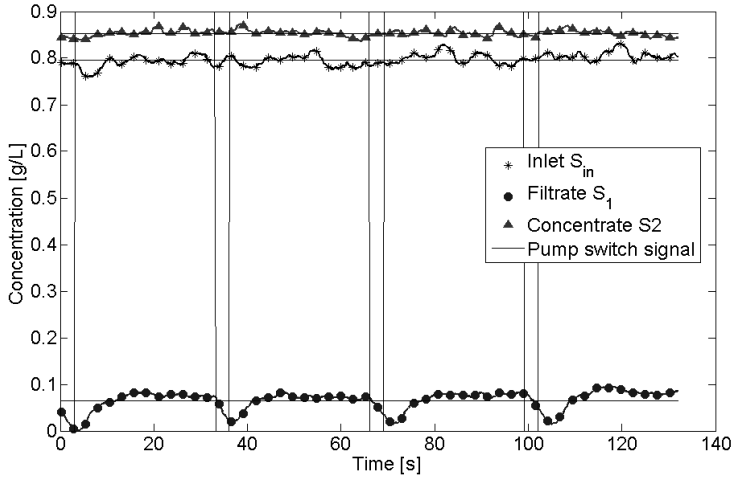


Figure 8.5: Dynamic experiment of inlet (S_{in}) and outlet concentrations (S_1 and S_2) showing four filtration cycles. Pump 1 and the ultrasound are switched on for 30 s and switched off for 3 s.

from the general state space form in Equation 8.4 and are given by:

$$k_1 = -\frac{Q_1(S_{1sson} - S_{in}) + Q_2(S_{2sson} - S_{in})}{S_{1sson} V_1} \quad (8.6)$$

$$k_2 = \frac{Q_1 Q_2 (S_{2sson} - S_{in})}{S_{1sson} * V_1} \quad (8.7)$$

$$k_4 = \frac{S_{1ssoff} V_1 k_2}{Q_2 (S_{2ssoff} - S_{in})} \quad (8.8)$$

(see Appendix D for details)

In order to estimate these parameters the volumes of the three compartments, the concentration of suspended particles in the stock solution and the filtrate and concentrate flow rates were needed.

With a known total volume (24 ml) and resonator volume (7 ml) of the BioSep and assuming that the volume of C3 is 10% of the volume of C1, the volumes of the three compartments were calculated. Thus, the volume of C1 is 6.36 ml, the volume of C2 is 17 ml and the volume of C3 is 0.64 ml. The flow Q_1 was fixed to 0.46 ml/s and Q_2 to 1.38 ml/s. During sound-off $Q_1=0$ ml/s.

The concentration of particles in the suspensions was calculated as a time average of all measurements. The outcome of this calculation was 0.797 mg/ml

Table 8.1: System parameter values in steady state analysis.

parameter	value	unit
V_1	6.36	ml
V_2	17	ml
V_3	0.64	ml
Q_{1on}	0.46	ml/s
Q_{1off}	0	l/s
Q_2	1.38	ml/s
S_{in}	0.797	mg/ml
S_{1sson}	0.075	mg/ml
S_{1ssoff}	0.015	mg/ml
S_2	0.853	mg/ml

for S_{in} and 0.853 mg/ml for S_2 . For S_1 the average of the steady state during the sound-on period was used, resulting in an $S_{1sson}=0.075$ mg/ml. During the sound-off period a minimum of S_1 of 0.015 mg/ml was found using an average of three minima. This value is used in Equation 8.8 as an estimate of S_{1ssoff} . A summary of the values obtained is given in Table 8.1.

8.4.3 Dynamic data analysis

As already mentioned in the previous section S_2 does not show a consistent dynamic response during switching of the sound over various runs. However, during the sound-off period a drop in S_1 is seen. The drop is most likely a result of particle settling inside the turbidity meter's chamber. If particles were released from C3 only to C1 one would at least expect a notable increase of S_1 right after pump 1 (Q_1) is switched on again. This increase is not visible, which implies that either the turbidity meter is insensitive to this concentration increase or particles have already settled from C1 to C2 as well, as described by k_2 . Hence, the dynamic experiments do not provide additional information to the steady state analysis.

This means that coefficient k_3 cannot be estimated from the steady state analysis nor from the dynamic data. However, in what follows we assume that the release of particles from C3 to C1 happens rather quickly, within the 3s in which BioSep is switched off, otherwise serious accumulation during multiple runs would occur. Also, from visual inspection, it was observed that particles are immediately scattered all over BioSep's chamber (C1, C2 and C3) during the sound-off period, which, during this time, implies a large k_2 as well. Consequently, k_2 is not

Table 8.2: Coefficients k_j of the control model obtained from steady state and dynamic analyses.

constant	value	unit
k_1	0.534	1/s
k_{2on}	0.075	ml/s ²
k_{2off}	1.65	ml/s ²
k_3	1.20	1/s
k_4	0.092	ml/s

a constant. When the transducer is off, equation 8.3 becomes:

$$\frac{dS_3}{dt} = -k_3 S_3 \quad (8.9)$$

so that

$$S_3(t) = S_{03} e^{-k_3 t} \quad (8.10)$$

with S_{03} the concentration right before particle release. If we then, based on visual inspection, assume 97% release (i.e. $S_3(t = 3) = 0.03S_{03}$) from C3 to C1 (resulting in an approximate homogeneous concentration in the entire chamber, because $(V_1 - V_3)/V_1 = 0.97$) it turns out that k_{3off} is approximately equal to 1.2. Higher k_{3off} means quicker release. As we concluded that k_2 is different under sound-on and sound-off conditions, k_{2off} should be of the same order as k_{3off} , we therefore assume $k_{2off} = k_{3off} Q_2$, while k_{2on} is estimated from Equation 8.7.

A summary of the estimated k_j values is given in Table 8.2.

8.4.4 Model validation

Given the estimated values of the parameters, the output behaviour of the piecewise linear system, is simulated during a period of one cycle (33s) and ten cycles (330s) with time step of 0.1 seconds. The outputs of the system are the three states - the concentrations of suspended particles in the three compartments (see Equation 8.5). The result of this dynamic simulation is shown in Figure 8.6. It shows that S_3 increases and decreases quickly during each on-off cycle and that both S_1 and S_2 remain rather constant due to their much larger associated volume, which corresponds to the measured signals. For comparison with the experiments the average steady state values of S1 and S2 can be calculated. The

average concentration for S_1 is 0.076 mg/ml and the average for S_2 is 1.02 mg/ml versus 0.075 mg/ml and 0.835 mg/ml in the experiments. The efficiency in the experiment was 91% and in the simulation 92%.

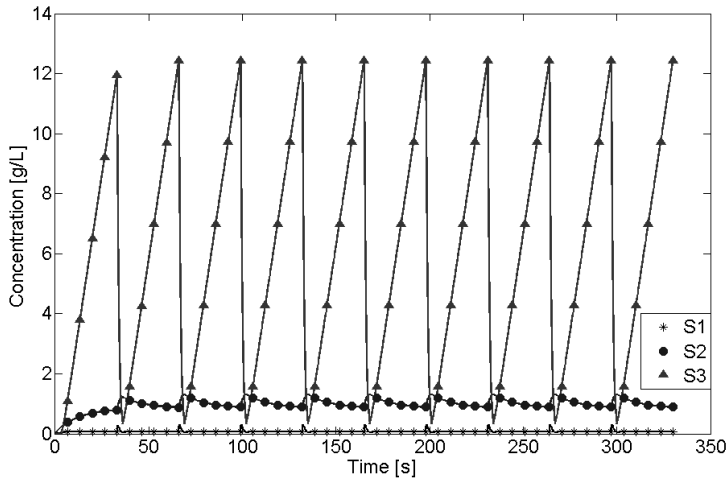


Figure 8.6: Dynamic simulation showing outlet concentrations (S_1 and S_2) and internal concentration (S_3) during 10 filtration cycles. Pump 1 and the ultrasound are switched on for 30 s and switched off for 3 s resulting in 92% separation efficiency.

8.4.5 Optimal switching control

Recall that there are three control inputs: transducer coefficient (α), filtrate flow rate (Q_1) and concentrate flow rate (Q_2). Considering a switching control strategy all of these inputs can have only two values, either in switched-on state or switched-off state, thus implying constant pump rates for Q_1 (0 or 0.46 ml/s) and Q_2 (0 or 1.38 ml/s) and α is either zero or one. Moreover, one cycle consists of two periods: a short one of 3 seconds and a long one of 30 seconds. Thus, there are eight possible combinations of the control inputs for each period. Consequently, for a full cycle of 33s, containing two periods, there are 64 ($8 \cdot 8$) combinations of the control inputs, which represent 64 different control strategies. In order to select the optimal control strategy by enumeration, each of the 64 combinations were simulated using exact solutions of the piece-wise linear systems defined by Equations 8.4 and 8.5 and given values for Q_1 , Q_2 and α . The optimal control strategy was then chosen by the following criteria:

a) The difference (Δm) between the total mass of suspended particles in the

concentrate m_c and filtrate solution (m_f), obtained after one cycle, should be maximised, with

$$\Delta m = m_c - m_f = \int_0^{t_{cycle}} (Q_2(t)S_2(t) - Q_1(t)S_1(t))dt \quad (8.11)$$

b) The total mass of suspended particles in the filtrate solution (m_f) after one cycle should be minimal, which implies that the desired value is actually zero. As can be seen from equation 8.11, the total mass of the filtrate will be equal to zero in two cases, when the filtrate flow rate is zero all the time ($Q_1(t) = 0$) or when the concentration of particles is zero all the time ($S_1(t) = 0$). If the filtrate flow rate is equal to zero this means that the volume of filtrate solution is also zero ($V_f = 0$), in other words, there is no production of filtrate solution. Consequently, in order to ensure that there is production of filtrate solution, its volume should be different from zero. As a result, the second criterion becomes: the total mass of suspended particles in the filtrate solution (m_f) after one cycle should be minimal with

$$m_f = \int_0^{t_{cycle}} Q_1(t)S_1(t)dt \quad (8.12)$$

and the volume of filtrate solution should be different from zero, thus $Q_1(t) > 0$ for $t \in [t_1, t_2]$ with $t_2 > t_1$.

c) The energy used during the process should be minimal, therefore assuming that the BioSep should be switched off as much as possible.

Table 8.3 shows the eight best of all 64 control strategies with associated Δm and m_f . Maximal mass difference and minimal filtrated mass is obtained with simulation 52 (i.e. $Q_1=0.46$ ml/s; $Q_2=1.38$ ml/s; $\alpha=1$ for 3s and $Q_1=0$ ml/s; $Q_2=1.38$ ml/s; $\alpha=0$ for 30s), which also satisfies the minimal energy criterion. The optimal control strategy satisfying the criteria consists of a short period during which the transducer and both pumps are working and a long period during which only pump 2 is working. This setting was simulated during 10 cycles as shown in Figure 8.7, resulting in 99% separation efficiency in the simulation and was then verified experimentally resulting in a separation efficiency of 96%. This is an efficiency improvement of 4% with respect to the initial experimental setting achieved by an optimal switching control strategy only.

Table 8.3: Initial set and best set of 64 simulated control strategy showing simulation number, mass difference and filtrated particle mass. Maximal mass difference Δm and minimal filtrated mass m_f is strived for, which corresponds to strategy 52.

Simulated strategy	Δm [10^{-2} g]	m_f [10^{-3} g]
initial	2.38	1.02
20	2.41	0.07
24	2.45	0.10
28	2.39	1.13
32	2.40	1.20
52	2.46	0.07
56	2.45	0.10
60	2.42	3.60
64	2.42	3.60

8.5 Discussion

An optimal control strategy was obtained from an averaged series of dynamic experiments using an ultrasonic separator combined with a dynamic model of the separator and open-loop switching control. There are various ways to control an acoustic separation process depending on the goal pursued. Initially, in the experiments for finding an optimal pump rate ratio, the flow rates of the filtrate (Q_1) and concentrate (Q_2) pump were varied such that a maximum difference in turbidity between concentrate and filtrate was obtained. In the second step, the maximum mass difference between concentrate and filtrate was used as the optimisation criterion. This seemed more appropriate, because the final aim was particle recovery. Ideally, the first experiments for an optimal pump rate ratio should be run again using this second criterion. However, the optimal pump rate experiments are quite time consuming and the, most likely, new pump rate ratio will not result in changes to the model or procedure. Moreover, in addition to the acoustic power, ideally flow rates will also be subject to (controlled) changes. In the current study, a high separation efficiency and thus high product purity were pursued with a given constant influent quality. In future work, when considering unknown and strongly time-varying influent quality, feed-forward and/or feedback controllers will be designed, while using both acoustic power and flow rates as control inputs. In that case a similar model applies, however, a more accurate (and still being designed) on-line turbidity sensor will be needed.

In the results presented, starch was used as suspended matter, because starch recovery from waste water in food industry is uncommon and expensive, whereas

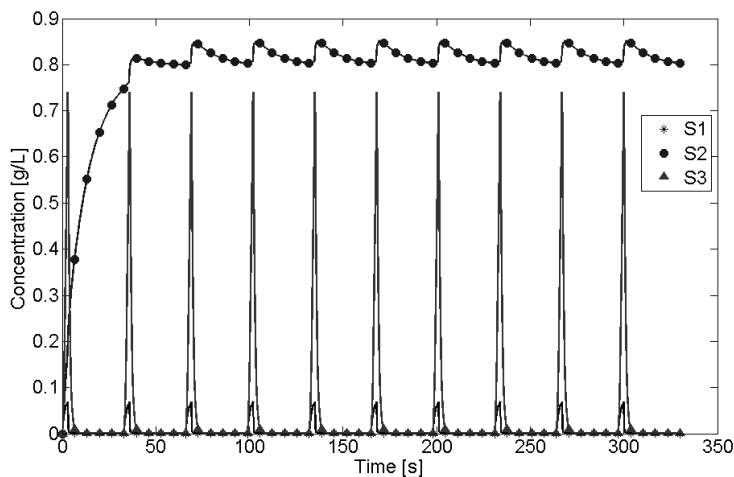


Figure 8.7: Dynamic simulation showing outlet concentrations (S_1 and S_2) and internal concentration (S_3) during 10 filtration cycles with optimal control. Pump 1 and the ultrasound are switched on for 3 s and switched off for 30 s resulting in 99% separation efficiency.

it induces a high biological oxygen demand in water treatment plants, even after the process of anaerobic digestion. However, the separation process has a wider range of application, as it was also evaluated successfully for suspended clay and much larger particles, like herbs.

Given the low signal-to-noise ratio, due to which system changes with time were not clearly visible, the estimated parameters were rather accurate: an average S_2 of 0.853 mg/ml was measured in the experiments while an average steady state S_2 of 1.02 mg/ml was obtained from simulation using the parameter estimated from Table 8.1. The concentration S_1 was even more accurate, 0.075 mg/ml in experiments and 0.076 mg/ml in simulation. Given the mass balance for the entire system in multiple cycles (no accumulation in BioSep) $S_{in}Q_{in} = S_2Q_2 + S_1Q_1$ in steady state, it can even be shown that in fact the 1.02 mg/ml for S_2 is more accurate than the 0.853 mg/ml measured. The mass balance, assuming S_2 to be the only unknown, results in an estimate of S_2 of 1.037 mg/ml. Of course also S_1 may have been measured inaccurately, whereas the stock solution S_{in} was accurately prepared and flow rates were rather accurately determined as well.

8.6 Conclusions

A model-based open loop switching control strategy of the commercially available device BioSep, which employs ultrasound enhanced sedimentation, was developed. Unknown system parameters in the model were estimated using steady states and limited dynamic data from experiments. The results showed that the setup used for turbidity measurements could not accurately detect the expected changes with time. Nevertheless, an optimal open-loop switching control strategy for the BioSep was designed such that high separation efficiency of 99% was achieved in simulation, resulting in a separation efficiency of 96% in the experiment.

9. DISCUSSION AND CONCLUSIONS

9.1 Discussion

9.1.1 Design methodology

The design methodology applied in this thesis was a numerical-experimental approach. A design based purely on experiments is quite expensive and also time consuming, as each single design change should be evaluated first, in order to perform the next step. Although numerical modelling can take quite some time as well, since predictive and detailed (finite element) models require proper validation, the insights gained are invaluable to the design process. Single or multi-parameter design changes can easily be evaluated using numerical models and numerical optimisation can be used to find the optimal solution to a (design) problem.

During this research, design changes were evaluated using a Design of Experiments (DOE) approach, using random (Monte Carlo), Latin-Hypercube and Full Factorial sampling methods within the design space. This sampling strategy was done during each design step of this study i.e. with respect to the piezoelectric transducer (Chapter 3), the resonator dimensions (acoustics and flow, Chapter 6) and the sensitivity studies (sections 3.4.3 and 6.5). The advantage of these methods is that they provide thorough insight into the effect of different design parameter changes on the system's performance. The risk of missing trends is minimised by this approach, especially when random sampling is used. However, the disadvantage is that the amount of simulations and thus CPU and analysis time tend to become quite large.

A DOE is essential when performing optimisation of a system with an irregular response surface (section 3.3.3), since there is a large chance of ending up in a local minimum (or maximum), unless multiple starting points are used. Moreover, design parameter optimisation along extremely irregular surfaces might not result in a practical design, simply because the accuracy needed to manufacture the optimised design is beyond practical feasibility. In such case, as seen during the determination of the resonator dimensions (Chapter 6), a DOE with practically feasible and fixed parameter steps is the best approach to find an optimal solution.

9.1.2 Finite element modelling

Existing one-dimensional models, as proposed and used by various researchers [23, 38], have the main limitation that the acoustic pressure field found is always

sine-shaped throughout the length of the resonator and thus analytical solutions have been found. Hence, the 1D approach supposes that any particle inside a fluid flow running through the resonance field surely will encounter an acoustic pressure peak or pit and can possibly be trapped. Therefore, as long as the acoustic pressure is large enough to trap the particle, the particle will never escape from the resonator. In practise, however, particles do escape, because the 1D field is a utopia in 3D structures.

2D models, as applied here, add an extra dimension, showing that the pressure patterns inside the resonance field cannot easily be predicted on the basis of analytical models. Moreover, when additional details are introduced, like transducers with size limitations, flow lanes, in- and outlets, physical boundaries and even fluid flow, the complexity of the model becomes such, that analytical solutions from 1D models will not suffice. The other extreme, the addition of a third dimension, might increase the accuracy even more, but will also increase the complexity to such an extent that the hardware becomes the limiting factor. The largest 2D models in this study had near 600.000 (small) elements subject to one first-order or one second-order partial differential equation (from the piezoelectric and acoustic domain) using quadratic finite elements. This resulted in frequency domain analyses taking several hours for a limited frequency sweep of 21 steps (Intel i5, quad core 3.1 MHz CPU). Particle tracing simulations of 5 s simulation time with highly fluctuating pressure fields of several MPa, took up to 12 hours of CPU time. A 3D approach would require significantly more CPU power, which was not available. The assumption was that the extra CPU time needed for 3D simulations would not compensate for the expected improvement of the result. In the end, it was proved that the 2D approach was adequate for proper system design (Chapter 7).

The current models used the principle of superposition for the determination of the system performance by means of particle tracing simulations. The results of the acoustic field simulations were projected on the flow simulations and combined to a third, particle tracing simulation. The assumptions made using superposition, were therefore as follows:

- The fluid flow does not influence the acoustic field. This assumption is justified because the maximum laminar flow speed (20 mm/s) is much smaller than the speed of sound (near 1500 m/s) and because no turbulence occurred ($Re < 120$);
- The particles in the fluid have no influence on the density of the fluid, which can be considered true for the small particle concentrations used (1 ‰) of near-neutral buoyant particles (1100 kg/m^3);

- The particles in the fluid have no influence on the acoustic field. This will be true for low concentrations as well;
- The particles in the suspension do not interact. This is true for low concentrations and randomly scattered particles, but is definitely not true for concentrated particles in the pressure nodes of the acoustic field (Chapter 7). Therefore, the current 2D model is not suitable for particle concentration simulations. The particle retention simulations are therefore only an approximation to the performance. On the other hand, agglomerated particles will form larger flocs, which are more easily captured by ultrasound and will decrease energy demand. Note, however, that the Gor'kov equations do not apply to large particles (Chapter 2);
- Sound scattering by the (spherical) particles and particle concentration do not affect the attenuation. Again, this is true for low concentrations, but not true for areas with agglomerated particles;
- There is no influence of Eckart streaming, resulting from attenuation. Since the attenuation is limited within small cavities, this assumption is justified. Moreover, two transducers were used on either side of the cavity, so that the effect of attenuation will be minimal.

The design approach taken here did allow a model update and subsequent validation step. At first, the filtration efficiency results obtained from the simulations were evaluated with respect to those of the prototype separator, followed by changes to the model (voltage and particle size) for a more valid comparison. A final validation step using the measured admittance (see Chapters 3 and 4), by implementing the updated properties of the transducer and the epoxy adhesive, and validating the changed model once more with another series of experiments, was beyond the scope. Although this is a fully valid step, it only contributes to having a better model, not to obtaining a better prototype. Improvement of the prototype itself is surely possible, but would require another iterative loop thereafter. Moreover, accurate prototype building is then the next step to actually improving the performance (see also section 9.1.3).

9.1.3 Parameter identification

Parameter identification and model validation were performed by comparison of the measured and simulated admittance of both the piezoelectric transducer (section 3.4.2) and the resonator model (section 4.3). This implies that the prototype

separator manufactured (Chapter 7) has similar material properties as used in the model-based design optimisation (Chapter 6). Generally, this is not true, since there will always be discrepancies between the two. In this study the transducer used in Chapter 3 and the demonstrator in Chapter 4 is different from the one applied in the prototype separator of Chapter 7 (although the modelled thickness was adapted to obtain the correct eigenfrequency). The SPC-140 transducer is an expensive (EUR 750), high quality device with well defined characteristics, whereas the Noliac NCE-41 transducer (EUR 15) is mass produced with less stringent specifications. This certainly had an influence on the separator performance (Chapter 7). The thought behind this was that the extremely expensive transducer would hardly contribute to a better performance of a handmade prototype device with many other deficiencies, like badly defined epoxy glue properties, to which the separator is very sensitive (Chapter 4). Applying the better transducer in separator devices requires well defined and precise manufacturing methods, especially in transducer bonding and wiring. These methods were not studied nor applied. Note, however, that the cheaper alternative might be adequate for many purposes.

9.1.4 Optimisation

Throughout the design process the acoustic pressure was used in the goal function for acoustic separator optimisation (Chapter 6). The question is then whether validation based on admittance is a satisfactory approach in the preceding steps (Chapters 3 and 4). It is known that the acoustic pressure in the fluid influences the electrical admittance of the transducer, both in reality and in the model. Transducer deformation or system mode shapes can also be verified with laser interferometry and pressure can be verified only in specific locations with a micro-tip (needle) pressure sensor, which will disturb the acoustic field at MHz frequencies (sub-mm wavelengths). However, neither of these methods was applied, because such setups require expensive and accurate equipment and their contribution to a better result should legitimate their use. Accurate measurements of various responses would certainly improve the accuracy of the estimated parameters, which included the geometrical parameters (section 4.3.2), but the influence of the subsequent unavoidable design changes to these geometrical parameters - the main issue in the separator optimisation - would still be undefined. Thus, the starting position would be well defined, but not the subsequent changes applied. Moreover, the unknown parameters were *estimated* with the measured admittance of an *empty* separator, and *validated* with a *filled* separator chamber. The admittance response changes, observed after filling the separator, were similar in the exper-

iments and the simulations, indicating that the admittance was a valid parameter to evaluate the system response; limited but valid.

Optimisation was performed using the average absolute acoustic pressure inside the resonator, which was found to be related to the particle displacement (Chapter 5). An average absolute pressure larger than 0.5 MPa was adopted as an adequate criterion for particle trapping. It is likely that even a pressure of 0.4 MPa will adequately trap all particles, thus reducing the power consumption (as voltage is linearly related to pressure in the model). In practical operation, a control strategy most likely aims at maintaining the separation efficiency of particles of any size. If this efficiency could be maintained by decreasing the power, the controller can certainly do so. In that sense, the chosen pressure criterion is indispensable for modelling and optimisation, but not directly of interest to the actual system operation. In practise, a high average pressure will be detrimental if it causes cavitation. Cavitation will have several effects on the suspension: turbulence, degassing and possibly (organic) particle oxidation and will therefore completely destabilise the acoustic separation process. Measures should be taken to minimise cavitation and maintain separation efficiency.

The final design is highly dependent on the objective chosen for optimisation. If minimal admittance, maximum pressure or minimal power were pursued, the result would be different. Even the particle size aimed for and the operation temperature will change the design. It is therefore very important to choose the right objective and practically operate likewise. Also the fluid and particle material properties will influence the best possible design, because they determine the density, stiffness and attenuation. This does not mean that the current design cannot be used in other circumstances, but it explains some of the limitations to the efficiency as found in Chapter 7.

9.1.5 Experiments

The final design was evaluated by means of a series of experiments with starch suspension of 1 g/l (Chapter 7). This is a relatively large concentration in terms of water quality, but has the advantage that it shows a rather quick saturation of the separator chamber. Even though a less efficient process was expected in reality as compared to the model, also the experiments in itself were far from optimal. The pulsating flow caused large fluctuations in fluid acceleration. This problem can be solved by using a pressurised or elevated reservoir, as will be discussed in Chapter 10.

Particle agglomeration and saturation were also indicated as possible causes of

limited concentration efficiency, because particles were by-passing the areas of high saturation. Optimisation of the operational process and taking into account the effects of saturated agglomeration is therefore recommended. Moreover, it is not exactly known to what extent smaller particles than aimed for ($< 10\mu\text{m}$ in this case) contribute to the turbidity found. Filtering a 350 NTU starch suspension with a $1.2\mu\text{m}$ Whatman filter still resulted in a filtrate turbidity between 30 NTU (newly made suspension) and 120 NTU (suspension after 2 hours), indicating that there is a significant contribution of small particles to the turbidity. One cannot simply extrapolate these numbers to a specific concentration, since also the relation between concentration and turbidity will change with particle size range.

However, the main limitation in the experimental evaluation of the model-based design of Chapter 7 was the limited power delivered by the ADI1015 amplifiers and, related to that, synchronisation problems with more than one amplifier. A more powerful and precise amplifier is recommended, which can control the frequency within a predefined narrow band. Modern electronics also provide more efficient methods for high frequency amplification compared to the more than a decade old ADI1015. The current ADI1015 amplifiers have a heat loss of more than 30% (30 W input versus 20 W maximum output), which is too much for large system applications.

Chapter 7 provided an evaluation of the separator performance, instead of a model validation step. The main reason is that there was a mismatch between the output of the model and the output of the experiments. As explained in section 9.1.2, the model was unable to provide particle concentrations in water as a result of the separation process, whereas it was concentration (turbidity) that was measured in the experiments. On the other hand the experiments could not provide acoustic pressure or particle trajectories, as did the simulation models. Furthermore, for proper validation of the model particles of $10\mu\text{m}$ and 1100 kg/m^3 , a steady, laminar flow and adequate power from the amplifiers would be needed. Even then, the validation would be hindered by precisely setting the correct frequency, not being the eigenfrequency, which produced the maximum pressure inside the resonator (see Chapter 6). Hence, validation of the numerical model of the resonator is still an open issue.

9.2 Conclusions

In this thesis a stepwise numerical-experimental approach to acoustic separator design was presented. Each layer in the separator was modelled and validated with experiments, starting with the piezoelectric transducer up to the acoustics and flow inside the resonator cavity. A model-based design optimisation was performed using a Design of Experiments (DOE) method, which resulted in a resonator with an optimal cavity size of 70×20×28.5 mm with three flow lanes and two transducers on each side of the cavity. The matching layer thickness of this system was 4.2 mm. The flow inside the resonator was perpendicular to the transducer surfaces.

The resonator had a theoretical particle retention of 100% at a flow rate of 5 ml/s (18 l/h) using particles with a diameter of 10 μ m and a density of 1100 kg/m³. The minimum power required was estimated to be 22-34 W, resulting in an average electric power of 1-1.5 kWh/m³. In order to obtain the desired flow rates of cubic meters per hour a modular setup with at least 50 parallel systems is recommended, which will be far more feasible than one large system, requiring a multiple of electric power.

The actual separation efficiency was calculated using the relative concentrations of influent and clarified fluid, both measured with a turbidity meter, since turbidity and concentration are linearly related. The maximum practical concentration efficiency obtained was 76% at a flow rate of 2 ml/s and a filtration efficiency of 54% at 1 ml/s with a real power input of 8.8 W. This is quite good compared to other studies presented in Chapter 2 (see Figure 9.1), indicating that numerical optimisation contributes to an improved separator design.

An optimal open loop control strategy showed that it is possible to operate an acoustic separator with high separation efficiency using the least power possible. Future control strategies should include inline turbidity measurements and feedback control to the voltage (power) and flow in order to optimise the operational filtering characteristics. Furthermore, modelling actual concentrations will provide the model output to actually validate the models used.

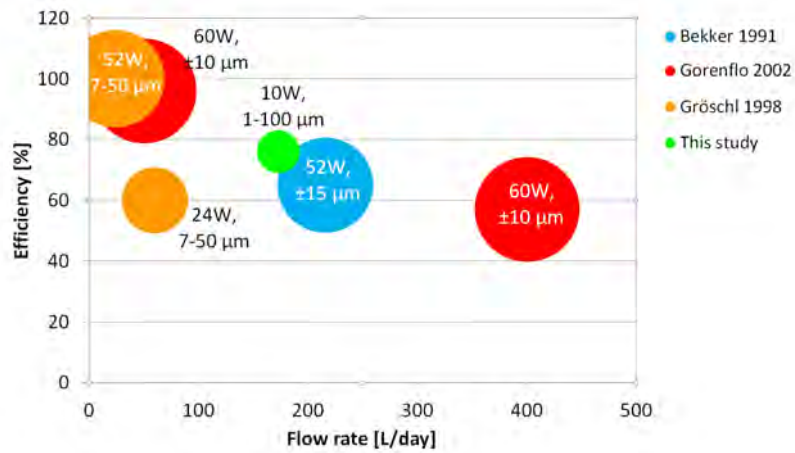


Figure 9.1: Concentration efficiency versus flow rate found in various studies (Chapter 2). The size of each balloon represents the given input power, while also the estimated particle size is shown for each study.

10. SYNTHESIS AND FUTURE PERSPECTIVE

10.1 Industrial size separators

The current prototype was built to treat a maximum of 18 l/hr of water, which means that multiple separators are needed to scale the process to larger dimensions. Although there is some room to increase the depth by at least 50% (to 3 cm), there is certainly a limit to the flow rate, as higher flow rates will induce turbulence. The current Reynolds number at 18 l/hr is near 115, so there is a laminar flow. Furthermore, the maximum flow rate depends on the application and the particle size. A rather easy way to increase the flow, is using two sides of each set of transducers, thus creating an array of parallel separators (Figure 10.1). Such construction also contributes to decreasing the energy demand, since two (resonant) transducer sides are used. Feeding such a large array of separators with suspension can be done by one reservoir, which is positioned above the array, so that water is fed to the systems by means of gravity. The outlets are connected to a second reservoir, from which the outlet flow is controlled by a valve. The resistance inside the separators is so low that the specified 18 l/hr per unit can be easily reached without additional pressure. A limitation of this parallelised setup is that the separators cannot be stacked vertically without additional flow control measures per separator unit.

Another option for device up-scaling is using a larger resonance chamber as was done in the Dissolved Air Flotation (DAF) system for whitewater (paper industry effluent) clarification [4]. Although this may seem to be an attractive solution, such large scale devices are far from optimal with respect to energy demand. If energy demand is not of importance, while maximum flow rate is, enlarging the dimensions is the most straightforward way to increase the flow. In order to increase the robustness, a stronger, stainless steel structure is recommended with large transducer plates and thus lower operating frequencies below 1 MHz. The lower frequency will require additional energy, but is less prone to attenuation and thus heat development in the large separator. Cooling is not considered to be a problem in any case, since the water itself acts as a coolant and its temperature will only increase slightly while passing through the separator, as the retention time at 5 ml/s is only 10 s.

10.2 Modes of operation

In this study only two modes of operation with fixed settings were used. In Chapter 7 a sequenced batch mode was used: the separator was operated until saturation took place and then concentrate was rinsed from the chamber by

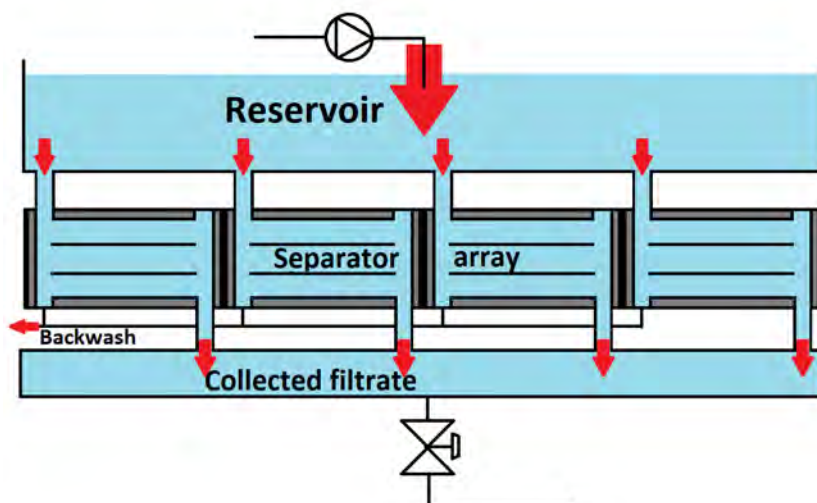


Figure 10.1: An array of separators with a reservoir on top (stock) and below (filtrate). The outlet valve controls the water level and flow rate inside the array and a backwash line washes out the concentrated suspension

backwashing. In Chapter 8 a continuous mode with pausing was applied: there was a continuous flow towards the concentrate outlet, thus continuously washing the chamber, while the filtrate flow and ultrasound was interrupted at set times, allowing settling and draining of the agglomerated particles.

Although these are the main modes of operation, there are many manipulated variables available for further optimisation:

- Switching times of both the ultrasound and the flow as in Chapters 7 and 8. Better separation might be induced by regularly switching off the sound without draining, thus allowing agglomerated particle flocs to settle, which can be done with a feedback controller on the basis of the measured filtering efficiency (turbidity).
- Phase or frequency differences between upper and lower transducer set, allowing movement of the particles towards one side of the chamber [18, 67].
- Active control of voltage (acoustic pressure) and frequency on the basis of measured concentrations (turbidity) at the filtrate and concentrate outlets.

- Angle of the chamber. If agglomerated particles do not settle at all, vertical operation like in Chapter 7 does not contribute to the process. However, if some settling occurs the might well be an optimal angle to the chamber, which is yet unknown.

Part of these parameters (switching times, phase and frequency differences) can be optimised by means of modelling. For optimisation of voltage based on turbidity and the angle, more advanced models are needed, incorporating particle agglomeration, particle concentration and interaction between the particles, the flow and the acoustic field.

10.3 Fields of application

Acoustic particle trapping started as a method to harvest biological cells from a suspension, like harvesting blood cells and bacterial colony flocs or yeast. During the last decade there has been little development in this biotechnological or medical area, while the technique has developed towards miniaturisation for particle detection, manipulation and characterisation purposes. Very little has been done on further development of water purification techniques with ultrasonic separators. In this research this relatively new filtration process was optimised and its efficiency was evaluated. It was found that electric energy demand of 1-1.5 kWh/m^3 limits the application of the technique to high value particles or toxic / hazardous particles, which must be recovered at all times. When larger particles are involved, the process becomes more feasible, due to lower power requirements, yet other techniques, like sand filtration, will then come in sight, as well. High product purity is a large advantage of acoustic separation over other techniques, while no additional agents or filter media, which might deteriorate product quality, are added to or interact with the water. A competing technology is the hydrocyclone, which is used in food industry for the concentration of starches. Trains of multiple hydrocyclones (up to 20) are used. Two advantages of acoustic separation are a low shear stress as compared to hydrocyclonation and the smaller chance of fouling.

A possible field of application is activated sludge-water separation after biological processes, like BOD removal or digestion. A series of experiments in which biological flocs were retained in the separator and the water was purified were reported by Keesman et al. [45]. The biological flocs did not show any deterioration due to the ultrasound and kept respiring dissolved organic material after ultrasonic exposure. Such system can be an interesting alternative to Membrane

BioReactor (MBR) technology, which has significant drawbacks due to fouling and plugging of the system by the activated sludge used. The separator presented in this study can be applied for sludge separation, but was not optimised to do so. A few tests were performed to test the feasibility of effluent polishing using communal wastewater effluent. The separator was shown to retain at least some of the particulate inside the chamber. Modelling of the fluffy particle flocs interacting with the acoustic field would be needed to optimise such a system. Such ultrasound separator models for soft matter, however, do not seem to exist.

Various applications related to acoustical particle trapping have been identified and patented during the course of this research:

- Enhanced disinfection focusing UV light beams on acoustically concentrated bacterial agglomerates (patent: NL1039050C);
- Particle/bacterial detection and sensors based on acoustically concentrated particle agglomerates (patent: NL1039051C);
- Ultrasound Standing-wave Bio-Reactor (USBR), mentioned above (patent: NL1039052C)
- Crystallisation or catalytic reactors, trapping crystals and/or catalysts in a USW matrix, while the water to be treated passes through the reactor (patent: NL1039053C)

Further modelling, optimisation and experimental work is required to develop each of these methods into mature and applicable technologies.

10.4 Model enhancements

As already stated, particle agglomeration modelling is the next step to further optimise the performance of ultrasonic separator systems as designed in this study. In general, particle properties are very important to determine the filtration efficiency. The effects of changing particle sizes with agglomeration, the effect of changing compressibility, non-perfect and non-rigid spheres and the use of soft materials with larger dimensions (floc) still need investigation in order to obtain the best solution for the future challenges in ultrasonic water treatment.

APPENDIX A. SENSITIVITY STUDY ON THE FINAL DESIGN

The sensitivity study in Chapter 6 involved changes to three factors, while monitoring the changes to the performance criteria. The results of all 27 simulations is shown in Table A.1. The before last column shows the minimum power required to obtain 0.5 MPa average absolute pressure, while applying variable voltage (see Appendix B). The associated frequency is shown in the last column. Note that this frequency is generally not at the main eigenfrequency.

Table A.1: Sensitivity of performance criteria to changes in the factors, changing all factors simultaneously. The reference design is shown in bold.

Separator length [mm]	Matching layer thickness [mm]	Flow lane height [mm]	$ p $ [MPa]	$Re(Y)$ [S]	AR [-]	U_{max} [mm/s]	U_r [mm/s]	Efficiency (for 0.5 MPa) [W]	@freq [MHz]
69.5	4.15	9.4	1.15	7.62	0.49	8	0.9	23	1.952
69.5	4.15	9.5	1.27	4.26	0.54	8	0.9	26	1.931
69.5	4.15	9.6	1.13	7.65	0.49	8	1.2	26	1.929
69.5	4.2	9.4	1.14	6.91	0.50	8	1.0	23	1.931
69.5	4.2	9.5	1.49	11.10	0.59	8	1.0	25	1.931
69.5	4.2	9.6	1.27	8.74	0.53	8	1.1	26	1.928
69.5	4.25	9.4	1.22	2.97	0.49	8	1.0	28	1.961
69.5	4.25	9.5	1.24	2.08	0.52	8	0.9	27	1.955
69.5	4.25	9.6	1.23	4.47	0.52	8	1.0	30	1.925
70	4.15	9.4	1.04	3.59	0.42	8	1.0	34	1.955
70	4.15	9.5	1.24	7.78	0.52	8	0.9	25	1.936
70	4.15	9.6	1.21	4.52	0.50	8	1.0	25	1.936
70	4.2	9.4	1.41	2.90	0.57	8	1.0	32	1.962
70.0	4.20	9.5	1.24	5.71	0.56	8	0.9	28	1.935
70	4.2	9.6	1.24	5.12	0.53	8	1.1	32	1.968
70	4.25	9.4	1.23	7.77	0.54	8	1.0	34	1.938
70	4.25	9.5	1.09	10.48	0.50	8	1.0	30	1.962
70	4.25	9.6	1.43	8.14	0.60	8	1.1	27	1.961
70.5	4.15	9.4	1.12	5.12	0.48	8	1.0	26	1.902
70.5	4.15	9.5	1.30	6.17	0.55	8	0.8	31	1.943
70.5	4.15	9.6	1.08	8.55	0.46	8	0.9	26	1.943
70.5	4.2	9.4	1.16	10.75	0.50	8	1.0	22	1.969
70.5	4.2	9.5	1.08	14.08	0.48	8	0.9	28	1.920
70.5	4.2	9.6	1.49	5.40	0.59	8	1.0	27	1.922
70.5	4.25	9.4	1.32	5.12	0.58	8	1.1	25	1.924
70.5	4.25	9.5	1.16	3.51	0.49	8	0.9	34	1.921
70.5	4.25	9.6	1.26	5.88	0.57	8	1.0	26	1.968

APPENDIX B. ENERGY CONSUMPTION OF THE FINAL DESIGN

In Chapter 6 the voltage was kept constant at 10 V during all simulations. In reality, voltage can be used to increase or decrease separation efficiency, thereby also changing the energy consumption (power). Fixing the power and varying voltage is another approach to the optimisation problem, however, with a different result. One can also find a maximum (average) pressure to power ratio at fixed voltage and adapt the voltage to obtain a certain lower pressure limit (e.g. 0.5 MPa), thus minimising power.

In the current (linear) model, for a given frequency f , V_{rms} is linearly related to acoustic pressure p and thus also to $|\bar{p}|$, which can be written as

$$|\bar{p}(f)| = \alpha_1(f)V_{rms} \quad (\text{B.1})$$

with $\alpha_1(f)$ a function of frequency. Doubling the voltage thus doubles the acoustic pressure, but quadruples the power (energy consumption), given by

$$P(f) = V_{rms}^2 Re(Y(f)) \quad (\text{B.2})$$

in which also $Y(f)$ is a function of frequency and dependent on the piezoelectric characteristics of the transducer, the acoustic properties of the separator materials used and of the fluid, and the separator dimensions.

Combining B.1 and B.2 results in

$$P(f) = \frac{|\bar{p}(f)|^2}{\alpha_1(f)^2} Re(Y(f)) \quad (\text{B.3})$$

In many cases the maximum average pressure is obtained at maximum real admittance, which occurs at the main eigenfrequency. This means that operation at the eigenfrequency results in maximum power.

Assume that at least 0.5 MPa absolute average pressure is needed to trap particles, so that

$$|\bar{p}(f)| \geq c_1 \quad (\text{B.4})$$

with $c_1 = 0.5[MPa]$. Then

$$\alpha_1(f)V_{rms} \geq c_1 \quad (\text{B.5})$$

so that

$$V_{rms} \geq \frac{c_1}{\alpha_1(f)} \quad (\text{B.6})$$

Combining B.2 and B.6 results in

$$P(f) \geq \frac{c_1^2}{\alpha_1(f)^2} Re(Y(f)) \quad (\text{B.7})$$

Hence, $P(f)$ is frequency dependent and can be minimised with respect to f while maintaining a minimum acoustic pressure ($c_1 = 0.5MPa$) in order to trap particles. The before last column of Table A.1 shows the power needed for the separators evaluated in the sensitivity study, when they are not operated at the eigenfrequency. The power ranges from 22 to 34 Watt, depending on size and frequency.

Figure B.1 shows the average absolute pressure at the eigenfrequency as well as at minimum power for each device in the sensitivity study with the nominal design encircled at the eigenfrequency and boxed at minimum power. The values calculated are connected by the dashed lines for each device in order to show that the minimum power is never obtained at the main eigenfrequency. The absolute average pressure is generally 2-3 times lower when operated at minimum power.

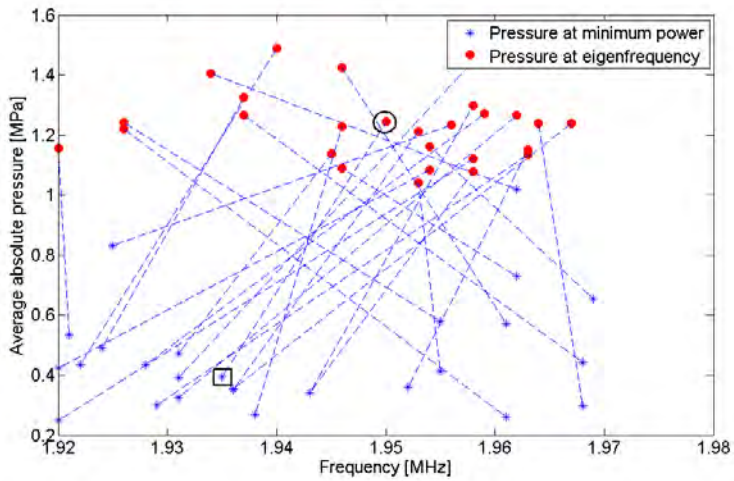


Figure B.1: Average absolute pressure for all 27 variations in the sensitivity study. The pressure at the main eigenfrequency and the pressure at minimum power of the same separator are shown.

APPENDIX C. TURBIDITY AND EFFICIENCY MEASUREMENTS

In Chapter 7 the mean results, confidence intervals and significance levels are presented. All measurements results are given in this appendix. The tables provide the measurements of each sample for Stock, Concentrate (Conc.) and Filtrate (Filt.), the average/mean, standard deviation (std) and 95% confidence interval (CI).

Table C.1: Runs: 2:30 minutes @ 60 mL/min (150 ml) and 30 s pause during which a backwash of 20 s @ 150 ml/min took place. US magnitude = 17.5 V amplitude @ 1945 kHz @ 10W

Blank	Sample	Stock			Conc.			Filt.		
	1	313	338	331	280	276	270	310	308	317
	2	362	359	342	253	275	266	299	285	312
	3	314	318	328	296	309	322	314	325	315
			mean	334		mean	283		mean	309
			std	17		std	21		std	11
			CI	13		CI	16		CI	8.4
Run 1	Sample	Stock			Conc.			Filt.		
	1	368	311	377	594	589	606	176	165	173
	2	352	378	336	458	442	465	180	176	174
	3	412	352	358	541	505	459	175	169	180
			mean	360		mean	518		mean	174
			std	27		std	62		std	5
			CI	21		CI	48		CI	3.5
Run 2	Sample	Stock			Conc.			Filt.		
	1	379	383	386	603	659	694	176	170	174
	2	327	363	364	455	508	573	177	200	156
	3	362	377	373	534	581	604	150	170	150
			mean	368		mean	579		mean	169
			std	17		std	69		std	15
			CI	13		CI	53		CI	11
t-test										
Blank					[S] vs [C]	0.000		[S] vs [F]	0.004	
Run1					[S] vs [C]	0.000		[S] vs [F]	0.000	
Run2					[S] vs [C]	0.000		[S] vs [F]	0.000	

Table C.2: Runs: 2:30 minutes @ 120 mL/min (300 ml) and 30 s pause during which a backwash of 20 s @ 150 ml/min took place. US magnitude = 17.5 V amplitude @ 1937-1942 kHz @ 10 W

Blank	Sample	Stock			Conc.			Filt.		
	1	319	324	296	335	346	341	316	336	346
	2	332	301	312	323	351	325	337	354	363
	3	342	286	296	418	389	378	335	299	310
			mean	312		mean	356		mean	333
			std	18		std	30		std	20
			CI	14		CI	23		CI	15
Run 1	Sample	Stock			Conc.			Filt.		
	1	317	340	346	549	665	619	268	285	264
	2	321	314	303	461	516	431	264	276	264
	3	342	325	256	457	520	563	288	281	241
			mean	318		mean	531		mean	270
			std	26		std	73		std	14
			CI	20		CI	56		CI	10
Run 2	Sample	Stock			Conc.			Filt.		
	1	317	352	379	641	685	685	246	236	270
	2	319	375	383	581	605	608	291	292	291
	3	307	362	329	552	562	571	281	278	288
			mean	347		mean	610		mean	275
			std	28		std	47		std	19
			CI	21		CI	37		CI	15
t-test										
Blank					[S] vs [C]	0.004		[S] vs [F]	0.041	
Run1					[S] vs [C]	0.000		[S] vs [F]	0.001	
Run2					[S] vs [C]	0.000		[S] vs [F]	0.000	

Table C.3: Runs: 2:30 minutes @ 180 mL/min (450 ml) and 30 s pause during which a backwash of 20 s @ 150 ml/min took place. US magnitude = 17.5 V amplitude @ 1937-1942 kHz @ 10 W

Blank	Sample	Stock			Conc.			Filt.		
	1	307	336	334	347	318	322	314	360	358
	2	343	333	354	313	317	335	346	330	339
	3	334	333	362	359	352	332	348	327	331
			mean	337		mean	333		mean	339
			std	15		std	16		std	14
			CI	11		CI	12		CI	11
Run 1	Sample	Stock			Conc.			Filt.		
	1	305	288	288	396	400	376	309	280	332
	2	328	316	338	318	367	357	299	279	273
	3	293	319	301	310	338	352	272	271	272
			mean	308		mean	357		mean	287
			std	17		std	30		std	20
			CI	13		CI	23		CI	16
Run 2	Sample	Stock			Conc.			Filt.		
	1	283	289	292	338	364	328	274	221	243
	2	301	268	324	296	291	298	240	229	241
	3	288	296	292	263	275	265	232	214	219
			mean	293		mean	302		mean	235
			std	14		std	33		std	17
			CI	11		CI	25		CI	13
t-test										
Blank					[S] vs [C]	0.556		[S] vs [F]	0.797	
Run1					[S] vs [C]	0.002		[S] vs [F]	0.039	
Run2					[S] vs [C]	0.469		[S] vs [F]	0.000	

APPENDIX D. STEADY STATE PARAMETER ESTIMATION

In Chapter 8 the steady state parameters were estimated. This appendix derives the formulae needed to calculate these estimates.

In steady state, all time derivatives of the states $\mathbf{S} = [S_1 \ S_2 \ S_3]^T$ are equal to zero:

$$\frac{d\mathbf{S}}{dt} = \mathbf{0} \quad (\text{D.1})$$

Therefore, Equation 8.1 becomes

$$0 = Q_1 S_{in} - Q_1 S_{1ss} + (1 - \alpha) K_3 S_{3ss} V_3 - \alpha k_1 S_{1ss} V_1 - \frac{k_2 S_{1ss} V_1}{Q_1 + k_4} \quad (\text{D.2})$$

$$Q_1 (S_{1ss} - S_{in}) = (1 - \alpha) K_3 S_{3ss} V_3 - \alpha k_1 S_{1ss} V_1 - \frac{k_2 S_{1ss} V_1}{Q_1 + k_4} \quad (\text{D.3})$$

Equation 8.2 then becomes

$$0 = Q_2 S_{in} - Q_2 S_{2ss} + \frac{k_2 S_{1ss} V_1}{Q_1 + k_4} \quad (\text{D.4})$$

$$Q_2 (S_{2ss} - S_{in}) = \frac{k_2 S_{1ss} V_1}{Q_1 + k_4} \quad (\text{D.5})$$

and Equation 8.3, only valid when the acoustic field is switched off, becomes

$$0 = \alpha k_1 S_{1ss} V_1 - (1 - \alpha) k_3 S_{3ss} V_3 \quad (\text{D.6})$$

In steady state this results in the following matrix form,

$$\begin{bmatrix} -\alpha S_{1ss} V_1 & -S_{1ss} V_1 & (1 - \alpha) S_{3ss} V_3 \\ 0 & S_{1ss} V_1 & 0 \\ \alpha S_{1ss} V_1 & 0 & -(1 - \alpha) S_{3ss} V_3 \end{bmatrix} \begin{bmatrix} k_1 \\ \frac{k_2}{Q_1 + k_4} \\ k_3 \end{bmatrix} = \begin{bmatrix} Q_1 (S_{1ss} - S_{in}) \\ Q_2 (S_{2ss} - S_{in}) \\ 0 \end{bmatrix} \quad (\text{D.7})$$

Furthermore two cases of operation exist: the acoustic field switched on and acoustic field switched off. When $\alpha = 1$ and assuming that $Q_1 \gg k_4$, Equation 8.4 becomes:

$$\begin{bmatrix} -S_{1sson}V_1 & -\frac{S_{1sson}V_1}{Q_1} \\ 0 & \frac{S_{1sson}V_1}{Q_1} \end{bmatrix} \begin{bmatrix} k_1 \\ k_2 \end{bmatrix} = \begin{bmatrix} Q_1(S_{1sson} - S_{in}) \\ Q_2(S_{2sson} - S_{in}) \end{bmatrix} \quad (D.8)$$

Consequently, the estimate of k_1 and k_2 are given by

$$\begin{bmatrix} k_1 \\ k_2 \end{bmatrix} = \begin{bmatrix} -S_{1sson}V_1 & -\frac{S_{1sson}V_1}{Q_1} \\ 0 & \frac{S_{1sson}V_1}{Q_1} \end{bmatrix}^{-1} \begin{bmatrix} Q_1(S_{1sson} - S_{in}) \\ Q_2(S_{2sson} - S_{in}) \end{bmatrix} \quad (D.9)$$

$$= \begin{bmatrix} -\frac{Q_1(S_{1sson} - S_{in}) + Q_2(S_{2sson} - S_{in})}{\frac{S_{1sson}V_1}{Q_1}} \\ \frac{Q_1Q_2(S_{2sson} - S_{in})}{S_{1sson}V_1} \end{bmatrix} \quad (D.10)$$

When the acoustic field is switched off ($\alpha = 0$), Q_1 also equals 0, so that

$$\begin{bmatrix} 0 & -S_{1ssoff}V_1 & (1 - \alpha)S_{3ssoff}V_3 \\ 0 & S_{1ssoff}V_1 & 0 \\ 0 & 0 & -S_{3ssoff}V_3 \end{bmatrix} \begin{bmatrix} k_1 \\ \frac{k_2}{k_4} \\ k_3 \end{bmatrix} = \begin{bmatrix} 0 \\ Q_2(S_{2ssoff} - S_{in}) \\ 0 \end{bmatrix} \quad (D.11)$$

and thus the estimate of k_4 is given by

$$k_4 = \frac{S_{1ssoff}V_1k_2}{Q_2(S_{2ssoff} - S_{in})} \quad (D.12)$$

BIBLIOGRAPHY

- [1] IEEE standard on piezoelectricity, ANSI/IEEE standard 176-1987.
- [2] EN50324 standard - piezoelectric properties of ceramic materials and components, 2002.
- [3] N. Aboobaker, D. Blackmore, and J. Meegoda. Mathematical modeling of the movement of suspended particles subjected to acoustic and flow fields. *Applied Mathematical Modelling*, 29:515–532, 2005.
- [4] F. Ahrens and T. Patterson. Final report, acoustic separation technology. Technical report, Institute of Paper Science and Technology, 2002.
- [5] M.A.B. Andrade, F. Buiochi, and J.C. Adamowski. Particle manipulation by ultrasonic progressive waves. *Physics Procedia*, 3:283–288, 2010.
- [6] D.M. Bates and D.G. Watts. *Nonlinear Regression Analysis and its Applications*. Wiley and Sons, New York, 1988.
- [7] M.C. Bekker, J.P. Meyer, L. Pretorius, and D.F. Van Der Merwe. Separation of solid-liquid suspensions with ultrasonic acoustic energy. *Water Research*, 31(10):2543–2549, 1997.
- [8] E. Benes, M. Gröschl, H. Nowotny, F. Trampler, T. Keijzer, H. Böhm, S. Radel, L. Gherardini, J.J. Hawkes, R. König, and Ch. Delouvroy. Ultrasonic separation of suspended particles. In *IEEE International Ultrasonics Symposium*, 2001.
- [9] R. Bosma, W.A. van Spronsen, J. Tramper, and R.H. Wijffels. Ultrasound, a new separation technique to harvest microalgae. *Journal of Applied Phycology*, 15:143–153, 2003.
- [10] H. Bruus. Microfluidics and ultrasound acoustophoresis. In *Ultrasound standing wave action on suspensions and biosuspensions in micro- and macrofluidic devices*, Udine, 7-10 June, 2010.
- [11] H. Cappon and K.J. Keesman. Numerical modelling of piezoelectric transducers using physical parameters. *IEEE trans. on Ultrasonics, Ferroelectrics and Frequency Control*, 59(5):1023–1032, 2012.
- [12] H.J. Cappon and K.J. Keesman. Design basis of industrial acoustic separators. In *IEEE UFFC International Ultrasonics Symposium, Prague, 20-25 July*, 2013.
- [13] H.J. Cappon and K.J. Keesman. Design of industrial acoustic separators. *Separation and Purification Technology*, submitted, 2013.

- [14] H. Cappon and K.J. Keesman. Numerical modeling, calibration and validation of an ultrasonic separator. *IEEE trans. on Ultrasonics, Ferroelectrics and Frequency Control*, 60(3):614–621, 2013.
- [15] H.J. Cappon, L.A. Stefanova, and K.J. Keesman. Concentration based flow control in acoustic separation of suspensions. *Separation and Purification Technology*, 103:321–327, 2012.
- [16] H. Cease, P.F. Derwent, H.T. Diehl, J. Fast, and D. Finley. Measurement of mechanical properties of three epoxy adhesives at cryogenic temperatures for CCD construction. Technical Report Fermilab-TM-2366-A, Fermi National Accelerator Laboratory, 2006.
- [17] Comsol AB, Stockholm. *Comsol Acoustics Module, User's Guide*, 2009.
- [18] C.R.P. Courtney, C.K. Ong, B.W. Drinkwater, P.D. Wilcox, C. Demore, S. Cochran, P. Glynne-Jones, and M. Hill. Manipulation of microparticles using phase-controllable ultrasonic standing waves. *Journal of the Acoustical Society of America*, 128(4), 2010.
- [19] Y. Dain, M. Fichman, C. Gutfinger, D. Pnueli, and P. Vainshtein. Dynamics of suspended particles in a two-dimensional high frequency sonic field. *Journal of Aerosol Science*, 26(4):575–594, 1995.
- [20] O. Doblhoff-Dier, Th. Gaida, H. Katinger, W. Burger, M. Gröschl, and H. Benes. A novel ultrasonic resonance field device for the retention of animal cells. *Biotechnology Progress*, 10:428–432, 1994.
- [21] O. Dron, C. Ratier, M. Hoyos, and J-L Aider. Parametric study of acoustic focusing of particles in a micro-channel in the perspective to improve micro-piv measurements. *Microfluid nanofluid*, 7:857–867, 2009.
- [22] D.D. Ebenezer and A.J. Sujatha. Errors in the characterization of piezoelectric ceramics. In *Proceedings of SPIE*, volume 5062, pages 182–189, 2003.
- [23] M. Gröschl (Ed.). Ultrasonic separation of suspended particles - part II: Design and operation of separation devices. *Acta acustica*, 84:632–642, 1998.
- [24] P. Glynne-Jones, M. Hill, N.R. Harris, R.J. Townsend, and S.K. Ravula. The design and modelling of a lateral acoustic particle manipulator exhibiting quarter wave operation. In: *Proceedings of Acoustics 08*, pages 5987–5991, 2008.
- [25] P. Glynne-Jones, R.J. Boltryk, N.R. Harris, A.W.J. Cranny, and Martyn Hill. Mode-switching: A new technique for electronically varying the agglomeration position in an acoustic particle manipulator. *Ultrasonics*, 50(1):68 – 75, 2010.
- [26] V.M. Gorenflo, L. Smith, B. Dedinsky, B. Persson, and J.M. Piret. Scale-up and optimization of an acoustic filter for 200 l/day perfusion of a cho cell culture. *Biotechnology and Bioengineering*, 80(4):438–444, 2002.
- [27] L.P. Gor'kov. On the forces acting on a small particle in an acoustical field in an ideal fluid. *Soviet Physics - Doklady*, 6(9):773–775, 1962.

-
- [28] R.K. Gould, W.T. Coakley, and M.A. Grundy. Upper sound pressure limits on particle concentration in fields of ultrasonic standing-wave at megahertz frequencies. *Ultrasonics*, 30(4):239–244, 1991.
- [29] A. Grinenko, P.D. Wilcox, C.R.P Courtney, and B.W. Drinkwater. Proof of principle study of ultrasonic particle manipulation by a circular array device. *Proceedings of the Royal Society A*, 468(2138):337–360, 2012.
- [30] M. Gröschl. Ultrasonic separation of suspended particles - part I: Fundamentals. *Acta acustica*, 84:432–447, 1998.
- [31] M. Gröschl, W. Burger, B. Handl, O. Doblhoff-Dier, Th. Gaida, and C. Schmatz. Ultrasonic separation of suspended particles - part iii: Application in biotechnology. *Acta acustica*, 84:815–822, 1998.
- [32] A. Haake and J. Dual. Positioning of small particles by an ultrasound field excited by surface waves. *Ultrasonics*, 42:75–80, 2004.
- [33] J. Hawkes, W. Coakley, M. Gröschl, E. Benes, S. Armstrong, P. Tasker, and H. Nowotny. Single half wavelength ultrasonic particle filter: Predictions of the transfer matrix multi-layer resonator model and experimental filtration results. *Journal of the Acoustic Society of America*, 111:1259–1266, 2002.
- [34] J.J. Hawkes and W.T. Coakley. A continuous flow ultrasonic cell-filtering method. *Enzyme Microbial Technology*, 19:57–62, 1996.
- [35] J.J. Hawkes and W.T. Coakley. Force field particle filter, combining ultrasound standing waves and laminar flow. *Sensors and Actuators B*, 75:213–222, 2001.
- [36] M. Hill, Y. Shen, and J.J. Hawkes. Modelling of layered resonators for ultrasonic separation. *Ultrasonics*, 40:385–392, 2002.
- [37] M. Hill, R.J. Townsend, and N.R. Harris. Modelling for the robust design of layered resonators for ultrasonic particle manipulation. *Ultrasonics*, 48:521–528, 2008.
- [38] M. Hill and R.J.K. Wood. Modelling in the design of a flow-through ultrasonic separator. *Ultrasonics*, 38(1-8):662 – 665, 2000.
- [39] H.W. Joo, C.H. Lee, J.S. Rho, and H.K Jung. Identification of material constants for piezoelectric transformers by three-dimensional, finite-element method and a design-sensitivity method. *Ultrasonics, Ferroelectrics and Frequency Control, IEEE Transactions on*, 50(8):965 – 971, 2003.
- [40] B. Kaltenbacher, M. Kaltenbacher, R. Lerch, and R. Simkovic. Identification of material tensors for piezoceramic materials. In *Ultrasonics Symposium, 2000 IEEE*, volume 2, pages 1033 –1036, Oct. 2000.
- [41] M. Kaltenbacher. *Numerical Simulation of Mechatronic Sensors and Actuators*. Springer, 2 edition, 2007.

- [42] M. Kaltenbacher, R. Simkovic, B. Kaltenbacher, and R. Lerch. Determination of piezoelectric material parameters using a combined measurement and simulation technique. In *Ultrasonics Symposium, 2001 IEEE*, volume 2, pages 1023–1026, 2001.
- [43] S. Kapishnikov, V. Kantsler, and V. Steinberg. Continuous particle size separation and size sorting using ultrasound in a microchannel. *Journal of statistical mechanics: theory and experiment*, 2006.
- [44] K.J. Keesman. *System Identification: an Introduction*. Springer Verlag, London, 2011.
- [45] K.J. Keesman, N. de Beus, J. Klok, and H. Cappon. Ultrasound standing-wave bio-reactor design and testing on aerobic activated sludge. In *IEEE UFFC International Ultrasonics Symposium, Prague, 20-25 July, 2013*.
- [46] F.N. Kemmer, editor. *The NALCO Water Handbook*. McGraw-Hill Book Company, 2 edition, 1987.
- [47] Louis V. King. On the acoustic radiation pressure on spheres. *Proceedings Royal Society London*, 147:212–240, 1934.
- [48] T. Lahmer, M. Kaltenbacher, B. Kaltenbacher, R. Lerch, and E. Leder. Fem-based determination of real and complex elastic, dielectric, and piezoelectric moduli in piezoceramic materials. *Ultrasonics, Ferroelectrics and Frequency Control, IEEE Transactions on*, 55(2):465–475, 2008.
- [49] N. Lamberti and A. Caputo. Characterization of piezoelectric ceramic elements by using ansys. In *Proceedings of the International Congress on Ultrasonics, 2007*.
- [50] T. Laurell, F. Petersson, and A. Nilsson. Chip integrated strategies for acoustic separation and manipulation of cells and particles. *Chemical Society Reviews*, 36:492–506, 2007.
- [51] A. Lenshof, M. Evander, T. Laurell, and J. Nilsson. Acoustofluidics 5: Building microfluidic acoustic resonators. *Lab Chip*, (12):684–695, 2012.
- [52] R. Lerch. Finite element analysis of piezoelectric transducers. In *Ultrasonics Symposium, 1988. Proceedings., IEEE 1988*, pages 643–654 volume 2, 1988.
- [53] T. Lilliehorn, U. Simu, M. Nilsson, M. Almqvist, T. Stepinski, T. Laurell, J. Nilsson, and S. Johansson. Trapping of microparticles in the near field of an ultrasonic transducer. *Ultrasonics*, 43:293–303, 2005.
- [54] B. Lipkens, M. Costolo, and E. Rietman. The effect of frequency sweeping and fluid flow on particle trajectories in ultrasonic standing waves. *IEEE sensors journal*, 8(61):667–677, 2008.
- [55] B. Lipkens, J. Dionne, A. Trask, B. Szczur, A. Stevens, and E. Rietman. Separation of micron-sized particles in macro-scale cavities by ultrasonic standing waves. *Physics Procedia*, 3(1):263–268, 2010.

-
- [56] A. Neild, S. Oberti, and J. Dual. Design, modeling and characterization of microfluidic devices for ultrasonic manipulation. *Sensors and Actuators B*, 121:452–461, 2007.
- [57] A. Neild, S. Oberti, A. Haake, and J. Dual. Finite element modeling of a microparticle manipulator. *Ultrasonics*, 44:e455–e460, 2006.
- [58] H. Nowotny and E. Benes. General one-dimensional treatment of the layered piezoelectric resonator with two electrodes. *The Journal of the Acoustical Society of America*, 82(2):513–521, 1987.
- [59] H. Nowotny, E. Benes, and M. Schmid. Layered piezoelectric resonators with an arbitrary number of electrodes (general one-dimensional treatment). *The Journal of the Acoustical Society of America*, 90(3):1238–1245, 1991.
- [60] S. Peterson, G. Perkins, and C. Baker. Development of an ultrasonic blood cell separator. In: *IEEE/Engineering in Medicine and Biology Society Annual Conference*, pages 154–156, 1986.
- [61] B. Piranda, S. Ballandras, T. Steichen, and B. Hecart. A model-updating procedure to simulate piezoelectric transducers accurately. *Ultrasonics, Ferroelectrics and Frequency Control, IEEE Transactions on*, 48(5):1321–1331, 2001.
- [62] L. Svarovsky. *Solid-liquid separation*. Elsevier Ltd., 4 edition, 2001.
- [63] G. Tchobanoglous, F.L. Burton, and H.D. Stensel. *Wastewater Engineering: treatment and reuse / Metcalf & Eddy, Inc.* McGraw-Hill Publishing Company, 4 edition, 2003.
- [64] R.J. Townsend, M. Hill, N.R. Harris, and M.B. McDonnell. Performance of a quarter-wavelength particle concentrator. *Ultrasonics*, 48:515–520, 2008.
- [65] R.J. Townsend, M. Hill, N.R. Harris, and N.M. White. Modelling of particle paths passing through an ultrasonic standing wave. *Ultrasonics*, 42:319–324, 2004.
- [66] F. Trampler, J.M. Piret, S.A. Sonderhoff, and D.G. Kilburn. Acoustic filter for separating and recycling suspended particles. US Patent 5626767, 1997.
- [67] G. Whitworth, M.A. Grundy, and W.T. Coakley. Transport and harvesting of suspended particles using modulated ultrasound. *Ultrasonics*, 29:439–444, November 1991.
- [68] M. Wiklund, R. Green, and M. Ohlin. Acoustofluidics 14: Applications of acoustic streaming in microfluidic devices. *Lab Chip*, 12(14):2438–2451, 2012.
- [69] F. Wolf, T. Lahmer, L. Bahr, A. Hauck, A. Sutor, R. Lerch, and M. Kaltenbacher. Finite element modeling of ultrasonic transducer by utilizing an inverse scheme for the determination of its material parameters. In *Ultrasonics Symposium, 2008. IUS 2008. IEEE*, pages 784–787, 2008.

LIST OF FIGURES

2.1	Single degree of freedom (SDOF) systems: a mechanical mass-spring-damper system (left) and an electrical inductor-resistor-capacitor system (right).	24
2.2	Sketch of ultrasonic particle trapping using standing waves. The transducer (left) and the reflector (right) build the standing wave field (with two nodes) in the intermediate fluid layer. Particles are first scattered (a), immediately line up (b) and agglomerate (c) in the nodes.	27
2.3	Experimental setup of an acoustic separator in air. Four piezo tweeters were mounted perpendicularly on a transparent base plate and driven by an amplified sinusoidal signal creating a resonance field.	34
2.4	Sequence of four snapshots of the process of particle concentration. The first photo shows the initial situation with randomly placed particles, the second and third show the process of separation and the last photo shows the final position of the particles after approximately 0.12s.	36
2.5	Particle displacement versus time in the acoustic pressure field. The value on the y-axis at time 0 represents the initial position of the particle. Particles are driven to three locations in 0.12s.	37
3.1	Setup for impedance analysis on a plate of piezoceramic material SPC-140.	46
3.2	Admittance Bode plot for the piezoceramic. Nine measurements with a frequency sweep from 2.0-2.1 MHz with 100 Hz intervals on a single new specimen.	50
3.3	Absolute value of the admittance versus frequency for a full factorial DOE varying s_{12} (6 values), s_{13} (6 values) and s_{44} (2 values).	51
3.4	Residual sum of squared differences between simulated and experimental admittance (z-axis) versus s_{12} (x-axis) and s_{13} (y-axis).	52
3.5	Admittance amplitude plot obtained with a least squares optimisation routine with 2D simulations. The theoretical quality factor Q needed to be reduced from 350 to the measured value of 129 to obtain the correct peak height. The 3D analysis was added for comparison and shows small differences with the 2D results.	53

3.6	Admittance phase plot obtained with a least squares optimisation routine with 2D simulations. The 3D analysis was added for comparison and shows small differences with the 2D results.	54
3.7	3D acceleration pattern of the quarter piezoceramic at the eigenfrequency of 2.05 MHz, verifying the first thickness mode.	55
3.8	Residual sum of squared differences between simulated and experimental admittance (z-axis) versus s_{13} (x-axis) and d_{31} (y-axis).	56
3.9	Eigenfrequency (peak location) of the admittance (z-axis) versus s_{12} (x-axis) and s_{13} (y-axis) at three different values of s_{33} (the three stacked layers). The figure was obtained using a 6×6×3 full factorial DOE. The figure shows that the set of three parameters is not unique at a given eigenfrequency.	58
3.10	Admittance amplitude plot obtained with a least squares optimisation routine with 2D simulations after decreasing d_{33} by 5%. This implied increasing quality factor Q as well.	59
4.1	The borosilicate cuvette, a basic non-flow separation device, with a BNC power connector on the right side.	65
4.2	Finite element model of the separator, top view. The five numbered areas are 1) glass cuvette, 2) water, 3) adhesive layer, 4) and 5) piezo halves.	66
4.3	Flow chart of the numerical calibration and validation process.	72
4.4	Admittance curve, magnitude and phase, measured on an the empty separator from 500 to 3000 kHz. The first main peak at 1.99 MHz is caused by the matching layer of the separator, the second at 2.29 MHz is the (shifted) eigenfrequency of the piezoelectric transducer.	73
4.5	Admittance curve (magnitude) measured on the water filled separator from 1950 to 2050 kHz at three different temperatures.	74
4.6	Experimental and simulated admittance curve of the empty separator based on the initial 2D model.	74
4.7	Model frequency response while varying epoxy E-modulus from 2.0 to 5.0 GPa in 0.5 GPa steps; increasing stiffness means shifting the second peak to the right (with increasing line thickness).	75
4.8	Model frequency response while varying epoxy quality factor from 25 to 150 in 6 steps; higher Q means higher (second) peak (with increasing line thickness).	75
4.9	Model frequency response while varying epoxy adhesive thickness from 30 to 50 μm in 5 μm steps; increasing thickness means shifting the second peak to the left (with increasing line thickness).	76

4.10	Model frequency response while varying the transducer Q-factor from 100 to 400 in 6 steps; increasing Q means higher (first) peak (with increasing line thickness).	76
4.11	Model frequency response while varying matching layer thickness from 4.15 to 4.30 mm in 0.05 mm steps; increasing thickness means a general peak shift to the left (with increasing line thickness).	77
4.12	Experimental and simulated magnitude of admittance of an empty separator. The simulated signal before and after calibration of the 2D model is shown.	77
4.13	Simulated magnitude of admittance of a water filled separator with varying channel width from 1.99 to 2.01 mm in 50 μ m steps; increasing channel width means a peak shift to the left (with increasing line thickness).	78
4.14	Experimental and simulated magnitude of admittance of a water filled separator showing four eigenfrequencies.	78
4.15	Simulated pressure profile in a 2D separator (top view) showing the typical nodal and anti-nodal pressure lines causing acoustic particle separation.	79
5.1	Side view of the model of the resonator chamber with two piezo transducers on the left and right. The transducers create the acoustic pressure field shown inside the chamber.	85
5.2	An example of a resonator chamber with short-circuiting flow pattern causing eddy currents	86
5.3	Preferred flow path inside a chamber with multiple, equally sized flow lanes (left) and inside a chamber applying geometrical flow splitting, resulting in almost equal flow in each lane (right).	88
5.4	Flow pattern with aligned and adapted partitions inside the chamber at 4 ml/s.	89
5.5	Flow pattern with adapted partitions and flow rates from 1-5 ml/s	90
5.6	Particle trajectories of the combined acoustic field and flow simulations with ultrasound (left) and without ultrasound (right).	90
5.7	Particle displacement versus acoustic pressure norms in a square resonator chamber. With peak acoustic pressure above 1 MPa or average acoustic pressure above 0.5 MPa particle displacement clearly decreases.	91
6.1	Example of the 2D resonator FE model consisting of two transducers on either side of the resonator, an inlet (top left) and outlet (bottom right) and three flow lanes with equalised flow velocity	95
6.2	Relation between the averaged absolute pressure and separator length	101

6.3	Relation between the averaged absolute pressure and matching layer thickness	102
6.4	Relation between the averaged absolute pressure and flow lane height (180 simulations)	103
6.5	Area ratio with pressure above 1 MPa versus real admittance Y	104
6.6	Area ratio divided by $Re(Y)$ versus average absolute pressure	105
6.7	Maximum flow velocity versus separator length	106
6.8	Maximum flow velocity versus separator lane height	107
6.9	Flow lane criterion versus separator length and flow lane height based on a full factorial DOE of 48 simulations	108
6.10	Flow velocity profile inside each lane at flow rates of 1-5 ml/s (left: lower lane, right: upper lane)	110
6.11	Frequency dependency of the minimum power required to obtain 0.5 MPa average pressure and the power at 10 V input (on the left y-axis) and average absolute pressure (on the right y-axis) for the new nominal design.	111
7.1	Prototype separator for experimental evaluation	115
7.2	The experimental setup used to test the separator (center) with ports numbered 1-4. The bottom power amplifier was used in this evaluation.	116
7.3	Magnitude of the measured admittance versus frequency for each individual transducer set at each end of the separator as well as both sets connected in series.	119
7.4	Turbidity of stock, concentrate and filtrate for one blank and two ultrasound experiments at a flow rate of 1 ml/s. The error bars indicate the 95% confidence interval.	120
7.5	Turbidity of stock, concentrate and filtrate for one blank and two ultrasound experiments at a flow rate of 2 ml/s. The error bars indicate the 95% confidence interval.	120
7.6	Turbidity of stock, concentrate and filtrate for one blank and two ultrasound experiments at a flow rate of 3 ml/s. The error bars indicate the 95% confidence interval.	121
7.7	Particle size distribution of the potato starch used in the experiments.	122
8.1	Three step acoustic separation principle: a) creation of the ultrasonic standing wave field, b) collection of particles in nodal lines, and c) agglomeration of particles forming clumps, which settle more easily.	127

8.2	Experimental setup using a BioSep, two peristaltic pumps and an in-line turbidity meter (left) and a zoomed in view of the BioSep resonator chamber (right).	129
8.3	Separation model of BioSep using three compartments, one inlet and two outlets for filtrate and concentrate flows.	130
8.4	Landscape of 81 experiments with nine flow rates for the filtrate pump and concentrate pump.	132
8.5	Dynamic experiment of inlet (S_{in}) and outlet concentrations (S_1 and S_2) showing four filtration cycles. Pump 1 and the ultrasound are switched on for 30 s and switched off for 3 s.	133
8.6	Dynamic simulation showing outlet concentrations (S_1 and S_2) and internal concentration (S_3) during 10 filtration cycles. Pump 1 and the ultrasound are switched on for 30 s and switched off for 3 s resulting in 92% separation efficiency.	136
8.7	Dynamic simulation showing outlet concentrations (S_1 and S_2) and internal concentration (S_3) during 10 filtration cycles with optimal control. Pump 1 and the ultrasound are switched on for 3 s and switched off for 30 s resulting in 99% separation efficiency.	139
9.1	Concentration efficiency versus flow rate found in various studies (Chapter 2). The size of each balloon represents the given input power, while also the estimated particle size is shown for each study.	149
10.1	An array of separators with a reservoir on top (stock) and below (filtrate). The outlet valve controls the water level and flow rate inside the array and a backwash line washes out the concentrated suspension	153
B.1	Average absolute pressure for all 27 variations in the sensitivity study. The pressure at the main eigenfrequency and the pressure at minimum power of the same separator are shown.	161

LIST OF TABLES

2.1	Studies on ultrasonic standing wave separation units and particle manipulators, highlighting the mainstream of the modelled and evaluated systems.	28
2.2	Input and output parameters with corresponding values	38
3.1	Material constants of piezo material SPC-140. The subscripts with numbers, e.g. d_{31} , indicate the coupling in direction 3 with the value in direction 1. For example: a mechanical displacement in z-direction (3) results in a voltage change in x-direction (1)	48
3.2	Material parameters of piezo material SPC-140 to be estimated and pre-defined range and parameter step for full factorial design of experiments [first value:step size:last value].	49
3.3	Material constants of piezo material SPC-140 estimated with a least squares optimisation routine	53
3.4	Sensitivity of admittance peak frequency and magnitude to 1% change in parameter value. The first row of each parameter corresponds to -1% change, the second to +1% change. The shift is calculated as a percentage of the given reference value	57
3.5	Result of optimisation with 10 parameters showing the initial values, derived from the previous optimisation, the final values and the deviation from the initial value.	57
3.6	Material constants of piezo material SPC-140 estimated with a least squares optimisation routine after decreasing d_{33}	58
4.1	Main dimensions of the cuvette	64
4.2	Parameter grid for model calibration	69
6.1	Ranges of factors (LH = Latin Hypercube; FF = Full Factorial; Ac. = Acoustic domain; Fl. = flow domain)	99
6.2	Optimal separator designs based on different criteria, shown in bold . . .	104

6.3	Sensitivity of responses to changes in the factors, changing one factor at a time. The last row shows the maximum deviation found, while changing all factors simultaneously.	109
6.4	Particle displacement results at various flow rates in the final design. A maximum displacement of 66 mm and average displacement of 63 mm indicates that no particles are trapped.	109
7.1	Test matrix of the experimental runs performed and the amount of samples taken per input/output port. The turbidity of each sample taken was measured trice, resulting in nine measurements per port per experimental run.	118
7.2	Concentration and filtration efficiency in % as compared to the stock solution with the associated significance (Student T-test using a 95% confidence interval). Only the numbers in italics show non-significant differences.	119
7.3	Simulated average displacement in mm of 25 particles released at the inlet after 15 s of simulated time as a function of particle size, without and with ultrasound applied.	123
8.1	System parameter values in steady state analysis.	134
8.2	Coefficients k_j of the control model obtained from steady state and dynamic analyses.	135
8.3	Initial set and best set of 64 simulated control strategy showing simulation number, mass difference and filtrated particle mass. Maximal mass difference Δm and minimal filtrated mass m_f is strived for, which corresponds to strategy 52.	138
A.1	Sensitivity of performance criteria to changes in the factors, changing all factors simultaneously. The reference design is shown in bold.	158
C.1	Runs: 2:30 minutes @ 60 mL/min (150 ml) and 30 s pause during which a backwash of 20 s @ 150 ml/min took place. US magnitude = 17.5 V amplitude @ 1945 kHz @ 10W	164
C.2	Runs: 2:30 minutes @ 120 mL/min (300 ml) and 30 s pause during which a backwash of 20 s @ 150 ml/min took place. US magnitude = 17.5 V amplitude @ 1937-1942 kHz @ 10 W	165
C.3	Runs: 2:30 minutes @ 180 mL/min (450 ml) and 30 s pause during which a backwash of 20 s @ 150 ml/min took place. US magnitude = 17.5 V amplitude @ 1937-1942 kHz @ 10 W	166

LIST OF SYMBOLS AND ABBREVIATIONS

Symbol	Description	Defined in section
Abbreviations		
AC	Alternating Current	2
ABS	Acrylonitrile butadiene styrene, plastic	7.2.1
BOD	Biochemical Oxygen Demand	10.3
CHO	Chinese Hamster Ovary (cells)	2.2.5
DOE	Design of Experiments, sampling method	3.3.4
FE	Finite Element	2.2.3
DAF	Dissolved Air Flotation	2.2.5
MEMS	Micro Electro-Mechanical Systems	3.2
MDOF	Multi-degree of freedom	2.1
NTU	Nephelometric Turbidity Units	7.4
PIV	Particle Image Velocimetry	2.2.5
PMMA	Polymethyl metacrylate, perspex	2.3.1
PVC	Polyvinyl chloride, plastic	7.2.1
PZT	Lead Zirconate Titanate, piezoelectric material	3.2
SDOF	Single degree of freedom	2.1
US	Ultrasound	3.3.1
USW	Ultrasonic Standing Waves	2.1
Acoustofluidics		
a	Particle diameter [m]	2.1
x	Space variable / position / displacement [m]	2.1
r	Position (x,y,z) [m]	2.1
v	Fluid velocity vector [m/s]	2.1
c	Speed of sound [m/s]	2.1
p	Pressure [Pa]	2.1
f	Frequency [Hz]	2.1
k	Wave number [1/m]	2.1
g	Gravity vector [m/s ²]	2.1
F	Force [N]	2.1
F_{rad}	Acoustic radiation force vector [N]	2.1
U_{rad}	Acoustic radiation force potential [Nm]	2.1
E_{ac}	Acoustic energy density [J/m ³]	2.1
E	Young's Modulus [N/m ²]	4.2.3
L_p	Sound level [dB]	2.3.2

Symbol	Description	Defined in section
V_p	Particle volume [m ³]	2.3.2
α	Attenuation [dB/m]	6.3.1
β	Viscosity ratio [-]	2.1
η	Dynamic viscosity [Ns/m ²]	2.1
κ	Compressibility [-]	2.1
ϕ	Velocity potential [m ² /s]	2.1
Φ	Acoustic contrast factor [-]	2.1
ρ	Density [kg/m ³]	2.1
ω	Angular frequency [rad/s]	2.1
∇	Gradient operator	2.1
Mechanics / Electronics		
m	Mass [kg]	2.1
b	Damping coefficient [Ns/m]	2.1
k	Stiffness [N/m]	2.1
L	Inductance [henry]	2.1
R	Resistance [Ω]	2.1
C	Capacitance [farad]	2.1
X	Reactance [Ω]	2.1
Y	Admittance [S]	3.2
Z	Impedance [Ω]	2.1
A	Amplitude of vibration [m]	2.1
V	Voltage, Electric potential [V]	3.2
I	Current [A]	3.2
P	Power [W]	3.4.1
Piezoelectrics		
Q	Quality Factor [-]	3.1
T	Stress matrix [N/m ²]	3.2.1
S	Strain matrix [-]	3.2.1
E	Electric field matrix [V/m]	3.2.1
D	Electric displacement matrix [N/Vm]	3.2.1
u	Displacement vector [m]	3.2.1
cE	Stiffness constant matrix	3.2.1
e, e_{ij}	Dielectric constant matrix, constant	3.2.1
d, d_{ij}	Coupling matrix, constant	3.2.1
$\epsilon_S, \epsilon_{ij}$	Permittivity matrix @ constant strain, constant	3.2.1
$\epsilon_T, \epsilon_{ij}$	Permittivity matrix @ constant stress, constant	3.2.1
s_E, s_{ij}	Compliance matrix, parameter [m ² /N]	3.2.1
k_{ij}	Coupling factor [-]	3.1
q_e	Surface charge [C]	3.2.1
η_m	Mechanical loss factor [-]	3.2.1
N_t	Frequency constant for thickness [Hzm]	3.1
$\tan \delta$	Dielectric loss factor [-]	3.1
β	First order differential operator	3.2.1

Symbol	Description	Defined in section
Δf	Peak width @ half peak height [Hz]	3.4.1
Optimisation		
\mathbf{n}	Normal vector	3.2.2
\mathbf{J}	Jacobian	3.3.3
\mathbf{b}	Estimator vector	3.3.3
\mathbf{F}	Residual vector	3.3.3
Cov	Covariance (matrix)	3.3.3
σ^2	Statistical variance	3.3.3
n	Number of function evaluations	3.3.3
p	Number of estimated parameters	3.3.3
U	(Relative) Flow speed [m/s]	6.2.4
AR	Area ratio [-]	6.2.4
h_{lane}	Lane height [m]	6.2.4
h_{ref}	Reference height [m]	6.2.4
Efficiency and Operational control		
ϵ_f	Filtration efficiency [%]	7.2.4
ϵ_c	Concentration efficiency [%]	7.2.4
$[S]$	Concentration of stock solution [mg/L]	7.2.4
$[C]$	Concentration of concentrate [mg/L]	7.2.4
$[F]$	Concentration of filtrate [mg/L]	7.2.4
C_i	Compartment i of separation chamber	8.3.2
S_i	Particle concentration in compartment C_i	8.3.2
V_i	Volume of compartment C_i	8.3.2
Q	Flow rate [m ³ /s]	8.3.2
k_j	Rate coefficient j	8.3.2
α	Digital on/off switch parameter	8.3.2
\mathbf{Y}	System output vector	8.3.2

SUMMARY

Due to limited water resources available in the world and the ever growing world population, there is an increasing need for water recycling, recovery and multi-sourcing strategies. In general, some sort of water treatment is needed when recycling water, in order to obtain the water quality needed. This water treatment often consists of several steps, called "unit operations", which can be divided into chemical, biological or physical processes and hybrids thereof.

The increasing need for water drives the innovation of new technology. One of the new physical process technologies being investigated for water purification and/or constituent recycling is ultrasonic particle separation. This technology is especially interesting for harvesting particles with an almost neutral buoyancy. An ultrasonic particle filter does not use a filter medium, like sand or a membrane, but filters on a basis of acoustic forces, which are able to immobilise particles in flowing water. The acoustic waves inside the fluid are reflected and scattered by the suspended particles, because the particles have different sound propagation properties than the surrounding fluid. This scattering results in a net acoustic force on the particles, forcing them toward acoustic pressure nodes or antinodes, depending on the particle properties with respect to the fluid. A state of acoustic resonance inside a separation chamber improves the separation efficiency, because forces (and pressures) resulting from standing waves are much higher than forces from travelling waves. The technique was demonstrated in ambient air with an experimental setup consisting of a signal generator, an audio amplifier, four small speakers and large, mm-size, polystyrene particles. The actual separation process, lining up the particles in the nodal lines of the standing wave field, occurred at 12.6 kHz in a matter of milliseconds.

Studies on acoustic separation are nowadays mainly focused on particle manipulators¹, including particle sorting (on the basis of their physical properties) and positioning of particles for sensing purposes. Few studies were performed on larger scale acoustic filters for water purification purposes. Therefore, the objective of this study was to develop an ultrasonic separation device for particle recovery and water purification. This separator should be fit for industrial applications treating cubic meters of water per hour.

In order to reach this objective, a combined numerical-experimental approach was proposed to develop a model-based design of an ultrasonic separator. Each individual component of this separator was modelled using a finite element (FE) approach. The numerical simulations were continuously cross-checked with experimental findings in a design loop in order to find the best solution possible.

¹A manipulator is able to control the position and orientation of a particle by specific changes to the acoustic field.

In this thesis, the source of the acoustic wave is a piezoelectric transducer. The transducer is attached to a glass matching layer of the acoustic cavity, which vibrates with the transducer and couples the transducer to the fluid inside the cavity, forming an acoustic resonator/separator. In order to obtain a valid transducer model, a limited set of material parameters for the piezoelectric transducer were obtained from the manufacturer, thus preserving prior physical knowledge to a large extent. The remaining unknown parameters were estimated from impedance (admittance) analysis with a simple experimental setup combined with a numerical optimisation routine using 2D and 3D FE models. Thus, a full set of physically interpretable material parameters was obtained. The approach provided adequate accuracy of the estimates of the material parameters, near 1%. A sensitivity study showed that small variations of 1% in the main parameters caused changes near 1% in the eigenfrequency, but changes up to 7% in the admittance peak, thus influencing the efficiency of the system.

A similar approach as used for the transducer was applied to an existing ultrasonic separator. The separator was calibrated and validated with the admittance measured on the transducer using non-linear optimisation techniques, again preserving known physical parameters and estimating the remaining unknown or less certain parameters. The results showed that the approach led to a fully calibrated 2D model of the *empty* separator, which was subsequently validated with experiments on a *filled* separator chamber. The large sensitivity of the separator to small variations indicated that either such system should be made and operated within tight specifications to obtain the required performance. Alternatively, the operation of the system should be adaptable to cope with a slightly off-spec system, requiring a feedback controller.

Starting from a fully characterised existing separator with all material parameters found so far, the subsequent step was the actual design of, or extrapolation to, a new separator. A basic design for an industrial scale acoustic separator was obtained based on simulated flow characteristics inside the separation chamber, on acoustic analysis within the chamber and simulated particle trajectories combining these two analyses. Results showed that positioning the piezoelectric transducer surfaces perpendicular to the flow direction and introducing chamber partitioning with multiple flow lanes to enforce laminar flow, resulted in high particle retention. The average particle displacement was found to be related to acoustic pressure in the fluid, showing large retention at peak pressures above 1 MPa or average pressures above 0.5 MPa for small (10 μm), near buoyant (1100 kg/m^3) particles at a flow speed of 3.5 cm/s, thus providing comprehensible criteria for subsequent optimisation.

This basic ultrasonic standing wave separator design was optimised with respect to separation efficiency, throughput and energy consumption. More than 300 finite element model simulations were run, in which acoustics, flow characteristics, particle retention and energy demand were evaluated. The methodology, using a design of experiments (DOE) approach, showed that it was possible to improve system performance based on acoustic pressure profiles, separation efficiency and flow robustness. Compromising the energy consumption and aiming for maximum separation efficiency with a laminar stable flow up to 5 ml/s resulted in a separator with inner dimensions of 70 mm length, 20 mm width and 28.5 mm height using two transducers perpendicular to the direction of flow

and three parallel flow lanes with 9.5 mm height each. The lowest power consumption (with an average of 30 W) with adequate pressure to trap the particles was obtained when it was not operated at the main eigenfrequency.

Finally, this new ultrasonic particle filter was built and evaluated experimentally. The particle filter was a three channel device, manufactured from glass with four in/outlet ports made of ABS. It was operated in sequenced batch mode - 150 s of filtering followed by a 20 s backwash with filtrate, which removed the collected particles from the separator as concentrate. The separation efficiency was determined at three flow rates ranging from 1 to 3 ml/s, using a stock suspension of insoluble potato starch of 1 g/l (1000 ppm). Concentrations of stock, filtrate and concentrate were measured using a turbidity meter and significant effects of acoustic particle concentration were measured at both outlets of the process. The maximum filtration efficiency and concentration efficiency were 54% and 76%, respectively. The performance found was lower than the 100% that was expected for 10 μm particles from the model based design study. The deviation in performance is mainly a result of (i) the pulsation of the feed pump, (ii) differences between the model and the actual prototype, (iii) the limited power supply of only 10 W used and (iv) (too) small particles, below 10 μm , occurring in the starch suspension.

The best dimensions for an acoustic separator were obtained, but thus far operational characteristics were not yet studied. Operational characterisation and optimisation is the last step in the process of obtaining the best possible solution for operation. Therefore, in the initial stage of the study, a commercially available acoustic separator, named BioSep, which employs ultrasound enhanced sedimentation, was used. With the aim to achieve a high separation efficiency with minimal energy consumption, a model-based open-loop switching control strategy was designed for the BioSep, using a numerical-experimental approach. Firstly, a dynamic BioSep model structure was derived from mass balances and its system properties were studied. Then, the unknown system parameters were estimated from steady state and dynamic experimental data and subsequently, the switching times of the control input were determined. The model with switching control outputs was then validated by experiments. Finally, the control strategy was implemented in an experimental setup and tested using suspended potato starch. Results showed that the optimal control strategy reached a mass separation efficiency of 96%, which was an improvement of 4% with respect to the initial settings, while using less energy. Extension towards the design of a feedforward / feedback control strategy and application of the newly developed separator is recommended.

Concluding, a stepwise numerical-experimental approach to acoustic separator design was presented in this study. Each physical layer in the separator was modelled and validated with experiments, starting with the piezoelectric transducer up to the acoustics and flow inside the resonator cavity. A model-based design optimisation was performed using a Design of Experiments (DOE) method. The resonator had a theoretical particle retention of 100% at a flow rate of 5 ml/s (18 l/h) using particles with a diameter of 10 μm and a density of 1100 kg/m³. The minimum power required was estimated to be 22-34 W, resulting in an average electric energy consumption of 1-1.5 kWh/m³. The practical concentration efficiency obtained was 76% at a flow rate of 2 ml/s and a filtration efficiency of 54% at 1 ml/s with a real power input of 8.8 W. An optimal open

loop control strategy showed that it is possible to operate an acoustic separator with high separation efficiency using the least power possible. Parallelisation, instead of enlarging the separator, is recommended to scale this system up to larger, industrial flows.

SAMENVATTING

Aangezien de watervoorraden op aarde beperkt zijn en de wereldbevolking groeit, is er een steeds grotere behoefte aan hergebruik van water, terugwinning van water en het gebruik van meerdere bronnen voor onze watervoorziening. Meestal is er bij waterhergebruik wel een vorm van waterzuivering nodig om de benodigde waterkwaliteit te krijgen. Deze zuivering bestaat vaak uit meerdere stappen, zogenaamde 'proceseenheden', die onderverdeeld worden in chemische, biologische of fysische processen of hybriden daarvan.

De toenemende vraag naar water leidt tot nieuwe technologische innovaties. Eén van de nieuwere, fysische technieken die onderzocht wordt als methode om water te zuiveren of stoffen daaruit terug te winnen, is ultrasone deeltjesscheiding. Deze techniek is met name interessant voor zwevende deeltjes, die nauwelijks bezinken of opdrijven. Een ultrasone deeltjesseparator gebruikt geen filtermateriaal, zoals zand of een membraan, maar filtert op basis van akoestische krachten, die deeltjes in het water kunnen tegenhouden in het verder stromende water. Deze akoestische krachten op zwevende deeltjes zijn een resultante van geluidsgolven, die weerkaatst en verstrooid worden door de deeltjes zelf, omdat deze deeltjes andere akoestische eigenschappen hebben dan de vloeistof of het gas, waarin ze zich bevinden. Akoestische resonantie in de separator verbetert de efficiëntie van het proces, omdat krachten en drukken in het akoestisch veld van een staande golf veel hoger zijn dan in het akoestisch veld van een lopende golf. De techniek werd gedemonstreerd in lucht met een experimentele opstelling, die bestond uit een signaalgenerator, een audioversterker, vier kleine luidsprekertjes en grote (mm) piepschuimbolletjes. De scheiding van de bolletjes, waarbij deze in de knooppunten van de staande golf kwamen te liggen, vond plaats binnen enkele milliseconden bij een frequentie van 12.6 kHz.

Onderzoek naar akoestische scheidingsmethoden richt zich vandaag de dag vooral op het (be)sturen van de deeltjes zelf, inclusief het sorteren van deeltjes (op basis van de akoestische eigenschappen), en op het positioneren van deeltjes, zodat ze gemakkelijker gedetecteerd kunnen worden. Een zeer beperkt aantal onderzoeken richt zich op groot-schalige toepassingen voor waterzuivering. Daarom was het doel van dit onderzoek om een ultrasone separator te ontwikkelen voor het terugwinnen van zwevende stof uit water en zuivering van het water zelf. De separator moet geschikt zijn voor industriële toepassingen, waarbij kubieke meters water per uur behandeld kunnen worden.

Om dit doel te bereiken, werd een numeriek-experimentele methode gekozen, waarmee de separator op basis van modelvorming ontworpen kon worden. Elk onderdeel van de separator werd gemodelleerd met eindige elementen (FE), waarbij de numerieke resultaten steeds kruislings gecontroleerd werden met experimentele resultaten, zodat met deze

ontwerpcyclus de meest optimale oplossing gevonden werd.

In dit onderzoek werd een piezoelektrische geluidsbron gebruikt. Dit piezo-elektrische plaatje, kortweg piezo genoemd, zat vastgeplakt aan de glazen buitenwand van de akoestische separator, die daardoor in trilling werd gebracht en de trilling overbracht van de geluidsbron en de vloeistof, die zich in de separator bevond. Deze componenten samen vormden de resonator/separator. Om een gevalideerd model van de piezo te maken, werden de door de fabrikant gespecificeerde materiaalparameters zoveel mogelijk gebruikt in het model, zodat reeds bestaande kennis zoveel mogelijk in het model geïntegreerd was. De overige onbekende parameters werden op basis van impedantie- (admittantie-)metingen geschat, door deze metingen te koppelen met een numerieke optimaliseroutine met 2D en 3D FE-modellen van de piezo. Op die manier werd een set materiaalparameters verkregen, die ook fysisch te interpreteren was. Deze werkwijze resulteerde in een nauwkeurigheid van 1% voor de geschatte parameters, hetgeen voldoende was. Een gevoeligheidsanalyse toonde aan dat door kleine veranderingen van 1% in de belangrijkste, geschatte parameters, de eigenfrequentie met 1% veranderde, maar de admittantie zelfs tot 7% kon veranderen. Deze verandering van de admittantie is direct van invloed op de efficiëntie van het systeem.

Eenzelfde modelmatige benadering, zoals toegepast werd op de piezo, werd ook gebruikt voor het model van een bestaande ultrasone separator. Het model werd gekalibreerd en gevalideerd met behulp van de elektrische admittantie, die aan de piezo van deze separator werd gemeten. Om de onbekende parameters te schatten, werd ook hier gebruik gemaakt van niet-lineaire optimalisatie, terwijl de reeds bekende parameters onveranderd bleven. Het resultaat leidde tot een volledig gekalibreerd 2D model van de *lege* separator, dat vervolgens werd gevalideerd met metingen aan een *gevulde* separator. De grote gevoeligheid van het model voor kleine parametervariëaties, echter, toonde aan dat dergelijke systemen of met grote nauwkeurigheid gebouwd en bestuurd moeten worden om de vereiste prestatie te halen, of dat de aansturing van het systeem moet kunnen compenseren voor kleine afwijkingen, waarbij een regeling met terugkoppeling nodig is.

Met een volledig gekarakteriseerd model van een bestaande separator als startpunt, kon de volgende stap gezet worden door het model te extrapoleren naar een nieuw ontwerp. Het basisontwerp voor een industriële separator werd bepaald op basis van simulaties van de vloeistofstroming in het systeem, het gesimuleerde akoestische veld en de gesimuleerde deeltjesverplaatsing. De laatst genoemde simulatie maakte gebruik van de resultaten uit de twee eerder genoemde simulaties. De resultaten toonden aan dat het positioneren van de piezo loodrecht op de stromingsrichting en het verdelen van de vloeistofstroming over meerdere kanalen een hoge mate van deeltjesretentie gaf. Bovendien bleek de gemiddelde deeltjesverplaatsing gecorreleerd te zijn met de akoestische druk in de vloeistof. Een hoge mate van deeltjesretentie werd gevonden bij een maximale druk boven de 1 MPa of een gemiddelde absolute druk boven de 0.5 MPa voor kleine ($10\ \mu\text{m}$), zwevende ($1100\ \text{kg/m}^3$) deeltjes bij een stroomsnelheid van 3.5 cm/s. Deze duidelijke criteria konden gebruikt worden voor de hieropvolgende optimalisatie.

De basisconfiguratie werd geoptimaliseerd op basis van scheidingsefficiëntie, debiet en energieverbruik. Meer dan 300 FE-modelsimulaties werden uitgevoerd, waarin akoes-

tiek, stroming, deeltjesretentie en energieverbruik werden geëvalueerd. De gebruikte experimentele ontwerpmethode toonde aan dat het mogelijk was om de prestaties van het systeem te verbeteren op basis van akoestische drukprofielen, scheidingsefficiëntie en robuustheid van de stroming. De maximale efficiëntie werd bereikt met een stabiele, laminaire stroming van 5 ml/s in een separator met binnenafmetingen van 70 mm lengte, 20 mm breedte en 28.5 mm hoogte, met twee piezo's aan beide zijden, die loodrecht op de stromingsrichting stonden, en met drie parallelle kanalen van elk 9.5 mm hoog. Het laagst mogelijke vermogen (gemiddeld 30W), waarbij voldoende druk werd bereikt om deeltjes vast te houden, werd bereikt als het systeem niet op de primaire eigenfrequentie draaide.

De laatste stap was de evaluatie van de efficiëntie van het nieuwe separatorontwerp. Het deeltjesfilter had drie kanalen en werd gefabriceerd van glas met vier in-/uitgangen, die van ABS waren gemaakt. Het systeem draaide met opeenvolgende batches - na 150 s filteren werd er 20 s lang teruggespoeld met filtraat, waarmee de verzamelde deeltjes uit de separator werden afgevoerd als concentraat. De efficiëntie werd bepaald met een aardappelzetmeelsuspensie van 1 g/l bij drie stroomsnelheden van 1-3 ml/s. De concentraties van de ingaande stroom, filtraat en concentraat werden gemeten met een turbiditeitsmeter en de akoestische scheiding was significant meetbaar aan beide uitgangen. De maximale filterefficiëntie was 54% voor het filtraat en 76% voor het concentraat. Deze uitkomst was lager dan de 100% die op basis van het model voor 10 μm deeltjes zou moeten gelden. De verschillen in prestatie waren met name te wijten aan (i) pulsing van de voedingspomp, (ii) verschillen tussen model en het gebouwde prototype, (iii) onvoldoende toegevoerd vermogen van slechts 10 W en (iv) de (te) kleine deeltjes, onder de 10 μm , die in de zetmeelsuspensie aanwezig waren.

Hoewel de optimale afmetingen van een akoestische separator nu bepaald waren, was de operationele werking van het systeem nog niet bestudeerd. Het karakteriseren en de optimalisatie van het filtratieproces was de laatste stap in een zoektocht naar de best werkende oplossing. Om dit te bereiken werd (reeds in een vroeg stadium van het onderzoek) een commercieel beschikbare akoestische separator ingezet, de BioSep, die gebruik maakt van versnelde sedimentatie met ultrageluid. Met als doel om een hoge scheidingsefficiëntie te vinden bij een zo laag mogelijk energieverbruik, werd een modelmatige open-loop aan/uit schakeling ontworpen voor BioSep met een numeriek-experimentele benadering. Eerst werd een dynamisch model van BioSep gemaakt, afgeleid uit massabalansen, waarmee de systeemkarakteristieken bestudeerd werden. Daarna werden de onbekende systeemparameters geschat uit steady-state en dynamische testgegevens en daarna werden de schakeltijden bepaald. Met het model werd de concentratie aan de uitgang berekend en vervolgens gevalideerd met experimenten. Als laatste werd de gevonden regelstrategie in een experimentele opstelling geïmplementeerd en getest met aardappelzetmeel. Een scheidingsefficiëntie van 96% werd daarbij gehaald, hetgeen een verbetering was van 4% ten opzichte van de basisinstelling, terwijl er minder energie werd verbruikt. Een aanbeveling is om de regelstrategie uit te breiden met een terugkoppeling en toe te passen op de nieuwe separator.

Samengevat werd in deze studie een stapsgewijze, numeriek-experimentele benadering gebruikt om een akoestische separator te ontwerpen. Elk onderdeel in de separator werd

gemodelleerd en met experimenten gevalideerd, te beginnen bij de piezo tot en met de akoestiek in de resonator en de vloeistofstroming. Optimalisatie van het ontwerp werd met behulp van een experimentele ontwerpmethode gedaan. De resonator had een theoretische deeltjesretentie van 100% bij een debiet van 5 ml/s (18 l/u) voor deeltjes van 10 μm en een dichtheid van 1100 kg/m^3 . De energie die minimaal nodig was, werd geschat op 22-34 W, hetgeen een energieverbruik van 1-1.5 kWh/m^3 zou betekenen. In de praktijk werd een efficiëntie van 76% behaald voor de concentraatstroom bij een debiet van 2 ml/s en 54% bij 1 ml/s voor de filtraatstroom bij een reëel vermogen van 8.8 W. Er werd aangetoond dat een hoge scheidingsefficiëntie bereikt kan worden met zo min mogelijk vermogen door gebruik te maken van een optimale open-loop regelstrategie. Om industriële debieten aan te kunnen, is het aan te raden om meerdere systemen parallel te schakelen, in plaats van de afmetingen van de separator zelf te vergroten.

ACKNOWLEDGEMENTS

First of all, I would like to express my gratitude to my loving wife, Mariska, and dearest children, Jorim, Luca and Noémi. Pappa zat vaak achter zijn laptop voor het werk, voor de studie, de kerk en nog allerlei andere dingen die tegenwoordig op een PC moeten. Het werd zelfs zo erg dat op jullie tekeningen pappa steeds achter de PC zat. Dat geeft te denken ... Bedankt voor jullie geduld, liefde en begrip. Jullie zijn schatten! Thanks to my mom and dad for taking care of our kids ever so often. I love you people!

Of course, I am extremely grateful to Karel Keesman, co-promoter and everlasting optimist. Karel always saw the bright side of things, while I was wondering why some of the results were dramatically bad and things did not seem to fit. We have had great discussions in your office, on board the train, in Vlissingen, at CISM in Italy, at the conference in Prague and at Wetsus. Thanks for your endless reading, corrections, insights, wisdom and support. Also for the fun we had in the Netherlands and abroad during the past five years of research. I'd wish all PhD students had a supervisor like you; you've been marvellous! I surely wish to continue this close collaboration.

Also many thanks to Gerrit van Straten, my promoter, who was always wondering, whether he really was the right person to be in charge of this specific topic. Yes, Gerrit, there was nobody else working in this field in the Netherlands, so you had little choice. Your correct and specific questions helped to sort out every detail and what we were really heading for. Naturally, you were well informed on all procedures I needed to fulfil to get to the point of my defence at the university.

MSc and BSc students from Wageningen University and HZ: Nurul, Lyubka, Niels, Rebecca and Zhengdao, in timely order. Each of you did some part or parallel project on this subject and provided some very nice basics, measurements, results and insights for the work in this booklet or the research which is yet to come. Special thanks to Nurul, for kicking-off this difficult subject with me, and Lyubka, for your thorough work and writing a paper with Karel and me. You girls are brilliant!

I almost forgot the real experts, who greatly helped me along with their insights, either on paper or by mail or orally at the USW training in Udine and the USW conference in Groningen, some of whom I visited. Jeremy Hawkes, Felix Trampler, Martin Gröschl, Peter Glynn-Jones, Henrik Bruus and Bruce Drinkwater.

I'm grateful to Michiel and Jasper 'fellow-sufferers' or 'partners in crime', combining a PhD with lecturing and other research tasks. I guess we made our mutual frustrations a bit more bearable. I've also had great coffee breaks with you guys and Eva, Tessa, Niels, Jan, Tony and Jorik (sorry, if I missed out anyone here). I should also mention Gide Wattez, for helping me out with the demo in air, Bert Janssen for his advice and borrowing his

electronics lab, and Jan and Jorien for materials and 3D-printing. It's indispensable to have great colleagues, without whom some work would be really boring! Also thanks to my room/office mates during the past years from Piet and Chris, via the Civil Engineering team, to my own Water Technology group, for the fun and for listening every now and then to the challenges of the wonderful world of research. It's great working with you people! Gratitude to Wim Brouwer, Monica, three of the Peters and Adri who realised the opportunity to doing this extensive research at HZ.

Then there's the SCO/BRD team at Wageningen University. People like Marja, Ellen, Jan, Jimmy, James, Xin, Kees, Rachel, Ton and Gerard. I know I'm forgetting people here, but you were the people who I encountered most often and who were there in the office and when we were biking through Holland or visiting the Corpus in Leiden. Special thanks, in this respect, to Marja, Ellen, Kees and Jan. You guys were/are the glue in this group, keeping the pack together. I'm also grateful to Maarten Schutyser for borrowing the BioSep and related stuff for several years. Thanks also to the other group of fellow (former) PhD students at Wetsus: Justina, Yvette, Ran, Johannes, Nadine, Slawomir (in random order). We were on the same boat, defending and promoting our research time and again. My topic always seemed so simple compared to yours...

Finally, last but surely not least, thanks to the coordinating people at Wetsus, like Maarten, Doekle, Mateo, Jan de Groot, Cees and Johannes. Things would have been far more difficult without you people. Wetsus is a great institute to work with! Thanks to the Advanced WasteWater Treatment theme for good questions and discussions on practical applications and possibilities for further investigation.

CURRICULUM VITAE

Hans Cappon is lecturer and researcher in the field of Water Technology at HZ University of Applied Sciences since 2007. His main topic of research is ultrasound technology used for growth inhibition of micro-organisms in water and particle harvesting or filtering using ultrasound.

Hans was born in Axel, the Netherlands on June 29, 1973. During his childhood he lived in Axel and on the island of St. Maarten in the Caribbean, where he started his secondary education, which he finished in 1992 in Goes, the Netherlands. At Eindhoven University of Technology he then studied Mechanical Engineering during his first year, in order to continue with Biome-



chanical Engineering, for which he received his Master's degree in 1997. Five years later, in 2002, Hans started his 'second career' as a part time theology student at the Christelijke Hogeschool Ede and in 2009 he received his Bachelor of Theology degree.

Prior to his current job at HZ, he already worked in the field of physical modelling and optimisation at Catholic University of Leuven in Belgium and at research institute TNO in Delft, Helmond and Eindhoven. The objects of (model-based) research included agricultural sprayers, crash test dummies, sports equipment (motor cycle helmets, artificial turf and golf clubs) and injury mechanisms of various parts of the human body under extreme loading conditions. In all of this work numerical models were combined with experimental validation and/or evaluation.

Hans is married to Mariska and they have three children, Jorim, Luca and Noémi. His main hobbies are playing drums, reading and collecting Lego trains.



Netherlands Research School for the
Socio-Economic and Natural Sciences of the Environment

C E R T I F I C A T E

The Netherlands Research School for the
Socio-Economic and Natural Sciences of the Environment
(SENSE), declares that

Hendrik Jannis Cappon

born on 29 June 1973 in Axel, The Netherlands

has successfully fulfilled all requirements of the
Educational Programme of SENSE.

Wageningen, 5 March 2014

the Chairman of the SENSE board

Prof. dr. Rik Leemans

the SENSE Director of Education

Dr. Ad van Dommelen

The SENSE Research School has been accredited by the Royal Netherlands Academy of Arts and Sciences (KNAW)



KONINKLIJKE NEDERLANDSE
AKADEMIE VAN WETENSCHAPPEN



The SENSE Research School declares that **Mr. Hendrik Jannis Cappon** has successfully fulfilled all requirements of the Educational PhD Programme of SENSE with a work load of 35.5 ECTS, including the following activities:

SENSE PhD Courses

- o Environmental Research in Context
- o Research Context Activity: Developing and presenting course module on Ultrasonic Water Purification as well as writing accessible press release on research findings

Other PhD Courses

- o Techniques for Writing and Presenting Scientific Papers
- o Certificate of Proficiency in English
- o Comsol beginner and advanced training
- o Matlab Fundamentals and Simulink

External Training at a foreign research institute

- o External training period Ultrasonic Standing Waves, International Centre for Mechanical Sciences (CISM), Udine, Italy

Management and Didactic Skills Training

- o Organising Workshop Water Technology

Oral Presentations

- o *Purification with high frequency ultrasound*. Wetsus Internal Congress, 25 November 2010, Leeuwarden, The Netherlands
- o *Acoustic waves for water filtration and purification*. Wetsus Internal Congress, 17 November 2011, Leeuwarden, The Netherlands
- o *Numerical modelling and calibration of an ultrasonic separator*. Benelux Meeting for Systems & Control, 27-29 March 2012, Heijen, The Netherlands
- o *Design basis of industrial acoustic separators*. IEEE UFFC International Ultrasonics Symposium, 22-25 July 2013, Prague, Czech Republic

SENSE Coordinator PhD Education

Dr. ing. Monique Gulickx

This work was performed in the cooperation framework of Wetsus, centre of excellence for sustainable water technology (www.wetusus.nl). Wetusus is co-funded by the Dutch Ministry of Economic Affairs and Ministry of Infrastructure and Environment, the European Union Regional Development Fund, the Province of Fryslân, and the Northern Netherlands Provinces. The author likes to thank the participants of the research themes "Capacitive Deionization" and "Advanced Waste Water Treatment" for the fruitful discussions and their financial support.

The research described in this thesis was also financially supported by HZ University of Applied Sciences.

The cover, designed by the author, shows a manipulated photo of a cirrocumulus.
Printed by: Gildeprint Drukkerijen - The Netherlands